RICE UNIVERSITY

Linking a Mitotic Oscillator to the Extracellular Environment: The Importance of Protein Network Structure and Multisite Phosphorylation

by

Ryan Christopher Vargo

A THESIS SUBMITTED
IN PARTIAL FULFILLMENT OF THE
REQUIREMENTS FOR THE DEGREE

Doctor of Philosophy

APPROVED, THESIS COMMITTEE:

Kyriacos Zygourakis, Chair, A.J. Hartsook Professor Chemical and Biomolecular Engineering, Professor Bioengineering

Ramon Gonzales, William W. Akers Assistant Professor Chemical and Biomolecular Engineering

Antonios G. Mikos, Louis Calder Professor Bioengineering, Chemical and Biomolecular Engineering

HOUSTON, TEXAS

JULY 2009

ABSTRACT

Linking a Mitotic Oscillator to the Extracellular Environment: A Bottom-up Approach Analyzing Protein Network Structure and Multisite Phosphorylation

by

Ryan Christopher Vargo

This thesis work contributes the first vital steps in the development of a biologically based proliferation model to advance a bioartificial tissue regeneration model. Specifically, this work presents a mitotic oscillator model incorporating ATP, which was linked to extracellular glucose. This model is the first mitotic oscillator linked to the extracellular environment. Furthermore, this work is the first to connect extracellular glucose to mitosis with ATP.

Taking a bottom-up approach, a base mitotic model was developed using the latest biology. The reaction network structure of mitosis is not fully understood, and the role of multisite phosphorylation is uncertain. Therefore, using bifurcation analysis and transient simulations, the effect of the mitotic reaction network structure and multisite phosphorylation on system behavior was analyzed by varying the MPF activation network structure, the number of positive feedback loops, and the number of phosphorylations on the positive feedback loop proteins.

The results suggest that the MPF activation network has evolved to efficiently utilize cyclin B and to generate switch-like transitions into mitosis. The behavior of the mitotic oscillator model was affected by the order and number of multisite phosphorylations, which are essential to generate sharp switch-like transitions into mitosis. Addition of multiple positive feedback loops into the model enhanced the signal to initiate mitosis.

Next, ATP was incorporated into the network. The model was then tuned to a relative ATP concentration, which is generic and therefore applicable to different cell lines. Multiple Wee1 networks were analyzed to elucidate the function of the two inhibition mechanisms, kinase inhibition and increased degradation. The results suggest that the inhibition mechanisms are redundant. Therefore, the model incorporates the Wee1 mechanism that allows the cell to maintain maximum control over the initiation of mitosis.

To generalize the mitotic model, the parameter set was tuned for to a relative ATP concentration and fibroblast division times. Finally, the relative intracellular ATP model was linked to the extracellular glucose. The model developed in this thesis work is the first to use ATP as the link between mitosis and the extracellular glucose, and the first mitotic model connected to the extracellular environment.

ACKNOWLEDGEMENTS

First and foremost, I would like to thank Professor Kyriacos Zygourakis for mentoring and guiding my development as an independent researcher. Throughout my time at Rice researching the many areas of theoretical biology, Dr. Zygourakis has provided me the flexibility and freedom necessary to gain a broad exposure to the field. I am especially grateful that Dr. Zygourakis allowed me to reach out to areas outside my core research project, providing me opportunities to expand my skill set and knowledge.

I thank Professors Ramon Gonzalez and Antonios Mikos for serving as my committee members. I acknowledge the valuable input from Dr. Nikolaos Mantzaris during the early stages of this work. In addition, my colleague Michalis Stamatakis offered me a crash course in the XPPAUT bifurcation program and greatly assisted me in the post processing of the bifurcation data. My colleague Konstantinos Spetsieris has been a great resource for my interest in heterogeneity and microscopy. Although the experiments did not come to fruition, I appreciate all Kostas did to help me in the lab.

Furthermore, I am grateful to have worked with Tom Jaber and Mark Whatley in the Shepherd School of Music. Likewise, I thank Master Ray Nelson and Mr. William Wallauer for beginning my journey in the Chayon Rhu tradition, and providing instruction for my first formal exposure to martial arts. I thank all my fellow GSA soccer teammates especially, Nick Parra-Vasquez, Oscar Coronado, Juan Duque, and Eelco Nederkoorn. These activities at Rice with great friends have provided me a balance to my scientific work.

In addition, Dr. Patrick A. Thompson has been a great friend and mentor to whom I am extremely grateful for exposing me to and helping me find a position in pharmacometrics. I extend my thanks to Dr. Peter L. Bonate for the generous use of his knowledge and time during my experience with Dr. Thompson. Likewise, I thank Dr. Jan Hewitt for continuously improving my writing skills. Her feedback helped me to effectively communicate the scientific work I proposed and accomplished while at Rice. I am extremely grateful for her time and attention to detail, which have significantly improved my writing abilities.

I appreciate the support from all of my friends, particularly Matt Pozzi and Jason Hatch. Thank you to the Dougherty family, especially, Bryan, Amy, Jackie, and Terry for welcoming me into their family. I am grateful for all of the great times and holidays we celebrated together in Houston.

Finally, and most importantly, I thank my family. Thank you, Mom and Dad, for your unending support in my education. I am beyond grateful that I was born into a wonderful family with dedicated parents who nurtured my education and abilities, allowing me to grow into the person I am today. I thank my brothers, Scott, Craig, and Kevin for continuing to make me laugh and appreciate the lighter side of life. I cannot leave out my first pug Buddha for being a constant positive outlet that would always bring my mind to peace and happiness at the end of every day. I am extremely appreciative for the support and dedication of my wife, Abby. Throughout my time at Rice, you have always been a source of encouragement. Thank you, and I love you.

Table of Contents

List of Figures

List of Tables

Chapter 1 - Introduction

During mitosis, a mother cell partitions it contents and divides into two daughter cells. The successful division of cells is necessary for all life forms from single cells like bacteria and yeast to multicellular organisms such as humans. In humans, cellular division occurs throughout our lifetimes and is a key process in wound healing and tissue regeneration. My thesis work implements the first steps in developing a proliferation model that can be implemented into a model for bioartificial tissue regeneration by creating a biologically based mitotic oscillator model that is linked to the extracellular environment.

Our group carries out experimental and modeling studies to increase the understanding of the fundamental processes involved in bioartificial tissue regeneration [1-9]. A model for bioartificial tissue regeneration incorporates many different submodels (Figure 1). All the submodels flow into the bioartificial tissue regeneration model at the bottom. One level above the bioartificial tissue regeneration model, the middle level, are the models for the individual cells, the scaffold, and the environment. All of the models interact within this level. For example, the individual cell model is reacting to the scaffold and the extracellular environment to migrate, proliferate or die.

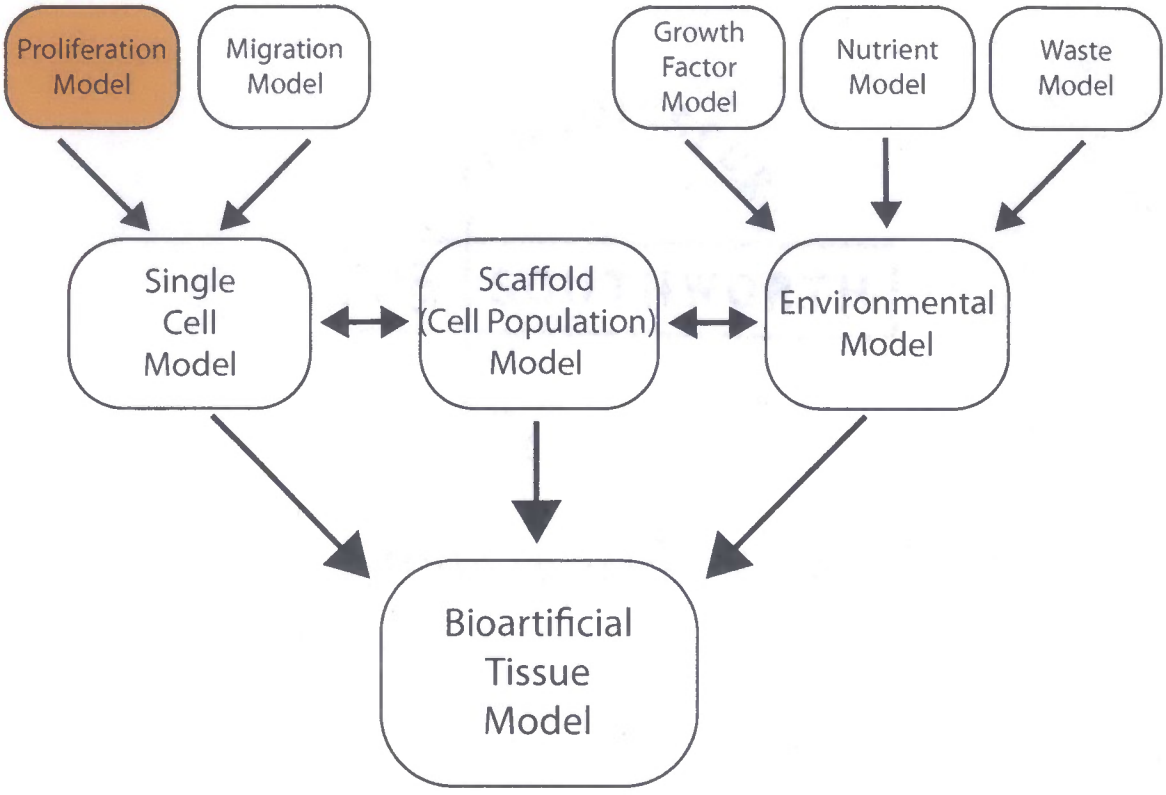

Figure 1 – Hierarchy of Bioartificial Tissue Model. At the bottom level is the full bioartificial tissue model. The middle level contains the key areas of the tissue regeneration process, individual cells, the tissue scaffold, and the environment. These models interact with each other and dictate the observed phenomena of the overall model. The processes dictating the behavior of the environment, scaffold, and individual cells compose the top level of the hierarchy. Individual cells have proliferation and migration models for individual cells, and the environment has mass transport, production, and consumption models for growth factors, nutrients, and waste products. All of these sub-models combine into the overall bioartificial tissue model. This work initiated the first steps developing a biologically based proliferation model for individual cells (red).

The processes dictating the behavior of the environment, scaffold, and individual cells are located at the top level. The environmental model incorporates the mass transfer, consumption, and production of growth factors, nutrients, and waste products. The scaffold model describes the three dimensional structure that dictates how and where cells have the ability to migrate and proliferation. Finally, the single cell models describe the cellular process of migration and proliferation.

Advances in any submodel improve the overall bioartificial tissue regeneration model. Therefore, this work focuses solely on the development of a single cell

proliferation model. I began by creating a mitotic oscillator model based on the core proteins of mitosis, and then incorporated ATP into the core model. Then, extracellular glucose was linked to the ATP concentration.

There remains uncertainty in the mitotic protein network structure, and how different mitotic protein network structures affect the behavior of the systems. Therefore, to gain insight into the effect of the mitotic protein networks structure, the initial mitotic oscillator was developed utilizing a bottom-up approach, which allowed the model to be minimal in the early stages. Implementing the bottom-up approach, I incorporated only the bare essential elements of mitosis while maintaining the model's biological integrity to create a base model.

After completing a sensitivity analysis on the base model, I began the mitotic protein network structure analysis. The base model was augmented to include six different networks for the activation of the central protein involved in initiating mitosis, the metaphase promoting factor (MPF). Each of the activation networks arranged the phosphorylation order on MPF differently, and therefore is coupled with multisite phosphorylation. Next, the number of phosphorylations on the protein in a positive feedback loop with MPF was varied to elucidate the effect of multisite phosphorylation. To gain insight into the role of multiple positive feedback loops involved in MPF activation, an additional protein was incorporated into the model. Finally, the number of phosphorylations on the protein in the additional positive feedback loop was varied to conclude the analysis of multisite phosphorylation.

With an ultimate goal of developing a proliferation model for the bioartificial tissue regeneration model, the next logical progression was to link the mitotic oscillator

to the environment. Therefore, I began by incorporating ATP, a cellular energy source, into the model. ATP is involved in multiple aspects of the model and is correlated with the extracellular glucose concentration [10], and thus bridged the link between the extracellular environment and the mitotic oscillator. However, there remains uncertainty in the mechanism involved in inhibiting the additional positive feedback protein, Wee1, at the initiation of mitosis. Therefore, four mechanisms were analyzed to gain insight into Wee1 inhibition during the initiation of mitosis. Utilizing the Wee1 mechanism that provided the cell with the most control over the initiation of mitosis, ATP was linked to extracellular glucose. The final mitotic model is linked to extracellular glucose through ATP, thereby producing a proliferation model modulated by the extracellular environment.

In the following chapter, the biology of the mitotic proteins is presented followed by a chapter on the prior cell cycle modeling. I then present the methods utilized in this work. The mitotic oscillator is developed including the mitotic protein network structure and multisite phosphorylation studies. The mitotic oscillator is then linked to the extracellular environment and the Wee1 inhibition network is analyzed. Finally, concluding remarks are presented along with proposed future projects.

Chapter 2 - Biology of Mitosis

The cell cycle has intrinsic, extrinsic, and external components [11]. The intrinsic components are executed during every cell cycle and include the essential proteins that compose the core of the cell cycle. The extrinsic components include proteins that arrest the cell cycle and act as checkpoints to problems that arise in the cell cycle including responses to DNA damage or unaligned chromosomes at metaphase. The external components balance growth between cells in an organism including cell-cell contacts, growth factors, and nutrients. This work focused on linking extracellular nutrients, an external component, to the intrinsic cell cycle components controlling the end of mitosis, but first a brief summary of the essential elements of the molecular control of mitosis is necessary. For a more thorough review of the molecular control of the mammalian cell cycle see Obaya and Sedivy's recent review and chapter 13 of Krauss's book [11, 12]

First, I introduce the central protein families that control the progression through the cell cycle, cyclin dependent kinases (CDKs) and cyclins. The key regulators of the mitotic CDK and cyclin are then presented. These include CAK, the Wee1 family of kinases, the Cdc25 family of phosphatases, and the anaphase promoting complex (APC).

2.1. Cyclin Dependent Kinases

The cell cycle is controlled by the activity of cyclin dependent kinases (CDKs) and their activating subunits, cyclins. Cyclins were discovered in 1983 in sea urchin embryos as proteins that oscillated with the cell cycle [13]. Cyclins activate their corresponding CDK by dimerization and determine substrate specificity of the CDK [11]. CDKs are Ser/Thr-specific protein kinases [11] and transduce their signal by utilizing

ATP to phosphorylate their substrates. Cyclin CDK dimerization allows ATP to bind to the active center of the CDK [11].

The yeast cells cycle incorporates only a single CDK: protein p^{34cdc2} in fission yeast and protein $p^{34cdc28}$ in budding yeasts [11]. However, mammalian cells have at least 10 CDKs, CDK1 to CDK10, [11] and multiple cyclins that are expressed during different phases of the cell cycle [12]. Cyclin-CDK activity is localized to the nucleus.

Quiescent cells are transitioned back into a proliferation state by mitogenic signals in their environment. The signal cascade initiated by the mitogenic signals triggers the synthesis of cyclin D. Unlike the other cell cycle cyclins, cyclin D concentration remains roughly constant throughout the cell cycle in proliferating cells. Cyclin D binds to CDK4 and CDK6, and both active cyclin D and the mitogenic signal stimulate the synthesis of cyclin E. Cyclin E binds to CDK2 and initiates DNA synthesis and S phase entry. S phase entry triggers the accumulation of the mitotic cyclins.

2.2. Mitotic Cyclins

Cyclin A and B are considered the mitotic cyclins [14], but the role of cyclin A is not completely understood. Cyclin A binds with both CDK1 (also known as Cdc2) and CDK2 to form an active complex. Cyclin B binds to CDK1 to form the metaphase promoting factor (MPF) which was first purified in 1988 from *Xenopus* [15]. Although both cyclins are considered the mitotic cyclins, they appear at different times during the cell cycle. Cyclin A begins to accumulate in late G1 and degrades in early mitosis. Cyclin B begins to accumulate in late S phase and degrades abruptly at the end of mitosis [11].

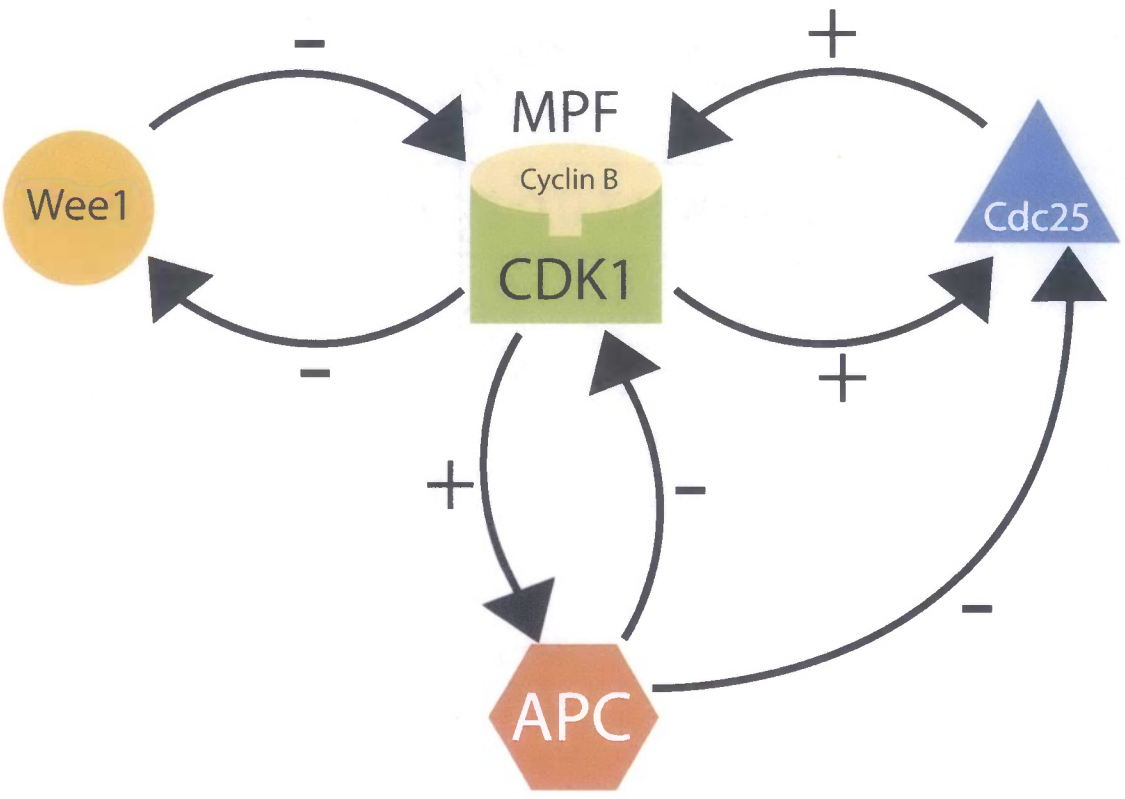

Figure 2 – Regulation of MPF during the cell cycle. The arrows with plus signs indicate that the lead protein up regulates the terminal protein. Conversely, the arrows with minus signs indicate that the lead protein down regulates the terminal protein. Upon dimerization of cyclin B and phosphorylation by CAK, CDK1 activates and is known as the metaphase promoting factor (MPF). The Wee1 family of kinases inhibits MPF by phosphorylating CDK1. MPF down regulates the Wee1 family of kinases by phosphorylation forming a double negative, or positive, feedback loop. The Cdc25 family of phosphatases removes the inhibitory phosphorylations on CDK1, thus activating MPF. MPF up regulates the Cdc25 family of phosphatases, thereby forming an additional positive feedback loop. MPF also up regulates the anaphase promoting complex (APC), a protease. Activated APC degrades cyclin B and the Cdc25 family of phosphatases forming a negative feedback loop.

The fall of MPF activity prompts the end of the cell cycle. In order to ensure that mitosis is not initiated before DNA synthesis and cellular material doubling occur, the cell maintains tight control of MPF activation. Cyclin B dimerization and subsequent phosphorylation control the activity of CDK1, and therefore MPF (Figure 2). CDK1 has 2 inhibitory phosphorylation sites, threonine 14 and tyrosine 15, and one activating phosphorylation site, threonine 161 [16]. The phosphorylations of CDK1 are facilitated by cyclin B binding [17]. Wee1 and Myt1 kinases are responsible for the two inhibitory

phosphorylations on CDK1, and Cdc25 phosphatases remove the inhibitory phosphorylations activating MPF. When CDK1 is phosphorylated at a single and both inhibitory sites, MPF has 10% and 1% the activity of unphosphorylated MPF, respectively [18]. CDK activating kinase (CAK) is responsible for the phosphorylation of CDK1 at the activating phosphorylation site. The following sections introduce the proteins that phosphorylate and dephosphorylate CDK1 including CAK, the Wee1 family of kinases, and the Cdc25 family of phosphatases.

2.3. CAK

CAK phosphorylates the t-loop of CDK1 (Thr161), CDK2 (Thr160), CDK4 (Thr172), and CDK6 (Thr172) [11]. CAK activity levels remain roughly constant throughout the cell cycle. Binding of cyclin and phosphorylation of the t-loop allows optimal access to the substrate binding pocket [11]. The t-loop blocks the substrate binding pocket when it is not phosphorylated [11]. When cyclin A-CDK2 is phosphorylated at Thr160, its activity is increased 300 fold [11]. In vivo, CAK phosphorylation stabilizes the cyclin B-CDK1 dimer which without phosphorylation at Thr161 cannot be observed experimentally [19].

2.4. Wee1 and Myt1

In vertebrates, CDK1 is phosphorylated at both tyrosine 15 (Tyr15) and threonine 14 (Thr14) [20]. Thr14 phosphorylation is not observed without Tyr15 phosphorylation which suggests that Tyr15 phosphorylation occurs before Thr14 phosphorylation [21]. Wee1 kinase phosphorylates CDK1 at Tyr15 and Myt1, another Wee1 family member, phosphorylates CDK1 at both Thr14 and Tyr15 [17, 22]. Thr14 and Tyr15 reside in the

ATP binding pocket and when phosphorylated prevent ATP binding, which inhibits the CDK [23]. In mammalian cells, there are two forms of Wee1, Wee1A and Wee1B [17]. Wee1A and Wee1B are synthesized in somatic and embryonic cells, respectively. Since this work focuses on the cell cycle of mammalian somatic cells, this section concentrates on the regulation of Wee1A, also known as Wee1Hu, and Myt1.

The catalytic region of the Wee1A was initially characterized by Igarashi and colleagues and subsequently the kinetic capabilities were analyzed [24, 25]. The full protein was isolated later, but found to have the same kinase activities [26]. Wee1A is localized to the nucleus [27]. In vitro, Wee1A is able to phosphorylate CDK1 and CDK2 when they are associated with cyclin A, B1, or E [20]. Wee1A cannot phosphorylate cyclin D1 associated CDKs [20]. Wee1A protein levels increase during S and G2 phases and decrease in M phase due to phosphorylation [20].

CDK1 regulates Wee1A activity through phosphorylation and subsequent proteolysis [28]. In vitro, CDK1 can phosphorylate Wee1A, but cannot inhibit Wee1A kinase activity [20]. Polo-like kinase 1 and CDK1 phosphorylate Wee1A on serines 53 and 123, respectively, which induces the proteolysis cascade. The key step appears to be CDK1 phosphorylation [17, 28]. Although this single site is necessary for degradation, human somatic cell Wee1A contains a total of 15 potential CDK phosphorylation sites [29]. This work analyzes the role of the 15 CDK phosphorylation sites on Wee1A in the initiation of mitosis.

In mitosis, hyperphosphorylated Wee1Hu has 8 to 15 fold decrease in activity when compared to the G2 phase when a similar amount of total Wee1Hu was measured [20]. The lower kinase activity is observed in the following G1 phase where Wee1Hu

has a 3 to 5 fold less activity when compared to the previous G2 phase activity at the same protein level [20]. Since Wee1A is inhibited during mitosis, this work elucidates the role of Wee1A inhibition as an additional feedback mechanism during MPF activation during mitotic initiation.

Embryonic Wee1, Wee1A in *Xenopus* oocytes and Wee1B in humans, is regulated in a different manner. There have been 5 mitotic phosphorylation sites identified in *Xenopus* Wee1, all of which are phosphorylated by CDK1 [22]. Two sites, Thr104 and Thr150, are conserved across species including somatic Wee1 and inhibit Wee1 kinase activity during mitosis [22]. The other three sites are not conserved across species, but are required for a mitotic gel shift in *Xenopus* [22]. Wee1 also positively autophosphorylates on Tyr90, Tyr103, and Tyr110 [22]. Embryonic Wee1 is down regulated by MPF by only kinase inhibition, and therefore permits the initial incorporation of Wee1 incorporated a simple mechanism.

The other CDK inhibitory kinase, Myt1, was purified and characterized a few years after Wee1A [30]. It is a membrane bound protein localized to the endoplasmic reticulum (ER) and Golgi complex [18]. Myt1 can regulate CDK1 activity by two mechanisms [31]. Myt1 can bind and sequester cyclin B-CDK1 keeping it from entering the nucleus and while bound phosphorylate CDK1 at its inhibitory sites. These mechanisms were shown in a set of experiments by Liu and colleagues [32]. First they observed that overproduction of kinase active Myt1 delays HeLa cells in the G2 phase. They then observed that overproduction of kinase inactive Myt1 was also able to delay the cell cycle in G2, but not as significantly as overproduction of kinase active Myt1. Overproduction of Myt1 with the cyclin B-CDK1 interaction domain deleted, restored

nuclear shuffling in vivo, and Myt1 would not bind with cyclin B-CDK1. CDK1 was not phosphorylated by Myt1 when the binding domain was deleted, and therefore cyclin B-CDK1-Myt1 complex formation is necessary for Myt1 inhibitory phosphorylation [32].

With the cyclin B-CDK1 interaction domain intact, Myt1 can phosphorylate CDK1 on Thr14 and Tyr15 when cyclin is bound, but preferentially phosphorylates CDK1 on Thr14 [18]. Myt1 phosphorylates CDK1 at Thr14 when Tyr15 is mutated to phenylalanine, but poorly phosphorylates CDK1 at Tyr15 when Thr14 is mutated to alanine [18, 30]. Thus, only a single Wee1 kinase is necessary to phosphorylate CDK1 at both inhibitory sites, and therefore, a mitotic model does not need to incorporate both Wee1A and Myt1.

Myt1 has 5 CDK phosphorylation sites and is inactivated directly in a phosphorylation dependent interaction which requires one or more of the five sites [31]. In vitro, CDK1 phosphorylation of Myt1 does not inhibit its kinase activity [33], but the phosphorylations could decrease the binding of cyclin B-CDK1 [32]. Hence, MPF down regulates Myt1 by multisite phosphorylation, which is a topic analyzed by this work.

2.5. Cdc25

The Wee1 family of kinases inhibits CDK1 prior to mitosis, but to initiate mitosis, the inhibitory phosphorylations must be removed from CDK1 to activate MPF. The Cdc25 family of phosphatases activates CDKs by sequentially removing the inhibitory phosphorylations Thr14 and then Tyr15 [34]. Cdc25 was first discovered in fission yeast as a factor that was required for mitosis [35], and therefore was an essential component included throughout modeling work. For more thorough reviews on the Cdc25

phosphatases and their role throughout the cell cycle, refer to the following papers [36-39].

Higher eukaryotes, including humans, have three forms, Cdc25A, Cdc25B, Cdc25C [11]. Cdc25A plays a general role in the cell cycle because it is involved in the initiation of both major cell cycle transitions, G1/S and G2/M [37]. The c-Myc and E2F transcription factors increase Cdc25A expression in mid to late G1 [40-42]. Cdc25A activates cyclin E-CDK2 which in turn activates Cdc25A through phosphorylation [43]. Cdc25A then activates cyclin A-CDK2 [44]. Cdc25A is liable during G1 and begins to accumulate during S and G2 [45]. The liable form of Cdc25A is degraded by SCF^{BTRCP} ubiquitin ligase [37]. During mitosis, Cdc25A is stabilized by MPF phosphorylation at serine 18 and serine 116 [46]. The stabilized form of Cdc25A is not recognized by SCF^{BTRCP} ubiquitin ligase. MPF is in turn a substrate of Cdc25A which contributes to MPF auto amplification at the onset of mitosis [46]. At the end of mitosis, Cdc25A is degraded by APC^{CDH1} to restart the cell cycle [37].

Cdc25B and Cdc25C are primarily involved in the G_2/M transition [47-49]. Cdc25B levels increase during S phase and peak at the G_2/M transition when it is hypothesized to initiate MPF activation [47, 50]. The small amount of activated MPF then activates Cdc25C which in turn fully activates MPF [51, 52]. Unlike Cdc25A and Cdc25B, Cdc25C protein levels remain roughly constant throughout the cell cycle [47, 49, 53, 54]. Cyclin A-CDK1 phosphorylates Cdc25B during mitosis which initiates degradation through ubiquitin proteolysis [55]. Both Cdc25A and Cdc25B have a nonphosphorylated site that is recognized by SCF for degradation [56].

The role of each of the isoforms of Cdc25 throughout the cell cycle is still not well understood. Overexpression of Cdc25A activates CDK2 prematurely leading to a shorter G1 phase [44, 57], but overexpression of Cdc25A also induces mitotic events [58]. Antibodies targeting Cdc25A induce G1 arrest [43, 54]. Overexpression of Cdc25B or Cdc25C results in premature mitosis, but Cdc25B overexpression is more efficient [38, 59]. Likewise, antibodies targeting Cdc25B or Cdc25C or transfection with inactive Cdc25B or Cdc25C induce G2 arrest [47-49]. Targeting either Cdc25A or Cdc25B results in G2 delay and targeting both leads to G2 arrest [50]. Although Cdc25B and Cdc25C are primarily involved in the G_2/M transition, both proteins were observed to be involved in S phase initiation in human cells even in the presence of functional Cdc25A [60, 61]. However, $Cdc25C^{-/-}$ knockout and $Cdc25B^{-/-}$ $Cdc25C^{-/-}$ double knockout mice develop normally suggesting that Cdc25A can compensate for all phosphatase functions throughout the cell cycle [62-64]. Therefore, this modeling work focused solely on the Cdc25A protein.

The exact biological mechanism between MPF and the Cdc25 phosphatases is still being investigated, but all involve multisite phosphorylation. Cdc25A has 12 potential CDK1 and CDK2 phosphorylation sites [39]. MPF stabilizes the protein by inhibiting SCF mediated degradation by phosphorylating serine 18 and serine 116 [46]. Cdc25B has 14 potential CDK1 and CDK2 phosphorylation sites, but their function is not known [39]. Cdc25C has 6 potential CDK1 and CDK2 phosphorylation sites and MPF mediated phosphorylation increases the phosphatase activity during the G_2/M transition [39]. Although the potential number of MPF phosphorylation sites and in some cases the function of the phosphorylation, the number of necessary phosphorylations and the order

in which they occur is still not understood, and therefore, this thesis work analyzes the effect of multisite phosphorylation on the mitotic system.

2.6. APC

Cyclins are also controlled by proteolysis throughout the cell cycle. SCF is active during G1/S, and APC (cyclosome) is active during mitosis [11]. SCF substrates must be phosphorylated at specific residues to be recognized, but APC substrates do not have to be phosphorylated [11]. APC is composed of 11 subunits and has high activity from late mitosis to late G1 [11]. APC has two activating subunits, Cdc20 and Hct1/Cdh1 [11]. Cdc20 activity is high during early anaphase through the exit of mitosis when Hct/Cdh1 activity rises and remains high until the end of G1 [11]. APC substrates include cyclin A, cyclin B, mitotic protein kinases, inhibitors of anaphase, spindle-associated proteins, and inhibitors of DNA replication [11]. MPF activates APC at the end of mitosis, and active APC degrades cyclin B species and Cdc25A the process by which the cell cycle is reset. Therefore, APC is an essential component for the mitotic process, and thus was included through all model iterations in this work.

Cell cycle modeling has been a prominent research area for over three decades. The first models based on biology incorporated only the negative interaction between cyclin B and APC, but recent work has produced highly complex models that incorporate multiple cyclins and their regulatory subnetworks. The following chapter presents the prior cell cycle modeling works.

Chapter 3 - Cell Cycle Modeling

This thesis work developed the first mitotic oscillator linked to the extracellular environment. Our model also incorporates recent biology that has not been accounted for in previous models. Furthermore, this model is the first to employ ATP as the link between the environment and mitosis. This chapter reviews the previous modeling work for the cell cycle.

Models for the cell cycle have been investigated for over 3 decades. Early models were based upon hypothetical oscillators that mimicked the oscillations observed in bacteria [65-67]. As the proteins involved in the cell cycle were discovered, cell cycle modeling shifted from hypothetical mechanisms towards deterministic models based on protein interactions. Similar to an experimentalist's approach, the first systems modeled were simple and were followed by the more complex systems. The first deterministic models were mitotic oscillators based on experimental data from frog embryos and extracts. Then, models capturing the protein dynamics of yeast systems were formed from experimental gene knockout data. Finally, models of the cell cycle checkpoints were analyzed which led to models of highly complex systems like mammalian cells.

3.1. Mitotic Oscillators

The first models of the mitotic oscillators were largely based on the negative feedback between cyclin and the Anaphase Promoting Complex (APC). The positive feedback mechanisms were incorporated and were followed by the addition of cyclin Dependent Kinase Inhibitors (CKI). These initial models were the precursors to more complex models that capture a broad spectrum of observed cell cycle phenomena.

The first mitotic model was proposed by Hyver and Guyader [68]. The intent of this model was to deduce whether cyclin and p34 kinase, a cyclin Dependent Kinase (CDK), dimerized to form Metaphase Promoting Factor (MPF), or whether cyclin activates pre-MPF into active MPF. They found that the system based on dimerization was able to oscillate without any constraints. Consequently, the system based on cyclin activation required that cyclin and MPF react stoichiometrically in order to observe oscillations. Both models incorporate active and inactive p34, cyclin, and MPF. Mass action kinetics are assumed for both mechanisms.

Norel and Agur proposed a mitotic oscillator that incorporated cyclin and MPF [69]. In the model, cyclin was synthesized and incorporated into MPF. MPF was created at a basal rate proportional to cyclin and autocatalytically proportional to cyclin and MPF. MPF promoted its own degradation with Michaelis-Menten kinetics. The system, composed of two species and four parameters, produced sinusoidal oscillations. This was the first model to incorporate MPF's autocatalytic activation.

Goldbeter developed a mitotic oscillator for the cyclin-CDK cascade that comprises three differential equations for cyclin, active cyclin-CDK, and a degradation protein [70]. In the model, cyclin promotes the activation of cyclin-CDK. Active cyclin-CDK then activates the degradation protein. The phosphorylated form of each species is active, and the inactive form is not phosphorylated. Only the active forms of the species are accounted for by differential equations. The degradation protein then degrades cyclin, generating a negative feedback loop. All the species were scaled by their maximum, and thus all species have a maximum value of unity.

Goldbeter's model utilized zero order ultrasensitivity and time delays to capture the cell cycle oscillations. Zero order ultrasensitivity dynamics are characterized by Michaelis-Menten rate forms with Michaelis-Menten constants that are orders of magnitude smaller than the maximum concentration. Zero order ultrasensitivity dynamics generate sigmoidal response curves that act as switches. Therefore, by turning the switches on and off in succession, the model generates oscillations.

Tyson and his coworkers have been working on stochastic and probabilistic models of the cell cycle throughout the 70s and 80s [71-79]. Tyson published his first deterministic mitotic model incorporating a biological mechanism in 1991 [80]. The model, like earlier models, captures the minimal mechanism of a single cyclin-CDK organism. Tyson's model started with six species that he reduces to two species to study with phase plane analysis. The phase plane analysis followed active cyclin-CDK with two key parameters: the active cyclin-CDK autocatalytic and degradation parameters. Tyson found that the autocatalytic activation of cyclin-CDK is essential for oscillation dynamics. In the model, the autocatalysis term is second order with respect to active cyclin-CDK, but when it is first order, limit cycle and an excitable lower steady state are not observed.

Obeyesekere and coworkers reviewed the previous cell cycle models and studied the physical limitations of the models [81]. All of the models capture the same behavior and differ mainly in the assumed phenomenological nonlinear terms. Obeyesekere and coworkers found that of the three proposed models by Norel and Agur, the first can go to negative concentrations, the second always has positive concentrations, and the third, which Norel and Agur were not able to get to oscillate, does oscillate with the right

parameter set. They also found that Tyson's model has the limitation that it can go to negative concentrations. Thron also reevaluated Norel and Agur's model and proposed three new models [82]. Obeyesekere and coworkers determined that Thron's first two proposed models always have positive concentrations and a stable periodic orbit for the correct parameter space, but Thron's last model can produce negative concentrations. Obeyesekere and coworkers also generated three models by combining aspects of the earlier models or using variations on the nonlinear assumptions. The newly generated models did not have the physical limitations of the previously published models. Overall, Obeyesekere and coworkers analyzed ten models. Each model would result in a different biochemical reaction network, and thus the models do not capture the biological mechanism. Rather, the models capture the behavior of the dynamics of the species. The studies published by Obeyesekere and coworkers reveal that multiple models can simulate the same behavior. For this reason, a thorough analysis of protein network structure is carried out in this thesis work.

The next advance in the mitotic oscillators was the incorporation of the proteins involved in the autocatalytic activation of MPF. The first mechanisms that were investigated involved the positive and double negative feedbacks generated by Cdc25 and Wee1, respectively. MPF activates Cdc25 that activates MPF to form a positive feedback loop. MPF inhibits Wee1, and Wee1 inhibits MPF to generate a double negative feedback loop.

Novak and Tyson extended Tyson's minimal model by incorporating Cdc25, Wee1, CAK, and INH [83]. The Cdc25 and CAK proteins activate the cyclin-CDK complex. In contrast, the Wee1 and INH proteins inactivate the cyclin-CDK complex.

The positive feedback loop between MPF and Cdc25 generates the instabilities necessary for oscillations in the model. Following the same strategy as Tyson's first work, the system was reduced to two species and analyzed with phase plane analysis. The parameters analyzed in the phase plane analysis were total cyclin and active cyclin-CDK. Novak and Tyson hypothesized that Cdc25 linked cell growth to the cell cycle, and that the ratio of Cdc25 to Wee1 controls the length of the cell cycle. Their model was the first attempt to link the cell cycle to cell growth utilizing the biological mechanism.

In their next model, Novak and Tyson then incorporated Wee1 as a dynamic species in the *Xenopus* model [84]. Again, the system was then analyzed with phase plane analysis and response curves. Total cyclin was used as the main modeling parameter because it is a controlled variable in *Xenopus* extracts. Novak and Tyson found that positive feedback between MPF and Cdc25 and Wee1 contributed to thresholds and time delays. The negative feedback loop drove oscillations, but the positive feedback loops would also drive oscillations if there were abrupt dephosphorylation of MPF.

The response curve for total cyclin versus active cyclin takes on a N-shape [84]. Thus, as total cyclin passes a threshold, there is a spike in the active cyclin concentration that triggers the activation of the protease. The protease then degrades the cyclin and resets the system to below the threshold.

Their model exhibits two types of oscillatory behavior. One is driven by MPF phosphorylation-dephosphorylation cascades, which are observed in *Xenopus* extracts. The other is induced by cyclin degradation due indirectly to MPF activity, which is observed in early *Xenopus* embryos. Novak and Tyson observed that increasing the

cyclin synthesis rate changes the oscillatory behavior from positive feedback dominated oscillations to negative feedback dominated ones.

Novak and Tyson then investigated how DNA damage, which is known to increase Wee1 activity and degrade Cdc25, shifted the response curve. DNA damage shifts the activation of Cdc25 and inactivation of Wee1 to higher concentrations of active MPF. By increasing Wee1 or decreasing Cdc25, the response curve shifts to higher total cyclin amounts, thereby resulting in division time delay or cell cycle arrest.

Borisuk and Tyson analyzed the *Xenopus* oocyte model with bifurcation analysis [85]. The primary bifurcation parameter was cyclin synthesis because this variable can be controlled experimentally in the *Xenopus* oocyte extracts. The system has a stable low MPF steady state, stable high MPF steady state, and limit cycle behavior. The upper bifurcation is a supercritical Hopf bifurcation, and the lower bifurcation is a saddle node. The system also produced multiplicity where the interphase MPF steady state coexisted with the mitotic MPF steady state. Also, the coexistence of two stable limit cycles with different amplitude and period was observed over a range of the parameter space. The system was also analyzed with two parameter bifurcation where cyclin degradation, total Wee1, and total Cdc25 were analyzed over the cyclin synthesis range.

Novak and Tyson's *Xenopus* oocyte model was then updated with a more accurate unreplicated DNA checkpoint [86]. The entry of mitosis is delayed by three mechanisms: activation of a CKI or Wee1, and inactivation of Cdc25. The updated model has 15 differential equations and 36 parameters with total Cdc25, Wee1, APC, and APC intermediate enzyme (IE) concentrations remaining constant. The model accounts for five states of the cyclin CDK complex, four states of the cyclin CDK CKI trimer, free

phosphorylated CKI, and active Cdc25, Wee1, APC, and IE. The work utilized the experimental data to gain better estimates of the rate constants in the model as well as update the protein interactions.

Around the same time, Romond and coworkers extended Goldbeter's minimal model by adding Cdc25 [87]. In the model, monomeric cyclin accumulates and activates Cdc25 that activates the cyclin-CDK complex. The active cyclin-CDK complex also activates Cdc25 forming a positive feedback loop. The active cyclin-CDK complex also activates a protease, which degrades the monomeric cyclin species forming the negative feedback loop. As in the earlier model, the species are scaled with their maximum values, and thus the maximum value of all species is unity.

Goldbeter and coworkers utilized two parameter bifurcation analysis to perform a stability analysis on the original minimal model and found that lowering the first order degradation of cyclin increases the region of oscillatory behavior. The oscillatory region is the largest when first order degradation of cyclin is zero. Thus, non-specific degradation of cyclin suppresses the oscillatory behavior of the system.

The stability analysis also reiterated that the Michaelis-Menten constants must be much smaller than the maximum concentration for the system to exhibit oscillations. Hence, the system must exhibit zero order ultrasensitivity. Cdc25 was then added to the model without autocatalysis. By adding the additional phosphorylation-dephosphorylation cascade to the model, the region of oscillations increased. In the model, surpassing a single threshold is sufficient to induce oscillations, and thus adding an additional species incorporates a threshold that can expand the region of oscillations. Finally, autocatalysis was added to the system, which increased the region of oscillations,

but not as significantly as adding an additional phosphorylation dephosphorylation cascade. Cyclin synthesis drives the oscillations, and therefore cyclin synthesis and degradation manipulate the oscillatory behavior of the system.

Goldbeter and Guilmot then utilized two parameter bifurcation analysis of Goldbeter's minimal mitotic oscillator to analyze how the cell cycle can be arrested [88]. Two sets of parameters were analyzed. The first compared the rate of activation of cyclin-CDK to the rate of inactivation of cyclin-CDK; the second compared the rate of protease activation to the rate of inactivation of the protease. In both bifurcations, the oscillatory region takes on the same shape and lies just above the bisector line.

Goldbeter and Gonze found that if cyclin-CDK is phosphorylated faster than dephosphorylated, then the system exists in a steady state with high levels of active cyclin-CDK kinase and protease and low levels of cyclin. However, if cyclin-CDK is dephosphorylated faster than phosphorylated, then the system resided in a steady state that corresponds to high levels of cyclin and low levels of Cdc2 kinase, a CDK, and phosphatase.

If the protease is phosphorylated faster than dephosphorylated, the system again resides in a steady state characterized by high levels of Cdc2 kinase and phosphatase. Alternatively, if the protease is dephosphorylated faster than phosphorylated, the system exists in a steady state with high levels of cyclin and Cdc2 phosphatase and low levels of Cdc2 kinase. Thus, from any starting point that oscillates, the system can be arrested into a steady state by changing the ratio of the rates to fall into one of the steady state categories.

After these studies of the Cdc25 and Wee1, the next protein interaction to be incorporated into the mitotic oscillators was the double negative feedback generated by cyclin dependent kinase inhibitors (CKI). The CKI proteins bind to and inactivate cyclin-CDK complexes. The formation of the cyclin-CDK-CKI complex inactivates the cyclin-CDK complex until the CKI is removed. Active cyclin-CDKs phosphorylate CKIs, which lowers their binding affinity releasing and activating cyclin-CDK.

Thron incorporated Suc1, a CKI, into his model to investigate an MPF pulse generator mechanism [89]. Thron found that Suc1 is necessary for mitosis because it affects three mechanisms. The amount of CKI sets the threshold of cyclin accumulation that triggers mitosis, which is accomplished by the large pool of inactive MPF sequestered. The feedback loop between Suc1 and MPF increases the reaction order of the autocatalysis that enhances the oscillatory characteristics of the system by increasing excitability and destabilizing the steady state. In Thron's earlier work, he proved that for the cell cycle system to oscillate, the reaction order of the autocatalysis must be higher than the reaction order of the degradation [82].

Gardner and colleagues incorporated a CKI into Goldbeter's minimal models and Novak and Tyson's yeast model [90]. Their data reveals that the cell division cycle can be controlled with CKI expression. The overall effect of the CKI on the system is determined on the CKI expression level, binding constant and binding rate. Gardner and colleagues found that the binding dynamics controlled the oscillatory characteristics of the system. Fast binding dynamics delayed the rise and fall of MPF due to buffering. Slow binding dynamics allowed the initial rise and fall of MPF to be fast. The magnitude of the effect was controlled by the CKI expression and equilibrium constant.

Since the two models utilized different mechanisms, the addition of a CKI induced different behavior. Goldbeter's model, which has no checkpoint mechanisms, increased the frequency of oscillations when there was slow binding and decreased the frequency with rapid binding. Novak and Tyson's model, which includes cell cycle checkpoints, had period doubling with low expression level of slowly binding CKI. The mean cell mass was decreased when the CKI had high expression level or rapid binding dynamics.

Novak and coworkers integrated a CKI into a generic cell cycle model [91]. The work began with a simplified model that incorporated a CDK and APC. The CDK inhibits APC, which is activated by an unknown activator protein. APC degrades cyclin inactivating the CDK. A CKI was added into the model to link the growth cycle to the cell cycle. This link was accomplished by setting the synthesis rate of CDK proportional to the cell mass. Finally, they incorporated Wee1 and Cdc25 into the model to induce a G2/M checkpoint.

Although models prior to Novak and coworkers generic cell cycle model followed a fairly similar path in their advancement, the continued research on mitotic oscillators branched in many directions to capture experimentally observed phenomena. Researchers investigated phenomenological models for cyclin and the dynamics of coupled oscillators. They also analyzed the contribution of the nucleocytoplasmic ratio and phosphorylation dephosphorylation cascades. Some groups researched the similarity between the cell cycle machinery between species including more complex models of *Xenopus* extracts. Stochasticity, feedback mechanism, and external oscillators have also been investigated.

Busenberg and Tang proposed an ordinary differential equation model and a delay differential equation model for the mitotic oscillator in early embryos [92]. The delay model is a phenomenological model for cyclin B. Through mathematical derivation, they develop a generic model for the MPF system that incorporates cyclin, preMPF, and MPF to gain insights into the underlying mechanisms.

Goldbeter and colleagues coupled two minimal oscillators through mutual inhibition to mimic the M and S phases of the cell cycle [93]. The first oscillator captures the G2/M transition with cyclin B, Cdc2, and ubiquitin ligase. The second oscillator captures the G1/S transition with cyclin E, CDK2, and an unknown ubiqutin ligase. To couple the oscillators, the current active CDK inhibits the counter cyclin's synthesis. Similar results were found by coupling the active CDK with the opposite ubiqutin ligase. Alternating oscillations are observed in the model when the inhibition is strong, which is likely what is observed in nature. When the inhibition is weaker, chaos is found over a large portion of the parameter space.

Ciliberto and Tyson incorporated the nucleocytoplasmic ratio into a model for sea urchin embryos [94]. The nucleocytoplasmic ratio is the ratio of the volume of the nucleus to the volume of the cytoplasm. As the cell grows and the DNA doubles, the nucleocytoplasmic ratio decreases.

The model is adapted from Novak and Tyson's *Xenopus* oocyte model and consists of MPF, positive feedback from Cdc25 and Wee1, and negative feedback from APC that is activated through an intermediate enzyme. Bifurcation analysis was utilized to observe the transition behavior as the nucleocytoplasmic ratio changed. In the model, the nucleocytoplasmic ratio affected the activation and inactivation of Wee1 and Cdc25

respectively. Asymmetric division was incorporated into the model to account for the standard deviation in the cell cycle time from the experimental data. Ciliberto and Tyson also performed preliminary simulations for communication between neighboring cells. Although the cellular communication model is not complete, the diffusion of proteins through junction gaps did affect the model behavior.

Gonze and Goldbeter developed a phosphorylation-dephosphorylation cascade model with positive and negative feedback [95]. In the model, the current active species phosphorylates the next species in the cascade activating it, and dephosphorylates a prior species in the cascade. The last species in the cascade phosphorylates the first species in the cascade thereby forming a looping cascade. The model utilized zero order ultrasensitivity to generate thresholds. To analyze the threshold's switching behavior, Gonze and Goldbeter generated response curves by plotting the amount of active kinase versus the ratio of the rates of phosphorylation to dephosphorylation. The initial model had four species with identical corresponding parameters.

Gonze and Goldbeter found that the generic phosphorylation-dephosphorylation cascade could generate a variety of dynamics. If the model had only positive feedback, the system exhibited bistability. When negative feedback is included, then damped oscillations were observed. To incorporate negative feedback, the current active species dephosphorylated the prior active species, which inactivated it. Gonze and Goldbeter observed that to generate oscillations the negative feedback must be applied at least two species prior to the current active species. When the negative feedback is two species prior to the current active species and there is only negative feedback, multiple steady states or oscillations are observed depending on the parameter selection. The model also

exhibited hard excitation, which Gonze and Goldbeter define as coexistence between a stable steady state and a stable limit cycle, also know as a subcritical Hopf bifurcation. The system can move from a sable oscillatory state to a stable steady state if any kinase is activated or inhibited from an outside source. The stable oscillations resume if the kinase or phosphatase is returned to its initial value.

Next, Gonze and Goldbeter analyzed the model with a bifurcation analysis. The bifurcation parameter was the ratio of phosphorylation to dephosphorylation rates, and since all species had the same parameter set, the data applied to each active species. The steady state followed a sigmoidal shape. Two subcritical Hopf bifurcation points enclose the unstable region, and thus there are two regions of hard excitation. In the regions of hard excitation, the system can be excited by a perturbation from the steady state to an oscillatory state and remain there after the parameter value is returned to its original value. Vice versa, the system in an oscillatory state in the hard excitation region attracts to the steady state with a perturbation from the stable steady state and remain there after the parameter is returned to its original value.

Gonze and Goldbeter also analyzed the system with two parameter bifurcation. They first analyzed the negative feedback strength versus the Michaelis-Menten constant. Their results reiterate that the Michaelis-Menten constant must be significantly small enough to generate oscillations. Thus, there must be zero order ultrasensitivity to produce oscillations in this model. They then analyzed the negative feedback strength versus the positive feedback strength and concluded that the negative feedback must be larger than the positive feedback for oscillations to occur. Finally, they analyzed the Michaelis-Menten constant versus the ratio of phosphorylation to dephosphorylation

rates. For the system to exhibit oscillations, the Michaelis-Menten constant must be orders of magnitude smaller than the maximum concentration, and the ratio of phosphorylation to dephosphorylation must be around unity.

Gonze and Goldbeter also analyzed the case where each phosphorylation dephosphorylation cascade had a unique parameter sets. With different parameter sets, the model exhibited asymmetric cycles, but was able to oscillate. This proved that the minimal model was able to capture more complex dynamics and was robust over a wide parameter space.

The number of species in the phosphorylation dephosphorylation cascade was then analyzed. They found that if there are an even number of cycles then, half the states would be high and the other half low. The states that were high or low depended on the initial condition. If there were an odd number of states or if half the number of states were odd (N or N/2 are odd), then the system oscillated with N/2 states overlapping. For example if there are 10 states, states 1,3,5,7, and 9 and 2,4,6,8, and 10 oscillate independently. Their most significant finding was that the system favors oscillations when there is both positive and negative feedback. Finally, Gonze and Goldbeter linked an external independent cAMP oscillator to the phosphorylation-dephosphorylation cascade and observed that the external oscillator was sufficient to drive oscillations in the phosphorylation-dephosphorylation cascade.

Recently, Battogtokh and coworkers linked an external oscillator to the cell cycle by periodically forcing specific species with small amplitude variability [96]. This work was later applied to a culture synchronization model that utilized periodic forcing from an external nutrient [97]. In contrast to Battogtokh and coworkers' models, our model links

the extracellular environment in a biologically mechanistic manner, and also links it to a specific source, extracellular glucose.

Tyson and Novak then investigated the link between fission yeast, *Xenopus* extracts, and cultured mammalian cells by building a generic cell cycle model [98]. They approached the model by beginning with a simplistic core model that represented a mitotic oscillator and added complexity to capture the dynamics of more complex systems in higher eukaryotes. The model began with two ODEs that captured the antagonism between cyclin and APC/Cdh1. A CKI was then added to the model to capture the basic fission yeast cell cycle, and finally Cdc20 and an intermediate activating enzyme were added to capture multicellular eukaryotes. The system is driven by the cellular mass, which regulates the total cyclin enzymatic rate. In all forms of the model, the cellular mass drives the total cyclin past a saddle node bifurcation that is reset when the cell divides and the mass is halved. Zero order ultrasensitivity is utilized in the activation and inactivation of Cdh1 and the active form of Cdc20 to capture the switch like properties of the protein interactions. The synthesis of total Cdc20 by total cyclin B utilizes a Hill function. Tyson and Novak draw upon the fact that many of the cell cycle proteins are conserved across species, and thus they hypothesize that there is a core cell cycle engine present at the center of all species regardless of the complexity that may be present in higher eukaryotes. More extensive bifurcation analysis was presented in a later review which linked molecular control systems and cell physiology [99].

Frankel built a two species model based on averaging cyclin and MPF to show that the lower bifurcation in the cell cycle model should be a saddle node bifurcation [100]. The model was able to explain long intermitotic times, quantized cell cycle times

and excitability. Rather than looking at cyclin independent synthesis rate or total cyclin, Frankel studied the autocatalytic nature of cyclin production. When cyclin production autocatalysis is zero, the model represents earlier two dimensional models, but by changing the amount of autocatalytic cyclin production, the system moved from nonexcitable behavior to excitable behavior. Thus, Frankel's results verify that MPF positive feedback is essential in the mitotic network.

Qu and coworkers created a model with the capability to simulate the dynamics of the G1/S or G2/M dynamics [101]. Since the model is created to capture either G1/S or G2/M, phase specific proteins are not used. Thus, the model includes a cyclin, and active and inactive cyclin CDK complex, Cdc25, Wee1, APC and CKI. They assume that protein synthesis rates are constant, and CDK concentration is constant and in excess. Cyclin synthesis is assumed proportional to cell size, and Cdc25 is assumed to need two phosphorylation sites to reach full activity. Also, Wee1 is assumed to have two forms, inactive and active.

Qu and coworkers analyzed the effects of positive and negative feedback with two parameter bifurcation. Positive feedback displayed low and high stable steady states with limit cycle and bistability in between. When adding negative feedback to the system, the bistable region was converted to limit cycle, and the limit cycle region grew substantially. The negative feedback converted the saddle node bifurcation points to Hopf bifurcation points.

They also analyzed the effect of negative feedback strength. At low feedback and cyclin synthesis, bistability or a low stable steady state is observed. At intermediate feedback and cyclin synthesis, limit cycle or a high stable steady state behavior is

observed. The effect of the delay of the negative feedback did not affect the region of limit cycle. Rather, as the delay increased, the period increased. Also, delayed negative feedback resulted in systems that were excitable.

Finally, Cdc25, Wee1, and CKI were analyzed. As Cdc25 synthesis increased, limit cycle behavior was observed at lower cyclin synthesis rates with little change in the cycle period. The opposite was observed for increased rates of Wee1 synthesis with little change in the cycle period. Positive feedback from Cdc25 and Wee1 creates bistability in the model. The lower Hopf bifurcation point moved towards the upper Hopf point as CKI synthesis increased until they merged and the limit cycle behavior was lost. As CKI synthesis increased, the oscillatory period also increased.

The model was able to capture a restriction point and the sizer and timer phenomena. Thus, cells must reach a certain size before DNA replication and mitosis. Qu and coworkers claim the G1 and G2 checkpoints are Hopf bifurcation points rather than Saddle Node bifurcation points as Tyson claimed in earlier papers. The contradiction in their work reiterates the uncertainty in the mechanism controlling the cell cycle, and therefore, this thesis work analyzed the protein network structure for mitosis.

Ciliberto and colleagues created a more extensive *Xenopus laevis* embryo model to account for the experimentally observed double peak in cyclin E activity in early cell cycles and the developmental timer [102]. The research combined experimental and theoretical approaches to design and support their model. The model is able to capture the dual peaks in cyclin E/CDK2 activity and the delayed degradation of cyclin E. The dual peaks in cyclin E/CDK2 activity was due to the proposed negative feedback between cyclin E/CDK2 and Wee1. Cyclin E/CDK2 inactivates Kin, the protein that inactivates

Wee1, thus activating Wee1, which inactivates cyclin E/CDK2 through phosphorylation. The delayed cyclin E degradation was linked to auto-phosphorylation, which marks the protein to be degraded. The degradation machinery has to be significantly delayed from the auto-phosphorylation to obtain the dynamics observed in experiments. Bifurcation analysis was used to support the observed phenomena.

Yang and colleagues analyzed the effect of multiple phosphorylation on ultrasensitive response of proteins involved in the cell cycle [103]. The model incorporated an extensive cyclin-CDK model that allowed Wee1 phosphorylations to occur in parallel with CAK phosphorylation. Cyclin binds with CDK to form an inactive dimer that can than be phosphorylated by either Wee1 or CAK. The positive feedback loops of Cdc25 and Wee1 were allowed to have up to five phosphorylation sites. CAK could have up to two phosphorylation sites. The activity of Cdc25, Wee1 and CAK were the sum of all the concentrations of the species multiplied by an activity for each conformation. This work did not analyze the effect of multi-site phosphorylation on the APC system. Rather, a second order Hill function was utilized to capture the nonlinear dynamics.

Yang and colleagues randomly searched parameter space to see the dynamics possible for each number of phosphorylations and counted the parameter sets that exhibited bistability or limit cycle dynamics. They found that bistability and limit cycles are observed if CDK, Cdc25, Wee1, or CAK have multi-site phosphorylation. As the number of phosphorylations increased on Cdc25, the number of bistable and limit cycle systems increased, but they report that "cooperativity" did not affect the system as much. The same behavior is observed for multiple Wee1 phosphorylations. CAK did not induce

as many instabilities even when it had two phosphorylation sites. This is due partly to the fact that Cdc25 and Wee1 phosphorylate CDK at two sites. Thus, there is an amplification of the nonlinear behavior because it already acts on a multi-phosphorylated species. CAK phosphorylates CDK at only one site. The addition of negative feedback increased the incidences of limit cycle behavior.

Also, combining multi-site phosphorylation cascades increases the robustness of the cell cycle machinery. Yang and colleagues defined robustness as the number of bistable and limit cycle systems in the parameter space when compared to other models. Bistability is the major dynamical behavior observed, and negative feedback converts bistable systems to limit cycle systems. Although many of the proteins that regulate cyclin/CDK activity have more than two phosphorylation sites, their study indicates that there is not a greater response after two phosphorylations.

When they analyzed their model of CDK activation with previous simplified models, the overarching feature of earlier models is the assumption that CDK is phosphorylated simultaneously in both spots by Wee1 and dephosphorylated in one step also. When CDK is simultaneously phosphorylated, it is linearly activated, and therefore, requires the nonlinearities in Cdc25 and Wee1 to have more phosphorylations.

The work pivotal work of Yang and colleagues was the first to analyze the effect of reaction network structure and multisite phosphorylation on the observable system behavior by quantifying the number of parameter set that exhibited limit cycle or bistable behavior. Although this work was the first to analyze the effect of reaction network structure and multisite phosphorylation on the observable system behavior, the results did not include how the observable system behavior changed when the reaction network

structure or number of multisite phosphorylations were varied. Rather, the results gave insight into which network structures would oscillate with the most parameter sets. This thesis work moves one step forward and analyzes the effect of protein network structure and multisite phosphorylation on the observed system behavior by analyzing the changes in the steady state behavior of the system for different reaction network structures and multisite phosphorylation.

The first attempt to add stochasticity to the cell cycle models was investigated by Steuer [104]. Steuer introduced white noise by converting Tyson and Novak's generic model [98] into stochastic differential equations. Steuer did not derive the noise terms; rather the noise was approximated and varied throughout the investigation. The addition of noise was able to account for quantized cycle times in Wee1/Cdc25 double mutants, and the noise was able to create oscillations, also known as noise-induced oscillations.

Zwolak, Tyson, and Watson developed an optimization approach to estimate the kinetic parameters from experimental data [105]. Data was used from frog eggs to minimize an objective function that was defined as the orthogonal distance between the model and experimental data. Although the method was applied to a mitotic oscillator and *Xenopus* extract data, the approach can be applied generally to estimate kinetic parameters from experimental data. This work was expanded upon to develop the JigCell parameter estimation environment utilized to estimate parameter in yeast cell models [106, 107].

Pomerening and coworkers developed a model to assess the importance of the positive feedback in the Cdc2/APC system while simultaneously performing the

necessary experiments with *Xenopus* extracts [108]. They investigated the Cdc2-Wee1/Myt1 and Cdc2-Cdc25 loops which on their own induce bistable switches.

The model they use is similar to the model proposed by Novak and Tyson's *Xenopus* oocyte model [84]. The main difference between the models is the form of ultrasensitivity utilized in the model. Pomerening and coworkers utilized the Hill function, and Novak and Tyson utilized zero order ultrasensitivity. Their model includes cyclin B, Cdc2, Wee1, Cdc25, PLX (an intermediate between active MPF and APC), and APC. The MPF activation mechanism for this model assumes that phosphorylations occur sequentially. Cyclin B and Cdc2 form an inactive dimer that is phosphorylated by Wee1 to form the second inactive dimer. The second inactive dimer is then phosphorylated in the activating phosphorylation site of Cdc2 at a constant rate to form the third inactive dimer. Finally, the third inactive dimer is dephosphorylated at the inactive phosphorylation site by Cdc25 to form the active species. APC degrades all forms of the dimer at the same rate. As mentioned earlier, APC is not directly activated by MPF, but rather by an intermediate PLX that still forms an indirect negative feedback loop. Pomerening and coworkers utilized nonlinear dynamics in all positive and negative feedback loops, whereas Tyson and Novak utilized only nonlinear dynamics in the Cdc25 and negative feedback loops. Pomerening and coworkers varied their strength of feedback as their modeling parameter.

From the data, they concluded that if the positive feedback is removed, damped, less temporally abrupt, faster oscillations are observed. Their model and experiments found that at low cyclin synthesis rates, bistability is required for oscillations, but at more realistic cyclin synthesis rates the requirement of bistability is relaxed. The positive and

negative loops of the cell cycle act as bistable switches. Their findings support the view that the Cdc2/APC system is a relaxation oscillator for which positive feedback is essential for sustained oscillations.

Han and coworkers investigated whether hysteresis is necessary or sufficient for cell cycle transitions [109]. They began with a complex model incorporating many of the known proteins and protein interactions for mitosis, including parallel phosphorylation by inhibitory and activating phosphorylations on MPF. The model is then simplified to a linear model that has three species: cyclin, and inactive dimer of cyclin-CDK, and an active cyclin-CDK dimer. Cyclin synthesis was assumed to occur at a constant rate, and CDK concentration was assumed to remain constant.

Han and coworkers then utilized bifurcation analysis to investigate the stability of subsystems of the cell cycle oscillator. They studied cyclin-CDK interactions with CKI, Rb-E2F and APC-CDH1 by incorporating each species into the simplified cyclin-CDK model one at a time. They analyzed each system over the cyclin synthesis range. They also created response curves, which plot active CDK versus total cyclin. There is no cyclin synthesis in these graphs, and total cyclin is controlled as an external variable.

They then analyzed the response curve of active CDK and cyclin in response to dynamical instabilities. They found that CDK phosphorylation and dephosphorylation or CKI double negative feedback induced the dynamical instabilities. Also, systems with hysteresis displayed more instances of dynamical instabilities than nonhysteretic systems do. Thus, if the system has a hysteretic, then it is more probable that a negative feedback loop converts the bistability to limit cycle than a system that does not have hysteresis. Han and coworkers also found it statistically likely that phosphorylation and

dephosphorylation of CDK is the cause of the bistable response in Xenopus experiments. Thus, they concluded that although hysteresis is neither necessary nor sufficient for cell cycle transitions, it is a better mechanism for cell cycle dynamics than nonhystertic mechanisms.

Recently, Tyson and colleagues proved that the quasi-steady state assumption that is utilized in Michaelis-Menten kinetics and Goldbeter's ultrasensitive switches is not applicable for protein interaction networks like the cell cycle because the enzyme concentrations are found at comparable concentrations as the substrate [110]. In order for Michaelis-Menten kinetics and Goldbeter's ultrasensitive switches to capture the kinetics of the underlying reaction network, the enzyme concentration must be much less than the substrate concentration. This is not the case in protein interaction networks like the cell cycle where enzyme and substrate concentrations exist in similar concentrations. Furthermore, proteins such as MPF and Wee1, which mutually inhibit each other, exist in competing states. Since the proteins mutually inhibit each other, only one exists in a high concentration, and therefore at different points in the cell cycle, they switch roles with one at a high concentration and the other at a low concentration.

When Tyson and colleagues unpacked an earlier cell cycle model that utilized ultrasensitive switches and Michaelis-Menten kinetics, they observed that the system lost bistability. The system gained bistability when the phosphorylated substrate retained some kinase activity rather than being fully inhibited. They also observed that the Wee1 MPF complexes accumulate to appreciable levels that capture the secondary inhibition of Wee1 on MPF through sequestration.

In a following work, Novak, Tyson and colleagues argued that irreversible cell cycle transitions occur because of system level feedback mechanisms rather than specific reactions such as activation or degradation of a specific protein [111]. They argue that systems-level feedback creates bistability that generates the irreversible transitions. Specific reactions can change as long as the systems-level feedback is retained.

3.2. Yeast

The yeast cell cycle was the next system researched both experimentally and theoretically. The cell cycle of yeast is a more complicated system than *Xenopus* extracts and embryos, but yeast populations can be mutated very easily. Fission yeast were the first system to be investigated and were followed closely by budding yeast.

3.2.1. Fission Yeast

Novak and Tyson were the first to model fission yeast data [112]. The model incorporated Wee1, Mik1, Cdc25, and MPF. Mik1 performs the same protein kinase activity as Wee1. They assume that the core cell cycle machinery has been conserved over evolution, and thus the fission yeast model utilized the *Xenopus* extracts model as a basis.

Novak and Tyson also incorporated checkpoints into the model. The first checkpoint at G2 determines if the DNA has replicated correctly and the cell is large enough to divide. The second checkpoint determines if the chromosomes are aligned on the metaphase plate, and the final checkpoint is the initiation of DNA synthesis where cell size is monitored.

Novak and Tyson utilized pseudo phase plane analysis to assess the dynamics of the system. The pseudo phase plane analysis plots total cyclin versus active MPF, but the system has not been reduced to two equations. The trajectories of the model through the plane can then be drawn. They then studied multiple different knockout scenarios with their model to capture the experimentally observed phenomena. The model consists of 20 differential equations and 46 parameters.

Novak and Tyson then added the biological mechanisms that control the start of DNA synthesis [113]. The phenomenological G1 checkpoint from the earlier model was replaced by the addition of Rum1, a CKI. The model was then updated to have checkpoint controls for G1/S, G2/M and metaphase/anaphase transitions [114] by combining the previous two models and testing them against mutant strains.

Quantized cycle times for Wee1/Cdc25 double mutants were simulated with a later model [115]. Sveiczer and colleagues found that in order to observe quantized cell cycle times, the systems must have weak positive feedback mechanisms. With the weak positive feedback, the system reverts to an oscillatory behavior that does not exhibit switch-like transition behavior. The model incorporated stochastic noise that varied one parameter to capture the quantized cell cycle times. A different hypothetical wiring diagram was used in a following investigation to explain the Wee1/Cdc25 double mutant [116]. Both wiring diagrams, though significantly different, were able to capture the same phenotypical behavior, a contradiction that displays the limitations of modeling protein interactions.

Sveiczer and coworkers also investigated the nucleocytoplasmic ratio by adding asymmetric division and variable nuclear volume into the fission yeast model [117]. This

was the first work to incorporate stochasticity into kinetic variables of the cell cycle to quantify population heterogeneity. Sveiczer and coworkers found that asymmetric division alone was not sufficient to quantify heterogeneity in fission yeast cells.

This work was followed by an investigation of the quantized cell cycle times in Wee1/Cdc25 double mutants [118]. In the model, nuclear volume was a stochastic random variable and asymmetric division was taken into account. The initial concentration of the Pyp3 protein, a phosphatase with that performs the same action as Cdc25, was taken as a stochastic random variable. The addition of the asymmetric distribution of Pyp3 at birth was able to capture the three quantized populations of Wee1-50 Cdc25Δ fission yeast. Sveiczer and Novak found that the nuclearcytoplasmic ratio was an essential element in determining cycle times.

In an effort to simplify a fission yeast cell cycle model, Srividhya and Gopinathan created a simple time delay model [119]. The time delay was incorporated into the activation of MPF by APC at the end of mitosis. By utilizing a time delay, fewer species are necessary in the cascade to activate APC. Bistability exists when the time delay is removed. As the time delay increases, MPF is allowed to activate before activating APC thus generating the oscillatory behavior of the system. Srividhya and Gopinathan incorporated stochasticity into the model by varying the cell birth length and incorporating white noise into their differential equations. The time delay model can capture many of the mutant strains, and the stochastic model captures quantized birth lengths observed in Wee1 Cdc25 double mutants.

3.2.2. Budding Yeast

The first cell cycle model based on budding yeast proteins captured a two phase system composed of G1 and S/G2/M [120]. The species were based on the earlier mitotic oscillator, but the model did not include Cdc25 or Wee1. The negative regulation of the CDK is through cyclin proteolysis and CKI inhibition.

The model captured two distinct states: G1 where the cyclin degradation machinery and CKI's are high, and S/M where cyclin/CDK activity is high and the inhibitory machinery is low. Cyclin B synthesis is modulated by the cell mass, and when it hits a critical concentration in the nucleus, cyclin B/CDK overcomes the negative inhibition and begins to accumulate. This triggers the activation of APC/Cdc20 that through cascading events degrades cyclin B and resets the system.

The following investigation expanded the complexity of the model, which accounted of wild type and 50 mutant strains of budding yeast [121]. The model incorporates three cyclins, Sic1 (CKI), Hct1 (Cdh1), and Cdc20. It also includes three transcription factors and exponential cell growth.

Utilizing a simplified representation of the budding yeast cell cycle model, Lovrics and colleagues followed the eigenvalues of the Jacobian with time to separate the regions of excitation and relaxation [122]. The analysis found four regions of excitation that were immediately followed by regions of relaxation. The excitation and relaxation regions corresponded with cell cycle transitions and cell cycle phases, respectively. Through dimensional analysis, Lovrics and colleagues found that the 13 species system could be represented by 7 species at any point in time in the model. The dimensional

analysis never fell below one, which corresponded with the cellular mass, which grows independently of the other species.

The morphogenesis checkpoint was later added to the model which was again verified by modeling mutant strains [123]. This model was reduced and extensively analyzed by one and two parameter bifurcation [124]. The most recent budding yeast model captured 120 of the 131 known mutant strains [125]. This model now incorporates 61 equations and well over 100 parameters.

Thornton and colleagues adapted the budding yeast model to investigate how fission yeast are able to cycle without APC (cyclosome) [126]. The model was modified to account for 31 different mutants and was able to capture the phenotypes of 28 mutants including the oscillating system without APC.

Rather than using ordinary differential equations, Li and coworkers developed a Boolean model for the budding yeast cell cycle and analyzed the model's stability and robustness with dynamical tool [127]. They found that the budding yeast cell cycle is highly robust with a global attractor for the G1 state. The cell cycle pathway (G1-S-G2-M) is also globally stable and relatively stable against perturbations.

The Boolean model by Li and coworkers was later expanded to include noise [128]. Utilizing a noise component that affected the entire system equally, they observed that when the noise was greater than the interaction strength, the network dynamics become noise dominated and lose their biological meaning. There is a critical noise limit below which the system maintains the biological function, namely the cell cycle. In Zhang and colleagues model, the cell cycle pathway falls in a valley on the potential surface and is stable against small perturbations induced by noise. In another work, Li

and coworkers original Boolean model was updated to include cell size as a variable [129]. In this work, Zhang and colleagues simulated the Boolean network utilizing a Markov Chain model.

Proctor and coworkers developed a stochastic model for the telomere uncapping during DNA synthesis [130]. The model incorporates great detail into the telomere uncapping during DNA synthesis, but it incorporates a phenomenological model for the cell cycle. Each phase has a cyclin that activates cyclins for the next phase. There are no feedback loops for the cell cycle transitions and therefore the cell cycle aspect of the model follows a dominos and clock model. One cyclin builds, which builds the following cyclin while the previous falls. These events occur in a clock-like fashion to produce the oscillatory dynamics of the cell cycle. Although their work incorporated a cell cycle model, the specific focus was to model telomere uncapping, and not the cell cycle events.

Ge, Qian, and Qian compared a stochastic budding yeast cell cycle model to its deterministic counterpart [131]. They observed a dominant cycle in the stochastic model that captures the deterministic model behavior. Ge and colleagues also found that the budding yeast cell cycle is very robust to small fluctuations.

A budding yeast cell cycle model was broken down into subnetworks to analyze them for multistability [132]. By analyzing the subnetworks, chemical reaction network theory can be applied. Within the subnetworks, Conradi and colleagues extracted multiple pathways for the system to exhibit multistability. The CDK and CKI negative feedback loop was found to have three plausible multistable mechanisms. This type of analysis allows for the parameter space to be estimated over which multistability is

observed. Contrary to breaking down a larger model into subnetworks, this thesis work used a bottom-up approach, and therefore, began with a minimal model and added complexity to elucidate the contribution.

Sriram, Bernot and Kepes developed a minimal model for the budding yeast cell cycle utilizing modules [133]. The positive feedback loops were analyzed separately from the negative feedback mechanisms and then combined into the full model where the topology of the network was investigated. Sriram and colleagues observed chaos within their reduced model over a small region of the parameter space.

Rather than minimize the budding yeast cell cycle model, Barberis and Klipp incorporated special regulation into their model [134]. In the model, nuclear transport of cyclin-CDK complexes is dictated by the environmental nutrient source. They demonstrated that spatial regulation, nuclear or cytoplasmic, plays a major role in correct onset of DNA synthesis.

3.3. Transition Models

As the cell cycle models grew more complex, some groups moved away from the oscillatory systems into investigating the switching behavior of the cell cycle transitions. Tyson and coworkers were the first group to analyze the system from this perspective [135]. They analyzed simple models for G1 and G2 checkpoints for various species with phase plane analysis.

Recently, the use of Michaelis-Menten kinetics in protein interaction networks was analyzed again by Sabouri-Ghomi and colleagues [136]. Utilizing bifurcation analysis, Sabouri-Ghomi and colleagues disassembled a bistable switch that was generated by Michaelis-Menten kinetics into the elementary reactions. They found that

the disassembled switch did not generate bistable behavior. Bistability was restored when the proteins were allowed to form a trimer complex where both proteins were attempting to phosphorylate their substrates. Sabouri-Ghomi and colleagues then ran stochastic simulations with the Gillespie algorithm and observed that the toggle switch is robust to small numbers of molecules.

The remainder of the transition models investigated the restriction point and DNA synthesis transition, or the transitions associated with mitosis. The section begins with a discussion of the restriction point and DNA synthesis transition models followed by the mitotic transition models.

3.3.1. Restriction Point and DNA Synthesis Transition Models

Kohn began with a core E2F and pRb G1/S transition model and added complexity to gain insight into the interactions of the proteins [137]. Kohn found that the binding and dissociation of E2F from Rb could produce a large wave of E2F activity. Cyclin E-CDK2 and finally cyclin D-CDK4 were then added to the model. Excessive cyclin E-CDK2 activity reduced the amplitude of the E2F activity wave. The extent of the effect was greater if Rb was phosphorylated both when complexed with E2F and unbound. Cyclin D decreased the delay in the E2F wave that occurred at later times with just the cyclin E circuit. Overexpression of either cyclin E or cyclin D under certain circumstances inhibited the start of DNA synthesis.

Hatzimanikatis and coworkers analyzed the G1/S transition with a nine component model [138]. The model included cyclin-CDK complexes, pRb, E2F-1, and a CKI. The model was analyzed with bifurcation analysis that revealed that changes in cyclin E or E2F can initiate proliferation, but co-overexpression results in quiescence.

Further analysis revealed that the concentration of CKI necessary to halt proliferation is independent of both E2F and cyclin E and only depends on the ratio of the bound and unbound forms of the CKI complex.

Deineko and colleagues adapted Aguda and Tang's G1/S model [139] to utilized sequence analysis tools to predict new potential target genes that are regulators of the cell cycle [140]. A mitogenic signal was added into the model and the system behavior was analyzed for different pulses of the mitogenic signal. If the duration of the pulse is longer than a critical time, the cell enters S phase. If the duration is less than the critical time, the cell enters a G0 state. The critical time of mitogenic signal corresponded to the exposure time necessary to pass the restriction point. The mitogenic signal increases AP-1 genes that up regulate cyclin E-CDK2. E2F and pRb are also included in the model. If there is an additional E2F and AP-1 positive feedback (E2F up regulates AP-1), the duration of the mitogenic signal necessary for transition is reduced five fold.

Swat and coworkers analyzed their G1/S model with bifurcation analysis [141]. The model included pRb, E2F1, Ap-1, cyclin D, CDK4/6, cyclin E, and CDK2. The restriction point is described by a transcritical bifurcation and the G1/S transition by a saddle node bifurcation. They began with a minimal model with E2F and pRb and added complexity to the model to investigate how the addition changed system behavior. The observed behavior of the core model was found in the more complex model. Hill functions and enzyme kinetics were incorporated throughout the model, and the mitogenic stimulation was utilized as the bifurcation parameter. Swat and coworkers found that as the positive feedback strength increased, multiplicity increased, and the G1/S transition became more irreversible. Similar to Swat and coworkers work, an

objective of this thesis work was to develop a model linked the environment and therefore, the final bifurcation parameter was extracellular glucose.

Aguda and Tang developed a model which addresses the G1 to S transition in mammalian cells to find the kinetic basis for the restriction point [139]. Aguda and Tang utilized this model to investigate the switching behavior of the G1 to S transition. The model includes cyclin D, CDK4, p16, p27, cyclin E, CDK2, Cdc25A, pRb, and E2F. The p27 protein is a CKI that interacts with both cyclin D-CDK4 and cyclin E-CDK2. The p16 protein is also a CKI which can bind to and inhibit cyclin D-CDK4 and inhibits the synthesis of pRb. The model has 11 kinetic equations for active cyclin E-CDK2, E2F, p27, p26, inactive cyclin E-CDK2, pRb, p27 bound cyclin E-CDK2, phosphorylated pRb, E2F pRb complex, cyclin D-CDK4, and p27 bound cyclin D-CDK4.

Aguda and Tang found that positive feedback between cyclin E/CDK2 and Cdc25 created a dynamical switching behavior. The switch behavior was also caused by the double negative feedback between cyclin E/CDK2 and $p27^{kip1}$. These two key interactions determined the switching behavior of the entire system.

A mesoscale liver regeneration model by Chauhan and colleagues linked cyclin E to DNA synthesis [142]. Since the model is mesoscale, the proteins of the cell cycle are lumped into groups, which limits the detail of the module. Utilizing this top-down approach, Chauhan and colleagues linked their cell cycle model to cytokines, growth factors released from damaged liver cells, and were able to simulate experimentally observed phenomena.

In their G1/S transition model for budding yeast, Barberis and coworkers incorporated compartmentalization of the proteins [143]. The model incorporates two

sizer mechanisms that are sugar source dependent. The parameter set was later assumed to be the mean values in a distribution of parameters to simulate a population of budding yeast. They observed that cell size is important for DNA synthesis initiation.

Pfeuty and colleagues developed a G1 model for mammalian cells that determines the cell's fate [144]. In their model, the G1 regulatory network dictates whether a cell remains quiescent in G0, begins G1, initiates DNA synthesis (S), or dies through apoptosis. The network generates a double-S bifurcation structure where the first and second saddle nodes capture the transition between G0 to G1 and G1to S, respectively. Tashima and coworkers designed a transition model for the G1/S phase to predict the key factor controlling the transition [145]. Utilizing systems analysis, Tashima and coworkers isolated the key factors, but their model was not able to reproduce phenomenological behavior. In their model, as pointed out in the discussion, cyclin A peaks before cyclin E, which is not consistent with what has been observed experimentally.

The DNA damage network was integrated with a G1/S transition network in the model developed by Iwamoto and colleagues [146]. In the work, Iwamoto and colleagues linked the oscillatory behavior of p53 to DNA damage into the G1/S transition network and analyzed the network through a sensitivity analysis. The model was able to qualitatively capture the dynamics of the G1/S transition with and without DNA damage including the delay of the onset of DNA synthesis when there is DNA damage.

Haberichter and coworkers developed a G1/S model that accounts for cyclin D independent activation of cyclin E that is observed in proliferating cells continuously exposed to growth factors [147]. This model is contrary to earlier restriction point

models where cyclin D is required to proceed through the checkpoint. Thus, cyclin E must inactivate pRB without the assistance of cyclin D. Haberichter and coworkers globally optimized for parameter sets and filtered the datasets to meet knockout criteria. They observed that the activation of CDK2 needs to be connected to a sizer mechanism from the cell.

3.3.2. Mitotic Transition Models

Thron expanded his MPF pulse generator model with the incorporation of the Cdc25 positive feedback loop [148]. Thron analyzed the autocatalytic positive feedback on MPF. The model was reduced to a single differential equation that was analyzed by phase plane analysis. The model does not include negative feedback in which MPF promotes the degradation of cyclin. Thron then added a titratable CKI and analyzed the proteins involved in the G1/S transition [149]. Multiple different positive feedback loops are proposed to create bistability.

Aguda began investigating the extrinsic instabilities of the G2-M DNA damage checkpoint [150]. The model included MPF, Cdc25, and Wee1. Each species had an active and inactive form in which the active form of MPF and Cdc25 is phosphorylated and the active form of Wee1 is not phosphorylated.

The G2/M DNA damage checkpoint model identified a transcritical bifurcation point that is the product of the total amount of MPF and Cdc25. The transcritical bifurcation occurs when two phosphorylation dephosphorylation cascades are coupled. Once the transcritical bifurcation is achieved, both proteins switch on. The phosphorylation dephosphorylation cascades involving Cdc25 and MPF cause dynamical instabilities.

Aguda expanded this initial model to include proteins p53 and Chk1 which signal that the DNA is damaged [151]. The p53 protein down regulates MPF and Cdc25, and Chk1 down regulates only Cdc25. This model captures the positive feedback bistable switch for the entry into mitosis that can be arrested by DNA damage.

This model also expanded the MPF and Cdc25 subsystems. The Wee1 subsystem has an active and inactive form like the previous model. In the MPF subsystem, a CKI, p21, is included in this model, which binds to MPF and renders it inactive. The synthesis of p21 is up regulated by p53 to link it to the DNA damage. MPF also catalyzes its own degradation with a second order feedback term. Thus, the model has three forms of MPF; preMPF, MPF, and MPF bound to p21. PreMPF is the Wee1 phosphorylated inactive form. The model phosphorylates both CDK1 inhibitory sites simultaneously.

The Cdc25 subsystem includes five forms of the species; an inactive form, an active form, an inactive form that is phosphorylated at Ser216, an active form phosphorylated at Ser216, and an inactive form phosphorylated at Ser216 and bound to the 14-3-3 protein. The 14-3-3 protein exports proteins from the nucleus and when Cdc25 is phosphorylated at Ser216 by Chk1 the 14-3-3 protein can bind to the inactive form of Cdc25. MPF and Plk1 activate Cdc25. The 14-3-3 protein is upregulated by the p53 protein, thereby linking the 14-3-3 protein to DNA damage.

Aguda found that Wee1 degradation is necessary for Cdc2 activation. G2 arrest due to DNA damage cannot be carried out solely by Rad3/Chk1 pathway and must have the help of p53. As established in his first model, the transcritical bifurcation point establishes the thresholds for the switching behavior. Therefore, if either species causes

the product to fall below the transcritical bifurcation point, both species shut off. This is why nuclear export of either species due to DNA damage may arrest the cell cycle in G2.

Recently, Ibrahim, Dittrich, Diekmann, and Schmitt investigated the activation of APC at the end of mitosis [152]. In their model, Mad2 sequesters Cdc20, which is required for APC activation, prior to anaphase to ensure that the cell divides DNA to each daughter cell accurately. They found that Mad2 could only reduce Cdc20 concentration by half. Therefore, they hypothesize that there is an additional mechanism present in the cell that reduces the remainder of Cdc20 during anaphase.

Toth, Queralt, Uhlmann, and Novak reduced an earlier G2/M model in order to analyze it with phase plane analysis [153]. They reduced the system to two dimensions, Clb2 and Cdc14. Clb2 is the main cyclin involved in initiating mitosis and Cdc14 is involved in the exit from mitosis. Toth and coworkers were able to report how the phase plane nulclines change as the mitotic exit network was activated.

3.4. Higher Eukaryotes

Unlike the cell cycle machinery in frog eggs and yeast, higher eukaryotes have multiple cyclins and CDKs that collaborate to initiate the cell cycle events [154]. The complexity of the system increases vastly because different regulatory proteins regulate the activity of each cyclin CDK. There have been models capturing the complex dynamics of finishing mitosis and apoptosis, but the majority of the models address the dynamics of the initiation of DNA synthesis.

The first task was to adapt the earlier mitotic oscillators by adding the proteins found in higher eukaryotes. Obeyesekere, Tucker, and Zimmerman were the first to tackle higher eukaryotes mitotic exit by designing a model with cyclin A and cyclin B

[155]. Cilberto and coworkers developed a model to capture the activation of APC [156]. Phosphorylated Cdc20 and Cdh1 have lower binding affinity than the unphosphorylated forms. The Cdc20 protein binds to phosphorylated APC. Conversely, Cdh1 binds to unphosphorylated APC. As MPF accumulates, it initially inhibits Cdc20, but at peak concentration, the activation of APC sequesters Cdc20. The activated APC begins to degrade MPF, which releases the inhibition on Cdc20 to finish the degradation.

In multicellular eukaryotes, programmed cell death, apoptosis, is an essential mechanism for controlling growth. Thus, Aguda and Algar developed a phenomenological model for linking apoptosis and the cell cycle [157]. A modular approach was used in the model assuming that the cell cycle machinery and apoptotic machinery could be separated. The work incorporated a simplified model that includes a basic level of connection between the two modules. The modules do not include specific proteins, but rather each module is considered a black box that captures the essence of each model. Thus, the module simulates the interaction between the two systems.

The work proposes four different signals that could affect the two systems. One signal would up-regulate both proliferation and death pathways. Another would up-regulate apoptosis and down-regulate the cell cycle and vice versa. Finally, a signal could down-regulate both modules. Their work focuses on the case where a signal up-regulates both modules.

One case, a negative feedback loop from the cell cycle reduced the mitogenic signal, which represses the apoptosis proteins. In this case, hyper-proliferation would reduce the apoptotic signal, and hyper-proliferating cells would not die when they should. Thus, the cell cycle must have some positive contribution to apoptosis. Consequently,

serum starved cells also become apoptotic, and thus lack of proliferation must positively affect apoptosis. The remainder of the work involves a thought experiment of the two systems and the complex interactions that must occur to allow the cell to proliferate normally.

One of the central proteins in apoptosis is p53. Utilizing a simplified model of the DNA damage mechanism, Ciliberto and colleagues were able to reproduce the experimentally observed constant amplitude oscillations in p53 [158]. The number of oscillations depends on the extent of DNA damage. The model system incorporated both positive and negative feedback mechanisms. The negative feedback loop was verified, and the next model hypothesized different positive feedback loops that would generate the oscillations [159]. Alternative activation schemes of p53 were also considered. The activation schemes would induce oscillations with negative feedback alone when there was a time scale separation. Four model structures were analyzed with bifurcation analysis, and the authors hypothesize that the response of p53 to DNA damage is digital, that is, coupled to the number of oscillations rather than an analog response.

Alarcon, Byrne and Maini adapted Tyson and Novak's mitotic oscillator [98] to include an environmental oxygen sensing mechanism [160]. By including p27, a CKI involved in sensing hypoxia, the model was able to capture G1/S arrest because of low oxygen levels. They found that only cancerous cells could achieve a quiescent state, and both normal and cancerous cells were able to arrest in G1/S.

Obeyesekere and colleagues then focused their attention on the DNA synthesis oscillator [161]. Their G1 phase model incorporated cyclin E/CDK2, MPF, and pRb. The goal of this model was to find the minimal number of variables that captures the

events occurring in G1. Obeyesekere and colleagues assumed that MPF has a negative feedback on cyclin E/CDK2, an autocatalytic activation, and first order degradation. Therefore, MPF is viewed as the negative feedback of G1, but its own negative feedback of APC is not taken into account. The model produced sinusoidal oscillations which did not fall to near zero concentrations when the species were out of phase.

Obeyesekere and colleagues then expanded their G1 oscillator to include an external growth factor [162]. Simulations of normal cells, transformed cells and Rb knockout cells were performed. The model captures normal cells and Rb knockout cellular arrest when growth factors are removed from the system, but transformed cells oscillate without growth factors. The growth factor level did not change the division time in the model, but rather it changed the amplitude of the active CDK complex. The model also predicts delayed S phase entry with Rb knockouts that is contrary to experimental evidence. This growth factor model was revised by replacing MPF with a cell progression indicator, which represents all the proteins involved in the end of the cell cycle [163]. Bistability in the form of a subcritical Hopf bifurcation was observed for low growth factor concentrations. Therefore, there is a hysteresis in growth factor response between the lower steady state and stable oscillatory state. Contrary to experimental evidence, the lower steady state where the cell has entered a state of quiescence had high levels of cyclin E/CDK2. The model parameters were updated, and the hysteresis in growth factor response was shown experimentally [164].

Kaern and Hunding incorporated cyclin E/CDK2 into Novak and Tyson's mitotic oscillator [83, 84] and found that cyclin E/CDK2 regulated the threshold activity of MPF; thus controlling the entry into mitosis [165]. The model arrests in G2 when active CDK2

is absent. Therefore, they suggest that cyclin A/CDK2 is a possible candidate to keep CDK2 activity present throughout S and G2 phases. High levels of CDK2 activity allowed for rapid repeated divisions in the model.

Chiorino and Lupi investigated the G1 variability with a mathematical model which included cyclin E, p27 (CKI), CDK2, pRb, and E2F [166]. The model varied reaction rates or initial protein levels to account for intercellular variability of division times and was linked to flow cytometry data.

Qu and coworkers designed a model of the G1 to S transition which was subdivided into modules [167]. Each module was added to the core module of cyclin E-CDK2 to assess its contribution and analyzed by steady state analysis. The proteins involved in the model are cyclin D, cyclin E, CDK2, CDK4, CDK6, Cdc25, E2F, Rb, and CKI. The model assumes mass action kinetics from biochemical reactions. Since the dynamics of the G1-S checkpoint are not completely known, both Hopf and saddle node bifurcations were considered.

The double negative feedback from Wee1 is not included in the model. The core module assumes that cyclin E binds to CDK2, which is already phosphorylated at all three sites. Cdc25 then unphosphorylates the two inhibitory sites simultaneously. Cdc25 has five phosphorylation sites, but is allowed an arbitrary number of phosphorylation sites in the model. The positive feedback from Cdc25 on CDK2 is then the sum of the number of species that are weighted by the number of phosphorylations. The phosphorylation of Cdc25 has a background rate and a rate catalyzed by active CDK2.

The same is true for Rb and CKI that have multiple phosphorylation sites. Rb must have at least M, a model parameter, phosphorylations to release E2F, but has a

larger possible number of phosphorylations. Likewise, CKI must be phosphorylated N, a model parameter, times before it releases cyclin E-CDK2 and is degraded.

For the main module that includes cyclin E, CDK2, and Cdc25, bistability, multistability, limit cycle, and excitable dynamics are observed. These dynamics occur when there at least two phosphorylation sites on Cdc25. Bifurcation analysis is performed with cyclin E synthesis as the bifurcation parameter. The system can have oscillations is a lower Hopf or saddle node bifurcation.

The effect of multiple phosphorylations on Cdc25 activation was also investigated. As the number of phosphorylations increased, the slope of the response curve and threshold of activation increased, a change that is essential to create instabilities. Also, fast phosphorylation is required to sustain oscillations. If the phosphorylation rate is lowered enough, the limit cycle behavior of the model disappears.

Simulation results show that a high level of free and bound cyclin E are required to keep active cyclin E-CDK2 levels low. If the degradation rate is low, then higher levels of active cyclin E-CDK2 are observed, a condition that is shown to be tumorigenic, and the system behaves like overexpression of cyclin E. Low levels of cyclin E result in cell cycle arrest in G1. Whereas, high levels result in early initiation of DNA synthesis.

Overexpression of Cdc25 shortens G1 phase. Cdc25 is down regulated if there is DNA damage, which delays the G1 to S transition. Conversely, overexpression of CKI results in G1 arrest. Including CKI module in the model resulted in limit cycle behavior at higher cyclin synthesis rates. E2F and Rb have little effect on the threshold for oscillations when total E2F is conserved and cyclin D is not present. When cyclin D is present, overexpression of E2F hastens G1 phase and overexpression of Rb delays or

blocks the cell in the G1 phase. Over expressing E2F or deleting Rb causes high levels of cyclin E-CDK2, another condition that is characteristic of tumor formation.

Multisite phosphorylation is essential for cell cycle instabilities that produce the oscillatory behavior. Cdc25 and CKI had to be phosphorylated in two or more sites to observe instabilities, and Rb required more than two sites.

Qu and coworkers then created a model that links a cell growth model with an external source to the cell cycle [168]. They hypothesized that cell surface area at birth determines the growth rate. They then compared their model with cycle time versus birth size in fission yeast, *Xenopus laevis*, and serum removal before the restriction point in mammalian cells. The model was able to capture the sizer and timer effects of the cell cycle when a cell is smaller than a critical size. The physiologically derived model can capture the sizer and timer effect in a number of different species and of all experimental data sets unlike the empirical equations and phenomenological linking in Tyson's work.

By introducing spatial concentrations in the cytoplasm and nucleus, Yang and colleagues simulated a cell that linked cell growth with the cell cycle [169]. The model included mitotic proteins cyclin B-CDK1, Cdc25, Wee1, Myt1, and APC. The cyclin B-CDK1 mechanism includes six species: cyclin B, hyper-phosphorylated cyclin B, inactive cyclin B-CDK1 complex, inactive cyclin B-CDK1 complex with hyper-phosphorylated cyclin B, active cyclin B-CDK1, and active cyclin B-CDK1 complex with hyper-phosphorylated cyclin B.

Cyclin B forms an inactive complex with CDK1 that is activated by Cdc25 to form the active complex. Wee1 or Myt1 can inactivate the active cyclin B-CDK1 complex by phosphorylation. The active complex autophosphorylates the cyclin species,

which are actively transported into the nucleus. Cdc25, Wee1, Myt1, and APC are assumed to have three phosphorylation sites which are catalyzed by both the active cyclin B-CDK1 complex and the active cyclin B-CDK1 complex with hyperphosphorylated cyclin B. The highest phosphorylated form of APC and Cdc25 are active and the unphosphorylated form of Wee1 and Myt1 are active. The non-phosphorylated form of Cdc25 can bind to the 14-3-3 protein to form another inactive form. Active proteins are transported from the cytoplasm to the nucleus and inactive proteins are transported out of the nucleus except Wee1 and Myt1 that are mainly nuclear and cytoplasmic, respectively.

The protein model is mechanistic and assumes mass action kinetics. Nonlinear dynamics in the form of a third order dependence of active forms of cyclin B-CDK complex are utilized to capture the hyperphosphorylation of cyclin B species. The active transport of active cyclin B-CDK2 had been show experimentally and is reprinted in the paper. The nuclear volume is assumed to be constant, and as the cytoplasm grows at a rate proportional to the surface area at birth. The model was simulated with a discritized PDE model and two compartmental problem to determine the effects of transport and protein localization on the cell cycle system.

Yang and colleagues determined early in the work that the two compartmental model captured the dynamics of the transport because there was a very small gradient within the nucleus and cytoplasm compartments in the full PDE model. They also found that the growth of the cytoplasmic volume makes the nucleus becomes a smaller sink term for the active species being transported between the two volumes. As the inactive cyclin B-CDK complexes accumulate in the cytoplasm, a threshold is past and then a spike occurs of active species, which are rapidly transported into the nucleus. The spike

in the nuclear concentrations is larger than the spike in the cytoplasmic concentration because the concentrating effect that is because the cytoplasmic volume is much larger than the nuclear volume.

The bifurcation analysis shows a lower steady state at low active cyclin-CDK and a high steady state at high active cyclin B-CDK levels. In between the steady states is a limit cycle region that separated by two Hopf bifurcation points. The model accurately captures the active transport of the active species into the nucleus and links cell growth to the cell cycle in a mechanistic form. One limitation in the model is that it does not include a dilution term in the cytoplasm and the model is written in concentrations.

Novak and Tyson developed a model that was able to capture the dynamics of the restriction point in mammalian cells [170]. Recently, a generic model that could capture cell cycle dynamics from *Xenopus* extracts to mammalian cells was developed in a modular form to display the similarities between the cell cycle machinery of all the species [171].

Although there has been great progress in the cell cycle modeling, there exists uncertainty in the protein network structure of the mitotic oscillator. Thus, this thesis work analyzed the effect of the reaction network structure and multisite phosphorylation on the observable system behavior. The next chapter presents the methods used in this thesis work to analyze the mitotic oscillator system behavior.

Chapter 4 - Methods

The systems of ordinary differential equations (ODE) developed in this work were analyzed by bifurcation analysis and transient simulations. Bifurcation analysis solves for the steady state behavior of the system of equations, and therefore, this work could elucidate the effect of protein network structure and multisite phosphorylation on system behavior. The system behavior was further analyzed by transient simulation, thereby allowing the protein dynamics to be observed. For a thorough presentation of the theory behind bifurcation analysis refer to the following books [172, 173]. Bifurcation analysis was performed by Ermentrout's *XPPAUT* program [174].

For bifurcation analysis, the dynamic terms from the system of ODEs is set to zero, and the resulting system is solved for steady state behavior for a bifurcation parameter. As the value of the bifurcation parameter changes, the steady state behavior of the system changes. The cell cycle exhibits two steady state behaviors: limit cycle and stable steady state. For limit cycle behavior, a key protein oscillates between a minimum and maximum concentration with a specific period, a behavior that simulates proliferating cells. Once the system reaches a stable steady state, all protein concentrations are constant for all time. Quiescent and arrested cells are in a stable steady state where the cell cycle proteins dynamics do not change with time.

Dynamic simulations for specific parameter sets were run with a program that I developed for this project. The program integrated an adaptive timestep Runge-Kutta-Fehlberg scheme with a Newton Raphson module. The two modules were integrated into a larger loop to accommodate a large number of parameter sets during a single simulation. For a specific parameter set, Newton Raphson was run to find the steady

state solution to the system. The key protein in the system, which in the case of the mitotic oscillator is MPF, was then perturbed to set the initial condition for the simulation. Adaptive time step Runge-Kutta-Fehlberg 45 was then run to generate the dynamic behavior of the perturbed system. This procedure repeated for each parameter set. For an in depth presentation on Newton Raphson and adaptive time step Runge-Kutta-Fehlberg 45 please refer to Chapra and Cannale's book [175].

Bifurcation analysis and transient simulation were utilized throughout this thesis work to elucidate the effect of protein network structure and multisite phosphorylation on the network behavior. Ultimately, this thesis work utilized bifurcation analysis and transient simulations to developed a mitotic oscillator linked to environment. For every analyzed parameter set, I observed how the system behavior deviates from ideal mitotic oscillator characteristics.

4.1. Ideal Mitotic Model Characteristics

An ideal mitotic model should capture the phenomenological behavior of a cell (Figure 3). First, a mitotic model should predict proliferating cells which are characterized by oscillating MPF levels [13]. A mitotic model should also capture quiescent and G2 arrested cells which are characterized by a low concentration of MPF [14]. Quiescent cells are non-cycling cells that are in a state of rest because they are completely surrounded by other cells or have not received a mitogenic signal from the environment. A mitotic model should also capture cells that are arrested in mitosis or have experienced mitotic catastrophe both of which are characterized by a high concentration of MPF. If cyclin B and CDK1 are over expressed, the cells enters mitosis

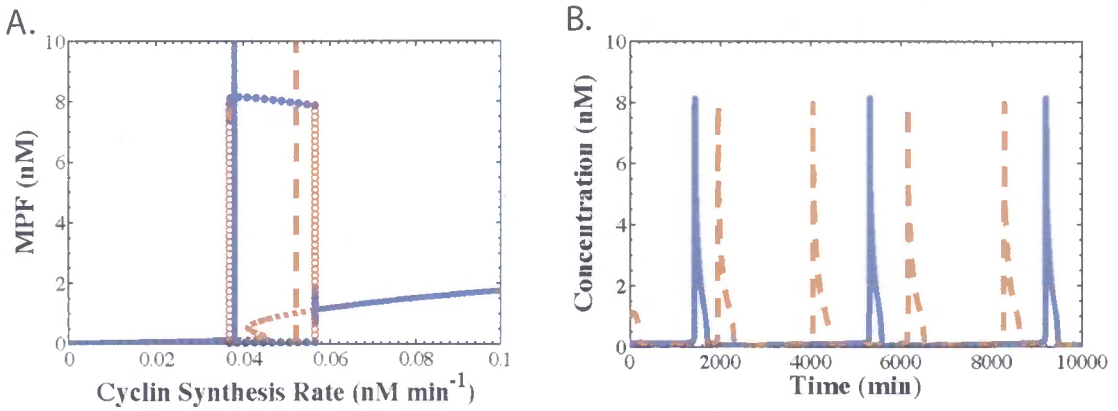

Figure 3 - A) General bifurcation diagram capturing the essential elements of the mitotic oscillator and B) dynamics. The main bifurcation parameter is cyclin synthesis rate, which is controlled by environmental factors and is the source for MPF generation. A low steady state represented by a solid blue line represents the quiescent cells and G2 arrested cells. The upper steady state, represented by the solid blue line, represents the mitotic arrested and mitotic catastrophe cells. The middle region has an unstable steady state, which is shown as a dashed red line, and is the region where oscillations are observed. The oscillations represent proliferating cells, which are represented by solid blue circles. The open red circles are unstable limit cycle.

before finishing DNA synthesis, consequently resulting in the death of the daughter cells. This behavior is known as mitotic catastrophe [176].

In the bifurcation diagram, the stable steady state with low concentrations of MPF at low cyclin synthesis rates represents all cells that are quiescent or G2 arrested. The stable limit cycle at intermediate cyclin synthesis rates represents proliferating cells, which have oscillatory MPF dynamics. MPF concentrations oscillate, a behavior which simulates multiple division cycles. The upper stable steady state with high MPF concentrations at high cyclin synthesis rates represents cells that have arrested in mitosis or that have experienced mitotic catastrophe. This thesis work takes the first vital steps to develop a proliferation model for a bioartificial tissue regeneration model. Therefore, I am particularly interested in the characteristics of stable limit cycle, otherwise known as the oscillatory region, where the cells are proliferating.

Specifically, I am interested in the size of the oscillatory region and the amplitude and period of the oscillations. Another model characteristic of interest to this work is hysteresis, which has been observed experimentally [177] with the MPF reaction network. Therefore, the model should be able to capture hysteresis. Hysteresis exists when there are multiple steady states for a singe value of the bifurcation parameter. Hence, I am interested if the model exhibits multiplicity of steady states for a given parameter set and network structure. The final model characteristic I am interested in is the shape of the change in amplitude with respect to the bifurcation parameter. Although it has not been observed experimentally yet, I hypothesize that the oscillations should be frequency encoded. When the oscillatory region is frequency encoded, as the key bifurcation parameter is changed over the oscillatory region, the period changes, but the amplitude remains approximately the same (Figure 3B). This behavior is ideal for a cell because the same peak in concentration is observed regardless of the division cycle time.

In the following chapter, this work develops a mitotic oscillator using a bottom-up approach. Thus, the initial model incorporates the minimal number of components while maintaining biological integrity. Than expanding from the base model, the MPF activation network, number of positive feedback loops, and number of multisite phosphorylations were varied to analyze their affect on system behavior.

Chapter 5 - Mitotic Oscillator

Cell mitosis has been the subject of many experimental and modeling studies. Even with all the new discoveries, there remains uncertainty about the protein network structure, and the effect of different protein network structures on the behavior of the systems is not fully understood. In an effort to elucidate the effect of protein network structure and multisite phosphorylation on system behavior, this work incorporated recent biological discoveries and a bottom-up approach to create a model for mitosis. Complexity was added to a base mitotic oscillator by increasing the number of phosphorylations and utilizing different protein reaction networks to analyze the effect of the different mechanisms and multisite phosphorylation on the oscillatory behavior of the model. This is the first work to analyze the effect of protein network structure and multisite phosphorylation on the system behavior of a mitotic oscillator.

For more than two decades, researchers have been developing models for the cell cycle, a subset of which is mitotic oscillators. Development began in the early 90s with minimal models describing the oscillatory behavior observed in frog embryos [69, 70, 80, 82]. The minimal models led to the development of more complex models for yeast [112, 113, 121] which were further generalized for eukaryotic systems [98] and expanded in complexity including a full model for the budding yeast cell cycle [125].

These models provided valuable insights into the cell cycle machinery and generated hypotheses that were later tested experimentally. However, all these models were developed with a top down approach. Each model incorporated the biological knowledge at the time, but assumed various nonlinear reaction rate expressions for protein-protein interactions. The model parameters were then fit to experimental data that

were based on postulated protein dynamics. However, the reaction rate expressions used in these models were not always supported by experimental evidence, and the mechanisms that generate the nonlinearities observed were not known.

Since the biological mechanisms generating these nonlinear reaction rates were not always fully understood, several groups developed bottom-up models to analyze how different sub-networks within the larger network contribute to the model's behavior [101, 137, 167, 171]. Utilizing a bottom-up approach, the modelers begin with a base or minimal model that can capture the basic behavior of the system. Then, proteins and protein interactions are added to the base model to analyze their contribution to the larger system. By utilizing the bottom-up approach, the modelers were able to gain insight into how different sub-networks contribute to the overall behavior of the complex network. Yet these works still assumed various nonlinear reaction rate expressions within the models that are presently not known. Furthermore, Tyson and colleagues recently proved that the Michaelis-Menten kinetics and ultrasensitive switches utilized extensively in earlier models do not accurately describe the dynamics occurring between proteins in cell cycle networks [110, 136].

The uncertainty in the functional form of the reaction rate expressions and the mechanisms that generate nonlinearities in the networks led Yang and colleagues to develop a bottom-up model for mitosis to analyze the effect of multiple phosphorylations on the observable behavior [103]. First, they developed a base model with the minimal assumption of mass action kinetics. Phosphorylation reactions were then added to the positive feedback loops and a Monte Carlo simulation was run. For each simulation, a random parameter set was chosen, and a bifurcation analysis was run.

Yang and colleagues observed that as the number of phosphorylations increased on the positive feedback mechanisms, the number of simulations that exhibited bistability and limit cycle increased. Bistability requires nonlinearities to exist within the network, and, therefore, the Yang and colleagues model suggests that multisite phosphorylation may be able to generate the nonlinear mechanisms that are present in mitosis. However, this study did not provide a systematic analysis of the parameter space where the model oscillates. Furthermore, this study did not provide details about the characteristics of the oscillations.

Moreover, recent experimental studies have also revealed new insights about the biology of mitosis. The central protein that initiates mitosis is the metaphase promoting factor (MPF) that is a composed of two subunits, cyclin B and cyclin dependent kinase 1 (CDK1). Larochelle and colleagues recently discovered that CDK1 must be phosphorylated at threonine 161 in order to stabilize the bond between cyclin B and CDK1 [19]. There have also been new discoveries about the activation of MPF. During the initiation of mitosis, the Cdc25 family of phosphatases activates MPF. All species of Cdc25 can activate MPF, but Cdc25A plays a general role in the cell cycle and is involved in both G1/S and G2/M [37]. Furthermore, $Cdc25B^{-/-}$ $Cdc25C^{-/-}$ double knockout mice grow normally, and therefore, do not display a unique phenotype [62]. Thus, Cdc25A can compensate for all CDK phosphatase functions throughout the cell cycle [62-64]. These results have not yet been incorporated into any of the models available in the literature.

Therefore, this work employed a bottom-up approach to add complexity to an initial base mitotic oscillator model incorporating the current biological knowledge.

Bifurcation analysis was utilized to assess how varying the number of multisite phosphorylation events and protein network architecture affect the system behavior. Specifically, this work investigated the MPF activation network that involves three phosphorylation events by varying the protein reaction network architecture that changes the phosphorylation sequence. In addition, this work analyzed the effect of varying the number of multisite phosphorylation events on Cdc25A on the oscillatory characteristics of MPF. Finally, an additional positive feedback loop was added to the model and the number of multisite phosphorylation events was varied to assess the biological relevance.

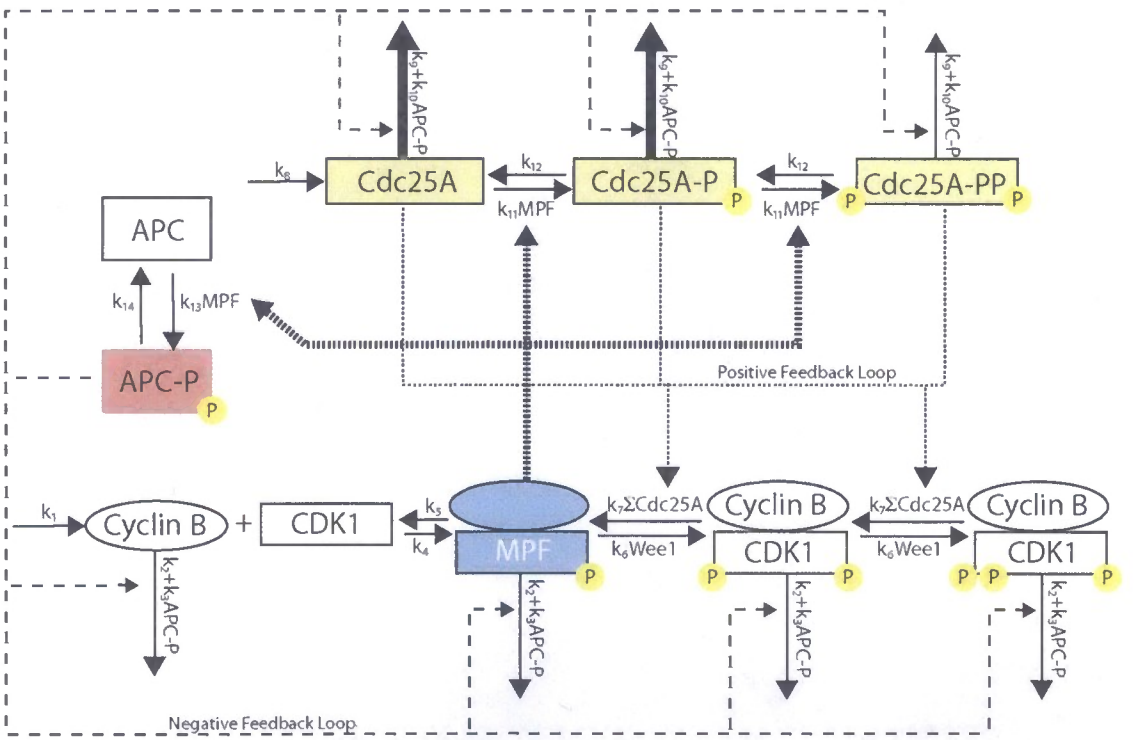

Figure 4 - Base Mitotic Model Reaction Network. MPF is generated by the dimerization of cyclin B and CDK1 thereby forming the active complex. MPF initiates mitosis and therefore is the central protein. The model has a single positive feedback loop where MPF stabilizes Cdc25A by phosphorylation and Cdc25A activates MPF by dephosphorylation. MPF activates APC by phosphorylation, and active APC in turn degrades all forms of cyclin B and Cdc25A thus generating the negative feedback loop

5.1. The Model

Employing a bottom-up approach, I designed a base mitotic model (Figure 4) that incorporates a minimal number of components while incorporating the current biological knowledge. The MPF subsystem has four species: monomeric cyclin B1, active MPF, and two inactive forms of MPF. CDK1 is in excess in cells [178], and therefore, is incorporated into the dimerization constant, k_4. This model is the first to include the recent biological discovery that CAK phosphorylation is required for the stabilization of the cyclin B-CDK1 dimer which is not observed otherwise [19]. In addition, CAK activity, which is observed to be constant in cells [179], and is also incorporated into the dimerization constant, k_4. The two inactivating phosphorylations by the Wee1 family of kinases are have been observed to occur sequentially in cells [34] and thus the model incorporates two inactive MPF species. By incorporating sequential inactivation phosphorylations and the requirement of CAK phosphorylation for MPF dimerization, this MPF activation mechanism is supported by the current biological knowledge, and this is the first mitotic model to incorporate this MPF activation network.

Although MPF is involved with multiple different proteins, which form positive feedback mechanisms during MPF activation, this work employed a bottom-up design and began by incorporating a single positive feedback loop by incorporating Cdc25A dynamics into the base model. All three species of Cdc25 can remove the inhibitory phosphorylations on MPF, but Cdc25A plays a general role in the cell cycle and is involved in both G1/S and G2/M [37]. Furthermore, $Cdc25B^{-/-}$ $Cdc25C^{-/-}$ double knockout mice do not display a unique phenotype [62]. Cdc25A can compensate for all

Table 1 – Mitotic Oscillator Base Model Rate Constants with Descriptions.

Parameter	Description	Base Model
k_1	Cyclin B synthesis rate	Bifurcation Parameter
k_2	Nonspecific Cyclin B degradation rate	0.0001 min^{-1}
k_3	Cyclin B degration rate by APC	0.015 nM^{-1} min^{-1}
k_4	Cyclin B CDK1 dimerization rate	6 min^{-1}
k_5	Cyclin B CDK1 dissociation rate	0.01 min^{-1}
k_6	MPF inactivation rate by Wee1 kinases	2.1 nM^{-1} min^{-1}
k_7	MPF activation rate by Cdc25A	0.5 nM^{-1} min^{-1}
k_8	Cdc25A synthesis rate	1.2 nM min^{-1}
k_9	Nonspecific lliable Cdc25A degradation rate	12 min^{-1}
k_{10}	Cdc25A degradation rate by APC	0.4 nM^{-1} min^{-1}
k_{11}	Cdc25A stabilization rate by MPF	7.5 nM^{-1} min^{-1}
k_{12}	Cdc25A desabilization rate	0.1 min^{-1}
k_{13}	APC activation rate by MPF	0.001 nM^{-1} min^{-1}
k_{14}	APC inactivation rate	0.45 min^{-1}
A_{tot}	Total APC Concentration	100 nM
Wee1	Total Wee1 Concentration	1 nM

phosphatase functions throughout the cell cycle [62-64], and therefore this work focuses solely on the Cdc25A species.

Cdc25A activity during mitosis is controlled by phosphorylation dependent stabilization [46]. Throughout interphase, Cdc25A is liable and degraded by the SCF protease [46]. During mitosis, Cdc25A is stabilized by MPF phosphorylation at serine 18 and serine 116 [46] thereby forming an additional positive feedback loop.

Cdc25A has three phosphorylation states in the base model. Unphosphorylated Cdc25A and Cdc25A with a single MPF phosphorylation are liable species and are degraded by a background protease. Cdc25A with two MPF phosphorylations is stabilized and is not degraded by the background protease. Since this work employed a bottom-up approach and therefore included only a single positive feedback mechanism in the base model, the positive feedback mechanism with Wee1 is not included and the activity of Wee1 is assumed to be constant.

In order to reset the system, MPF must activate its negative feedback mechanism, which is the anaphase promoting complex (APC). MPF can phosphorylate APC on at least 15 sites which facilitates the binding of its activating subunit Cdc20 [180]. The APC has two activating subunits, Cdc20 and Hct1/Cdh1 [11]. Cdc20 activity is high during early anaphase through the exit of mitosis when Hct/Cdh1 activity rises and remains high until the end of G1 [11].

Since the reaction network of the activation of APC is highly complex, the base model incorporates a simplified model of APC. APC has two forms, active and inactive, and the total concentration of APC is assumed to be constant during the cell cycle. MPF activates APC, which degrades all species containing cyclin B and all Cdc25A species. The base model was formulated with the minimal assumption of mass action kinetics and can capture the mitotic oscillations observed in proliferating cells (Figure 5). Rate constants for the base model are displayed in Table 1 with descriptions. The model equations are presented below.

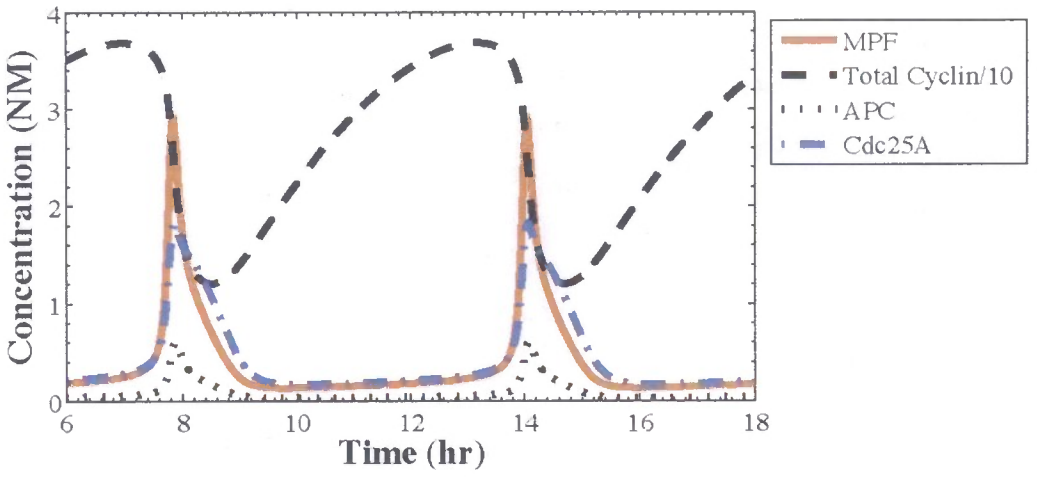

Figure 5 - Dynamics of mitotic oscillator. Cyclin B accumulates until a threshold of active MPF has been reached. Past the threshold, MPF rapidly stabilizes Cdc25A, which in turn activates MPF. Both concentrations peak at approximately the same time. MPF then activates the APC, which degrades cyclin B before Cdc25A, thus restarting the cell cycle. This is only a single parameter set, so a sensitivity analysis to determine how the model parameters change the oscillatory characteristics was performed. ($k_3 = 0.1$ nM^{-1} min^{-1})

$$\frac{d[CycB]}{dt} = k_1 - k_2[CycB] - k_3[APC-P][CycB] - k_4[CycB] + k_5[MPF] \tag{5.1}$$

$$\begin{aligned}\frac{d[MPF]}{dt} &= k_4[CycB] - k_5[MPF] - k_3[APC-P][MPF] - k_6[Wee1A][MPF] \\ &+k_7\left([Cdc25A]+[Cdc25A-P]+[Cdc25A-PP]\right)[MPF-P] \\ &-k_2[MPF]\end{aligned} \tag{5.2}$$

$$\begin{aligned}\frac{d[MPF-P]}{dt} &= k_7\left([Cdc25A]+[Cdc25A-P]+[Cdc25A-PP]\right)[MPF-PP] \\ &-k_2[XW]+k_6[Wee1A][MPF]-k_6[Wee1A][MPF-P] \\ &-k_3[APC-P][MPF-P] \\ &-k_7\left([Cdc25A]+[Cdc25A-P]+[Cdc25A-PP]\right)[MPF-P]\end{aligned} \tag{5.3}$$

$$\begin{aligned}\frac{d[MPF-PP]}{dt} &= -k_7\left([Cdc25A]+[Cdc25A-P]+[Cdc25-PP]\right)[MPF-PP] \\ &-k_2[MPF-PP]-k_3[APC-P][MPF-PP] \\ &+k_6[Wee1A][MPF-P]\end{aligned} \tag{5.4}$$

$$\frac{d[Cdc25A]}{dt} = k_8 - k_9[Cdc25A] - k_{10}[APC-P][Cdc25A] - k_{11}[MPF][Cdc25A] + k_{12}[Cdc25A-P] \tag{5.5}$$

$$\frac{d[Cdc25A-P]}{dt} = k_{11}[MPF][Cdc25A] - k_{12}[Cdc25A-P] - k_{11}[MPF][Cdc25A-P] + k_{12}[Cdc25-PP] - k_9[Cdc25A-P] - k_{10}[APC-P][Cdc25A-P] \tag{5.6}$$

$$\frac{d[Cdc25A-PP]}{dt} = k_{11}[MPF][Cdc25A-P] - k_{12}[Cdc25A-PP] - k_{10}[APC-P][Cdc25A-PP] \tag{5.7}$$

$$\frac{d[APC-P]}{dt} = k_{13}([APC_{tot}]-[APC-P])[MPF] - k_{14}[APC-P] \tag{5.8}$$

Equation 5.1 describes the dynamics of cyclin B monomers, CycB. CycB is synthesized at a constant rate, k_1. All species that incorporate cyclin B, CycB, MPF, MPF-P, and MPF-PP, degrade at a background rate, k_2, and at a rate proportional to the anaphase promoting complex, k_3. CycB dimerizes with CDK1 and is phosphorylated by CAK to from MPF at a rate of k_4. MPF dissociation to CycB and CDK1 occurs at a rate of k_5.

Equation 5.2 describes the dynamics of MPF, which is the protein that initiates mitosis. MPF dynamics include the dimerization and dissociation of cyclin B monomers and CDK1. Since MPF incorporates cyclin B, it has the same degradation terms. In addition, MPF is phosphorylated by Wee1 at a rate of k_6 and is formed by the dephosphorylation of inactive singly phosphorylated MPF species, MPF-P, by Cdc25A at a rate of k_7.

Equations 5.3 and 5.4 capture the dynamics of the inactive MPF species, MPF-P and MPF-PP. MPF-P has a single inactivating phosphorylation, whereas MPF-PP has

both inactivating phosphorylations. Both species incorporate cyclin B, and thus are degraded at a background rate of k_2 and proportional to APC, k_3. Both species are created by phosphorylation of the prior MPF specie by Wee1 at a rate of k_6. The removal of the inhibitory phosphorylation by Cdc25A converts each species to the prior species, and occurs at a rate of k_7. For example, MPF-PP becomes MPF-P when dephosphorylated by Cdc25A.

The Cdc25A species are described by equations 5.4 through 5.6. Cdc25A is synthesized at a constant rate of k_8. MPF phosphorylates Cdc25A at a rate of k_{11}. Cdc25A-P is the singly phosphorylated species, and Cdc25A-PP has two MPF phosphorylations. Cdc25A and Cdc25A-P are liable and therefore degraded at an accelerated rate, k_9. APC degrades all Cdc25A species at a proportional rate, k_{10}. MPF phosphorylation stabilizes Cdc25A, and therefore, Cdc25A-PP does not have accelerated degradation. The MPF phosphorylations are removed at a rate of k_{12}. The interactions between MPF and Cdc25A generate a positive feedback loop. MPF stabilizes Cdc25A, and Cdc25A removes the inhibitory phosphorylations on MPF, thereby activating it.

The final equation, 5.7, captures the dynamics of the active form of anaphase promoting complex, APC-P. The model assumes that the total APC concentration remains constant throughout the cell cycle, APC_{tot}. The inactive APC species, which is calculated as the total APC concentrations minus the active concentration, is activated by MPF phosphorylation at a rate of k_{12}. The MPF phosphorylation is removed at a rate of k_{13}, thereby inactivating APC. MPF activates APC, which in turn degrades all cyclin B species and Cdc25A species, thus forming a negative feedback loop.

This work analyzed the effect of multisite phosphorylation and protein network structure on the oscillatory characteristics of the mitotic oscillator, but first the effect of parameters on oscillatory behavior must be elucidated. Thus, I began with a sensitivity analysis of the base model. With a thorough understanding of how parameters affect the oscillatory characteristics of the mitotic oscillator, I began the investigation of the protein network structure. The protein network structure analysis included an analysis of the MPF activation network and the effect of multiple phosphorylations and multiple positive feedback loops.

The six MPF activation networks in the study are grouped by their phosphorylation order (Figure 10). The activating phosphorylation can occur in parallel (Figure 10A and B) or sequentially (Figure 10C, D, E, and F) with the inactivating phosphorylations. Within sequential activating phosphorylation, cyclin B and CDK1 can form either an active (Figure 10C and D) or inactive (Figure 10E and F) dimer. Finally, the inactivating phosphorylations can either happen sequentially (Figure 10A, C, and E) or simultaneously (Figure 10B, D, F). MPF activation that includes multisite phosphorylation requires sequential inactivating phosphorylations. As discussed earlier, mechanisms A, B, D, and F have been utilized in prior modeling efforts. Current biological knowledge supports mechanism C, which is incorporated into the base model in this work for comparison.

The model was then expanded to increase the number of sequential phosphorylations on Cdc25A. MPF is known to phosphorylate Cdc25A at two sites, serine 18 and 116, which stabilizes Cdc25A during mitosis [46], but Cdc25A has a total of 12 potential CDK phosphorylation sites [39]. For each additional phosphorylation, a

species was added to the system, but the model parameters remain constant. The Cdc25A species with the most phosphorylations was assumed to be stabilized.

In mammalian cells, multiple positive feedback loops are involved in the activation of MPF. To analyze the effect of multiple positive feedback loops I incorporated Wee1 dynamics into the base mitotic model. Since multiple Wee1 kinases are involved in the inhibition of MPF, Wee1A and Myt1, and their regulation by MPF differs, the model assumes that Wee1A can phosphorylate both inhibitory sites on MPF as is observed in fission yeast [181]. Wee1 inhibits MPF [20] and MPF indirectly inhibits Wee1 through phosphorylation [182] which forms a double negative, or positive feedback loop.

Although two MPF phosphorylation sites lead to Wee1A inhibition [182], there are a total of 15 potential CDK phosphorylation sites on Wee1 [29]. Therefore, sequential MPF phosphorylations are added to Wee1 to investigate the effect of multiple phosphorylations with a second positive feedback mechanism. The Wee1A species with the maximum number of phosphorylations is assumed to be inactive for each Wee1A network.

Throughout this work, bifurcation analysis was run on XPPAUT [174] with the stiff integrator function. Transient simulations were run with an adaptive timestep RK45 integrator on the three key mitotic regions (quiescent, proliferation, mitotic catastrophe) of the bifurcation diagrams in the sensitivity analysis. To generalize the results from the MPF activation reaction networks, multiple parameter sets were chosen from the base model to capture the full range of observed bifurcation structures. Since the base model incorporates the current biological knowledge, each tested MPF activation network is

compared to the base model with the parameter sets that capture the base model's full range of observed bifurcation structures. The analysis for the effects of additional phosphorylations and positive feedback loops employed the base mitotic model which incorporates the current biological knowledge.

5.2. Sensitivity Analysis

The majority of the model parameters can be separated into two groups: the parameters that increased the negative feedback strength and the parameters that increased the positive feedback strength. As the negative group parameters (k_2, k_3, k_6, k_9, k_{10}, k_{12}, k_{13}) are increased, the size of the oscillatory region increases and is shifted to higher synthesis rates (Figure 6). The amplitude, period, and size of the region of multiplicity decrease, and the oscillations become less frequency encoded.

By increasing the negative feedback strength, the system must produce more MPF and thus more cyclin to activate MPF through Cdc25A that causes the shift of the oscillatory region to higher synthesis rates. The increase in the negative feedback parameters down-regulate MPF by increasing MPF degradation (k_2, k_3), MPF inactivation (k_6), Cdc25A degradation (k_9,k_{10}), Cdc25A inactivation (k_{12}),or APC activation (k_{13}). As the negative feedback strength approaches the positive feedback strength, the difference in the MPF concentration necessary to activate APC and stabilize Cdc25A decreases, thus shrinking the delay between the positive and negative feedback activation generating non-frequency encoded oscillations.

The positive feedback group (k_8, k_{11}, k_{14}) has the opposite effect on the oscillatory characteristics as the negative feedback group (Figure 6). Increasing the parameters in the positive group decreases the oscillatory region and shifts it to lower synthesis rates. The amplitude, period, and size of the region of multiplicity increase, and the oscillations become more frequency encoded.

Increasing the positive feedback group parameters decreases the amount of MPF necessary to trigger the onset of mitosis, which causes the shift of the oscillatory region to lower cyclin B synthesis rates. Increasing Cdc25A synthesis (k_8) or stabilization (k_{11}) rates raises the amount of stable Cdc25A in the system. Increasing APC inactivation raises the amount of MPF necessary to active the negative feedback loop. Therefore,

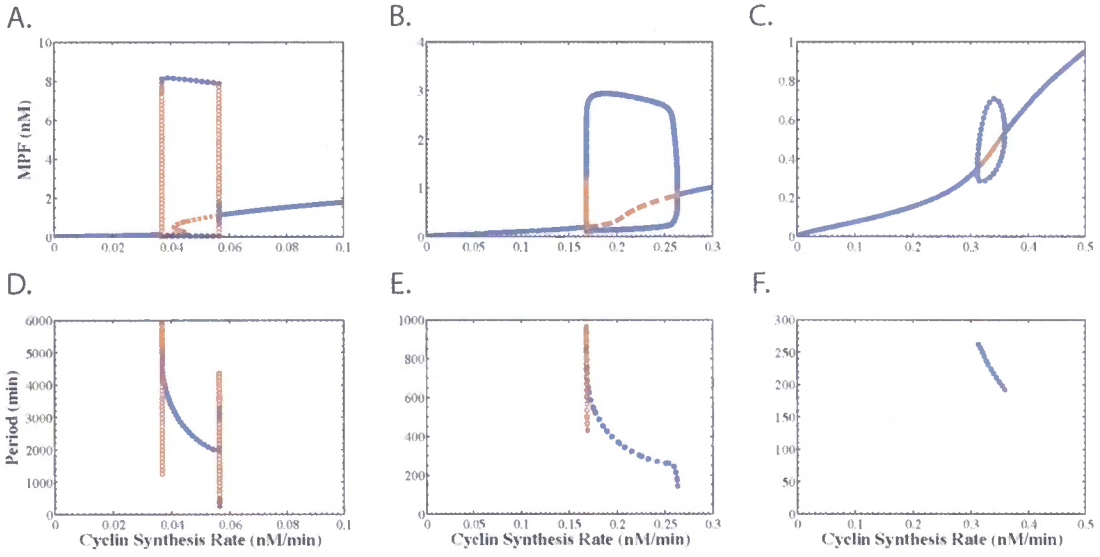

Figure 6 - Increasing negative feedback strength/Decreasing positive feedback strength. From left to right, negative feedback strength increases (k_3 = 0.015 nM^{-1} min^{-1}, 0.1 nM^{-1} min^{-1}, 0.2 nM^{-1} min^{-1}). As the negative feedback strength increases, the size of the oscillatory region increases and shifts to higher synthesis rates. The size of the region of multiplicity and amplitude decrease, and the oscillations become less frequency encoded. Also, observe the decrease in the period in the lower plots. From right to left, the positive feedback strength increases, and has the exact opposite effect on the oscillatory characteristics of the system as increasing the negative feedback strength.

increasing the positive feedback group up-regulates MPF by lowering the activation threshold of MPF or raising the activation threshold of the negative feedback loop.

Although normally considered a positive group parameter, MPF activation by Cdc25A (k_7) actually displays biphasic behavior (Figure 7). This work defines biphasic behavior as a change from increasing positive feedback characteristics to increasing negative feedback characteristics as the parameter is raised. Initially increasing the parameter increases the positive feedback strength. The size of the oscillatory region decreases and shifts to lower synthesis rates. The size of the region of multiplicity, amplitude, and period (data not shown) increase and the oscillations become more

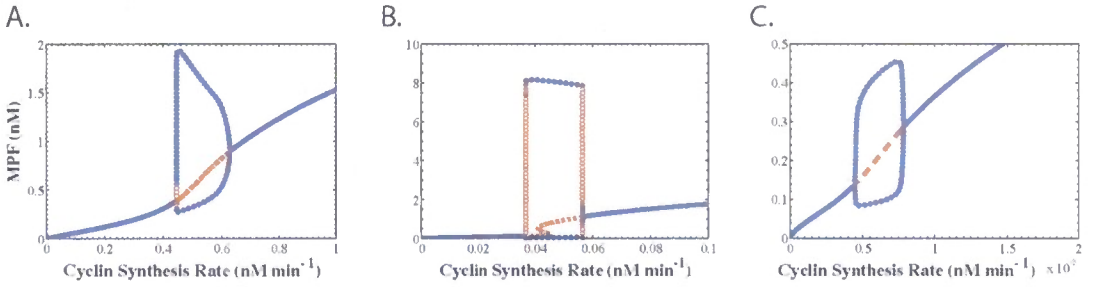

Figure 7 – Biphasic behavior of MPF activation by Cdc25A (k_7). As the activation rate is increased, the region of oscillations is shifted to lower synthesis rates and there is a decrease in the size of the region of oscillations. Initially, increasing the activation increases the region multiplicity and creates more frequency encoded oscillations, but further increase destroys the region of multiplicity and creates less frequency encoded oscillations. From left to right, $k_7 = 0.1$ nM^{-1} min^{-1}, 0.5 nM^{-1} min^{-1}, 7 nM^{-1} min^{-1}.

frequency encoded.

However, further increase in MPF activation rate weakens the positive feedback strength because of the protein network structure of the Cdc25A stabilization mechanism. As MPF activation rate increases, the concentration of Cdc25A necessary to activate MPF decreases. Thus, the unstable, rapidly degraded Cdc25A species concentrations become more significant decoupling the positive feedback mechanism of MPF induced

stabilization of Cdc25A. Since less Cdc25A is necessary to activate MPF, the oscillatory region is decreases and shifts to lower cyclin synthesis rates. The weakened positive feedback does not fully activate MPF before APC is activated which decreases the amplitude, period, and size of the region of multiplicity, and the oscillations are less frequency encoded.

The dimerization and dissociation of cyclin B and CDK1, k_4 and k_5, do not affect the positive or the negative feedback strength. Rather, both parameters affect the total amount of monomeric cyclin B observed in the system and where it oscillates (Figure 8). When dimerization of cyclin B and CDK1 is rapid and stable, cyclin B concentrations are negligible because all cyclin monomers are dimerized with CDK1. Slow dimerization rates create a barrier to the MPF activation subsystem, and thus monomeric cyclin B accumulates in order to dimerize into MPF. Hence, monomeric cyclin B accumulation is driving the oscillations in the system. Accumulation of monomeric cyclin B is inefficient for the cell since the majority of the cyclin B synthesized is not utilized in MPF to initiate mitosis. Alternatively, high cyclin B CDK1 dissociation rates destabilize MPF during mitosis. During interphase, cyclin B and CDK1 dimerize to form MPF that is rapidly inactivated by the Wee1 family of kinases, and therefore cyclin B monomer concentration is negligible. When Cdc25A activates MPF during the initiation of mitosis, the rapid dissociation results in MPF splitting into cyclin B and CDK1 that generates a spike in cyclin B monomer concentration. Thus, a high dimerization rate and low dissociation rate allow a cell to efficiently utilize synthesized monomeric cyclin B and generate an autocatalytic peak concentration in MPF.

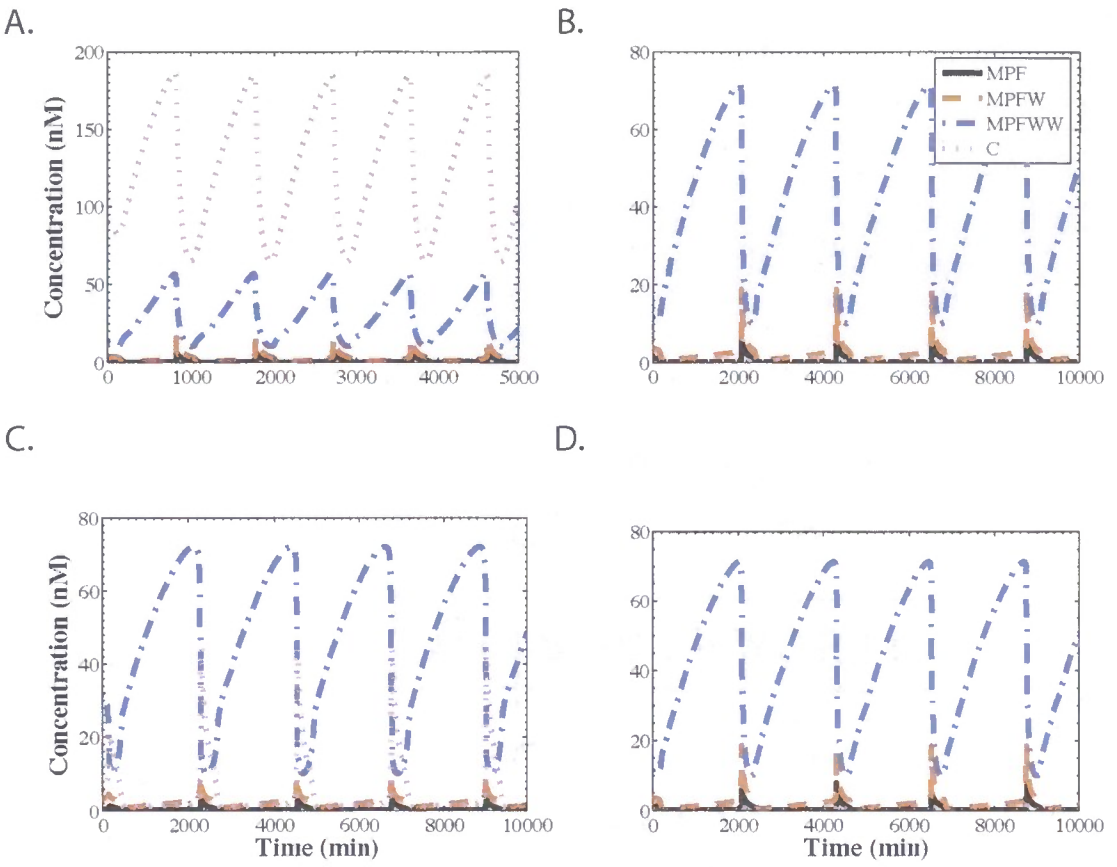

Figure 8 - Dimerization and dissociation of cyclin B and CDK1. Figure A has a low dimerization rate (k_4 = 0.0006 min^{-1}). Monomeric cyclin accumulation drives the system oscillations. Figure B has a high dimerization rate (k_4 = 0.6 min^{-1}). Monomeric cyclin efficiently dimerizes into MPF and MPF dynamics drive the oscillations. Figure C has a high dissociation rate (k_5 = 100 min^{-1}). The MPF dimer is unstable and quickly dissociates. Thus, the autocatalytic activation of MPF generates a monomeric cyclin concentration peak rather than a MPF concentration peak. Figure D has a low dissociation rate (k_5 = 1 min^{-1}). MPF is a stable dimer, and the autocatalytic activation of MPF generates a MPF concentration peak.

With a thorough understanding of the effect of the parameter values on the oscillation characteristics, I grouped the observed parameter sets into four categories. The first category has both multiplicity of steady states and frequency encoded oscillations to capture ideal mitotic oscillator characteristics (Figure 9A). The second category has frequency encoded oscillations without multiplicity of steady states, and the third category has multiplicity of steady states without frequency encoded oscillations.

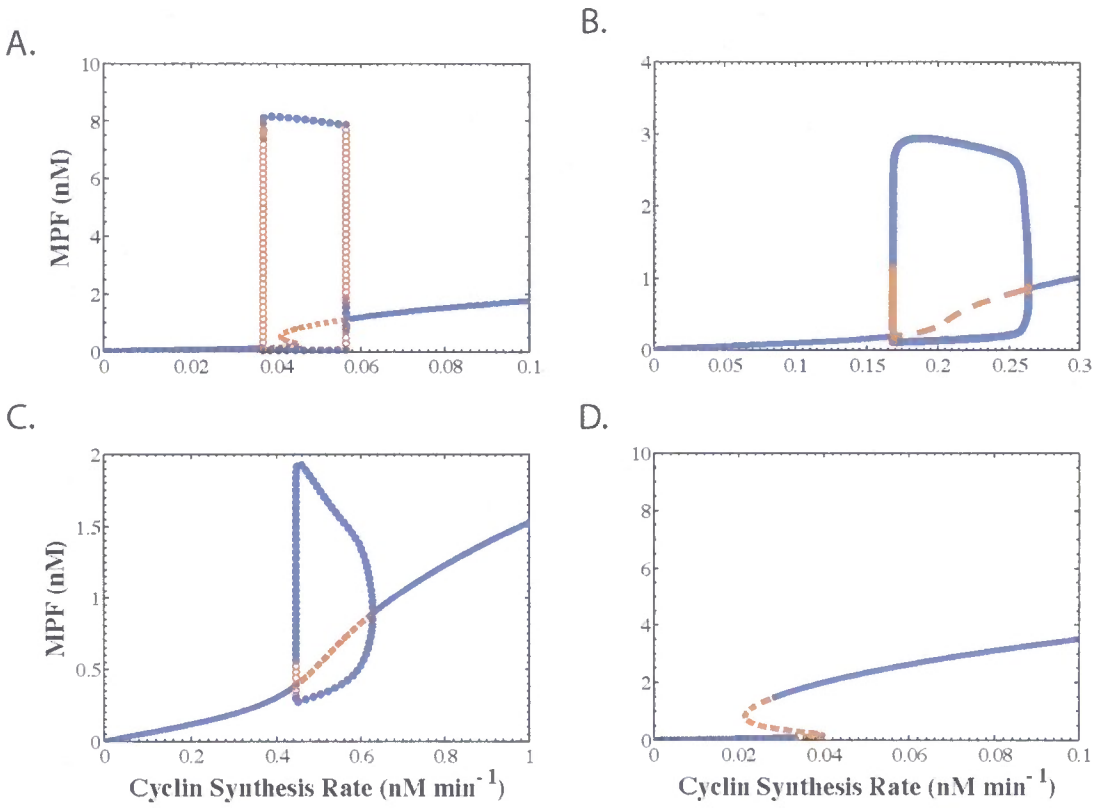

Figure 9 - Observed system behavior for base mitotic model. All oscillatory behaviors have a lower steady state that represents quiescent and G2 arrested cells and a high steady state that represents mitotic arrested and catastrophe cells. System A has frequency encoded oscillations and a region of multiplicity of steady states (base parameter set). System B has frequency encoded oscillations but does not have a region of multiplicity of steady states ($k_3 = 0.1$ nM^{-1} min^{-1}). System C generates nonfrequency encoded oscillations and does not have a region of multiple steady states ($k_7 = 0.1$ nM^{-1} min^{-1}). System D is bistable ($k_{10} = 0.1$ nM^{-1} min^{-1})

The final category is bistable without oscillation. One parameter set from each of these categories was analyzed for all MPF network structures.

In the following section, this work switches from analyzing the varying parameter values to elucidating the effect of different protein network structures. Many different MPF activation networks were employed in prior models, and therefore this analysis shed light into the motivation for cells to evolve to the present day mechanism. One parameter set from each of the categories from the sensitivity analysis was analyzed for every MPF activation network to generalize the results.

5.3. MPF Phosphorylation Reaction Network

The MPF reaction networks are grouped into 3 different groups by their phosphorylation order (Figure 10). First, parallel and sequential activating and inactivating phosphorylations are compared. Then, active and inactive cyclin B CDK1 dimerization are compared. Finally, sequential and simultaneous inactivating phosphorylations are compared. A parameter set from each of the four categories discussed in the sensitivity analysis was utilized to ensure the observed results are generalizable different regions of the parameter space. All six networks were analyzed, and the results were qualitatively consistent based on the phosphorylation structure.

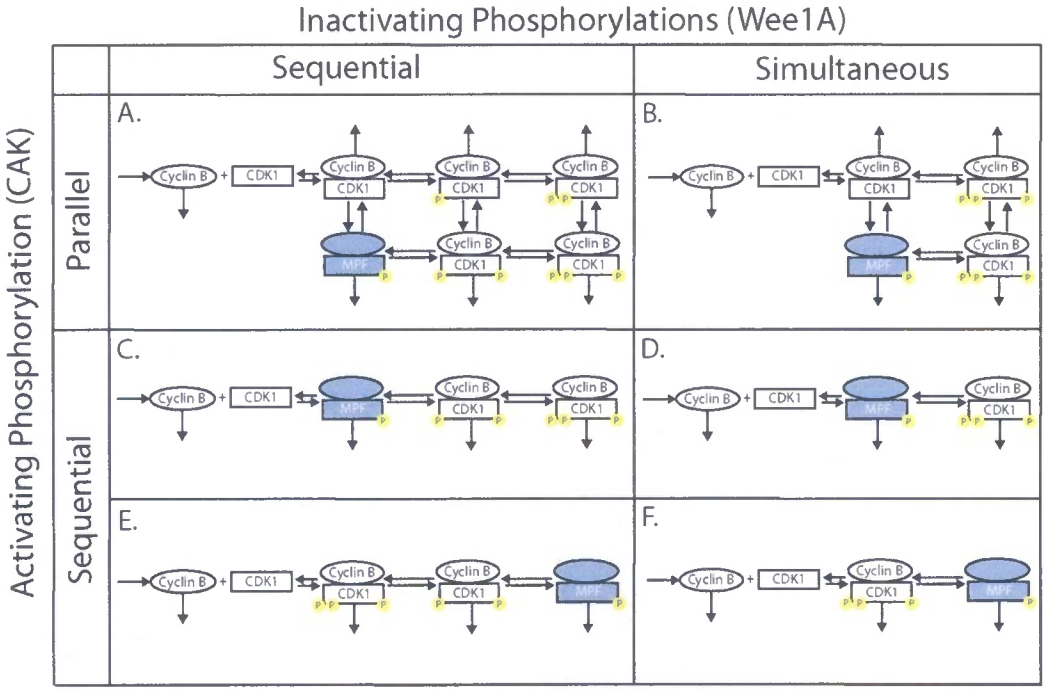

Figure 10 - MPF phosphorylation reaction networks. The reaction networks are organized by their phosphorylation structure. The squares represent CDK1 and the ovals represent cyclin B. The small circles represent the phosphorylations. The inhibitory phosphorylations are on the left side of CDK1 and the activating phosphorylation is on the right. Active MPF is shaded blue. The activating phosphorylation can occur in parallel (A and B) or sequentially (C, D, E, and F) with the inactivating phosphorylations. Within sequential activating phosphorylation, cyclin B and CDK1 can either form an active (C and D) or inactive (E and F) dimer. Finally, the inactivating phosphorylations can either happen sequentially (A, C, and E) or simultaneously (B, D, F).

The first group has parallel activating and inactivating phosphorylations. Cyclin B and CDK1 dimerize to form a complex without phosphorylations on CDK1that can then be phosphorylated by either CAK or Wee1 species. Two parameters (k_{cak} and k_{dcak}) are added to the model to describe the rate of phosphorylation and dephosphorylation at the activating site of CDK1, respectively. The ratio of k_{cak}/k_{dcak} was employed to compare parallel and sequential activating phosphorylations. When the ratio is very large, the activating phosphorylation event is rapid and stable and transforms the parallel models (Figure 10A and B) into sequential models (Figure 10C and D).

All MPF species that do not have the activating phosphorylation by CAK including monomeric cyclin B cannot be activated by Cdc25A to initiate mitosis. These inactive MPF species are referred to as CAK unphosphorylated MPF species. The remaining MPF species can be activated by Cdc25A to initiate mitosis and are referred to

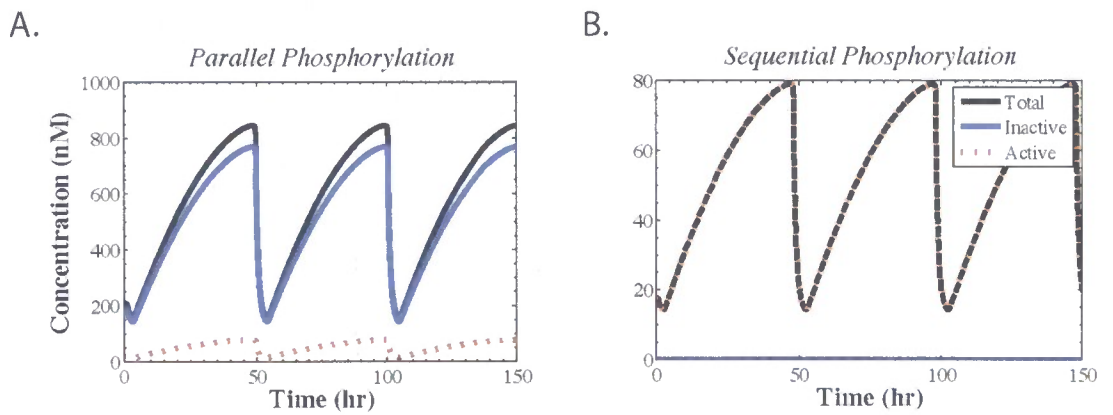

Figure 11 - Parallel vs. sequential activating phosphorylation sequence. The black line is total cyclin B concentration. The blue line represents concentration of CDK1 species that have not been phosphorylated at the activating site and monomeric cyclin B. The dashed red line represents the concentration of CDK1 species that have been phosphorylated at the activating site and therefore have the ability to become active MPF. When the activating phosphorylation occurs in parallel with the inactivating phosphorylations, the majority of the CDK1 remains inactive and therefore cannot become active MPF. When the activating phosphorylation occurs sequentially with the inactivating phosphorylations following, the majority of CDK1 has the activating phosphorylation and can be activated by Cdc25A to active MPF. (Mechanism A base parameter set, Parallel $k_{cak}/k_{dcak} = 10/100 = 0.1$, Sequential $k_{cak}/k_{dcak} = 10/0.0001 = 100000$)

as CAK activated MPF species. When the ratio of k_{cak}/k_{dcak} is small there is parallel phosphorylation, and the majority of cyclin B remains in CAK unphosphorylated MPF species (Figure 11). When the ratio of k_{cak}/k_{dcak} is large the activating phosphorylation occurs before the inactivating phosphorylations, and the majority of the cyclin B is in CAK activated MPF species (Figure 11). Therefore, the more efficient usage of cyclin B occurs when the activating phosphorylation occurs sequentially before the inactivating phosphorylations and is supported by experimental observations. CAK phosphorylation is required for the stabilization of the cyclin B CDK1 dimer [19], and cyclin B must bind CDK1 before Wee1 and Myt1 can phosphorylate CDK1[17].

The next group is defined by the dimerization of cyclin B and CDK1 into an active (Figure 10C and D) or inactive (Figure 10E and F) MPF complex. To form an active dimer, the activating phosphorylation occurs before the inactivating phosphorylation. To form an inactive dimer, both the activating and inactivating phosphorylations occur at dimerization.

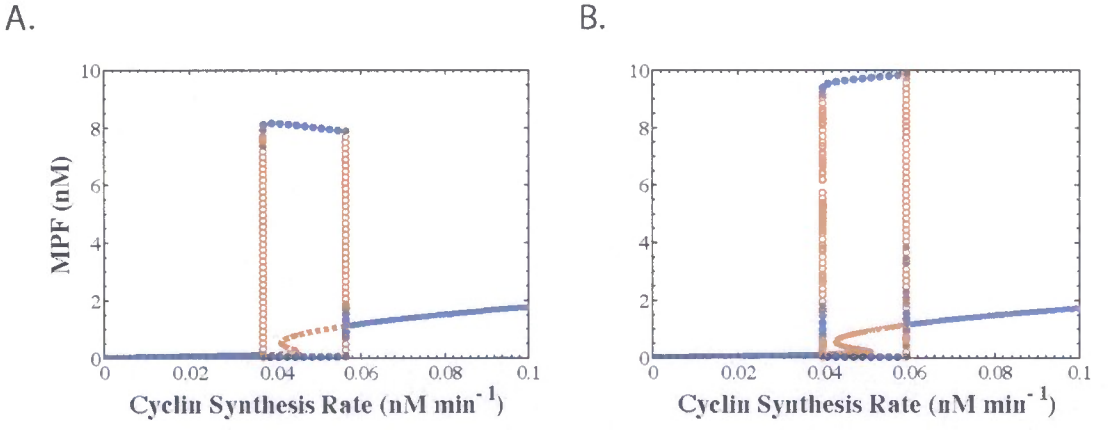

Figure 12 - Cyclin B CDK1 dimerization to active (A) and inactive (B) complex. MPF mechanism C is shown in figure A with the base parameter set and when comparing the MPF mechanism E in figure B, there is little qualitative difference. Both systems exhibit frequency encoded oscillations and a region of multiple steady states. Similar qualitative results were obtained when comparing MPF mechanisms D and F.

The results show that is not a qualitative difference in bifurcation diagrams for the active dimer and inactive dimer groups (Figure 12). The main qualitative difference between the active and inactive dimerization is observed when analyzing two parameter bifurcation plots (Figure 13). When cyclin B and CDK1 dimerize to an active MPF species, the MPF activation rate by Cdc25A has a lower bound, and below the lower bound the system does not oscillate (Figure 13A). Furthermore, there is a bounded region for the liable Cdc25A degradation rate (Figure 13C). Thus, if the liable Cdc25A degradation rate is unregulated above a certain rate the system no longer maintains the ability to oscillate. Up-regulated degradation of CDC25A is a mechanism utilized by the cell to arrest the cell cycle in response to DNA damage [46].

Alternatively when cyclin B and CDK1 dimerize to an inactive MPF species, the MPF activation rate by Cdc25A has a limitless lower bound (Figure 13B). Moreover, the liable Cdc25A degradation rate can increase orders of magnitude, and the system has the ability to oscillate if it synthesizes cyclin fast enough (Figure 13D). Hence, the cell has lost two mechanisms to arrest the cell cycle. Furthermore, since cyclin B binding is necessary for CAK and Wee1/Myt1 phosphorylation [17], and CAK phosphorylation is necessary for stabilization of the dimer [19], the dimerization cannot form an inactive MPF species.

The final grouping of MPF networks is whether the inactive phosphorylations occur sequentially (Figure 10A, C, and E) or simultaneously (Figure 10B, D, and F). When the inactivating phosphorylations occur sequentially, two phosphorylation events, there exist parameter sets that can generate ideal cell cycle oscillatory characteristics. Sequential dephosphorylation by Cdc25 has been observed experimentally [34], and Y15

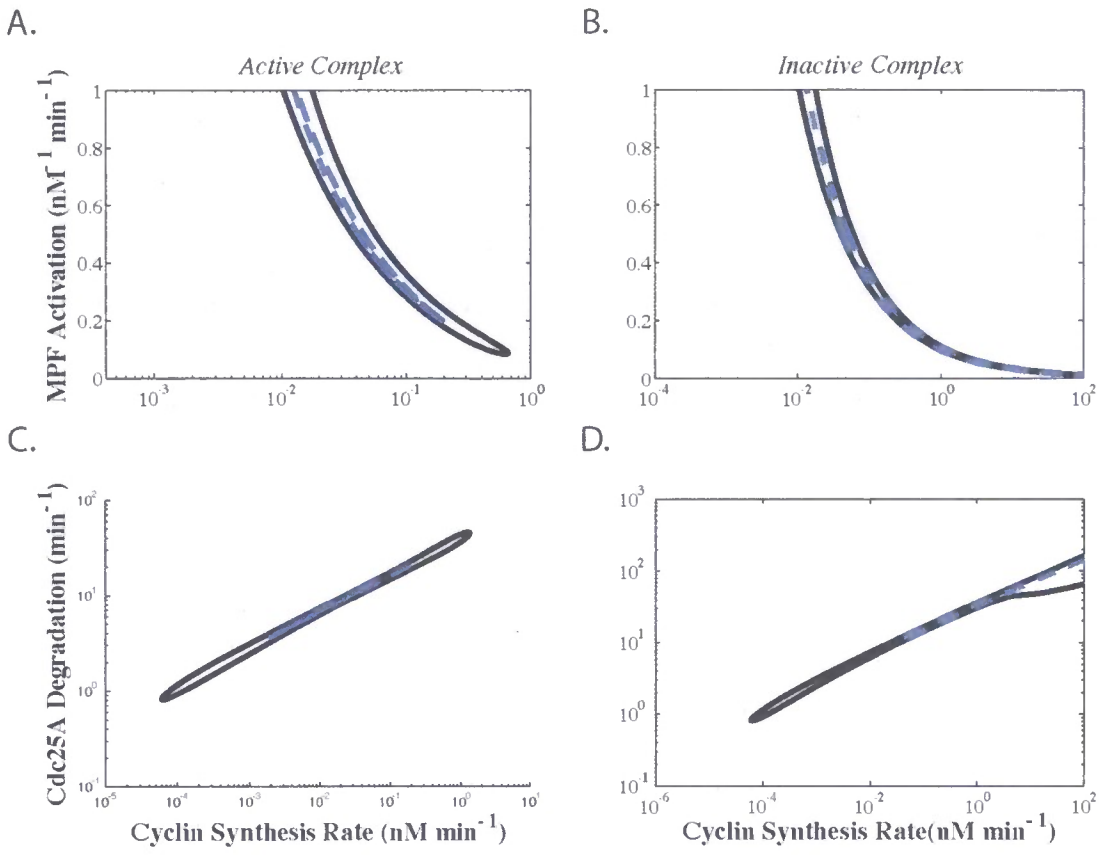

Figure 13 - Dimerization to active vs. inactive MPF complex. In the two parameter bifurcation plots, the dashed lines are the limit points, which enclose the region of multiplicity of steady states, and the solid lines are the Hopf points, which enclose the region of oscillations. Figures A and B plot the rate of Cdc25A activation of MPF vs. cyclin B synthesis rate for MPF mechanisms C and E, respectively. Figures C and D plot the nonspecific degradation rate of liable Cdc25A species vs. cyclin B synthesis rate for the same respective mechanisms. Both the Cdc25A activation rate of MPF and nonspecific degradation rate of liable Cdc25A are bounded when cyclin B and CDK1 form an active complex (A and C). On the other hand, when cyclin B and CDK1 form an inactive complex, the system retains the ability to oscillate at low MPF activation rates and high nonspecific liable Cdc25A degradation rates (B and D).

phosphorylation has only been observed with T14 phosphorylation [21] which suggests sequential phosphorylation.

When the inactivating phosphorylations occur simultaneously in one phosphorylation event, the mechanism does not generate ideal cell cycle dynamics (Figure 14A). The oscillations are sinusoidal, and thus the transition into mitosis is not abrupt. This behavior is in stark contrast to the switch-like transitions observed experimentally. In fact, multiplicity is not observed over the entire oscillatory space of

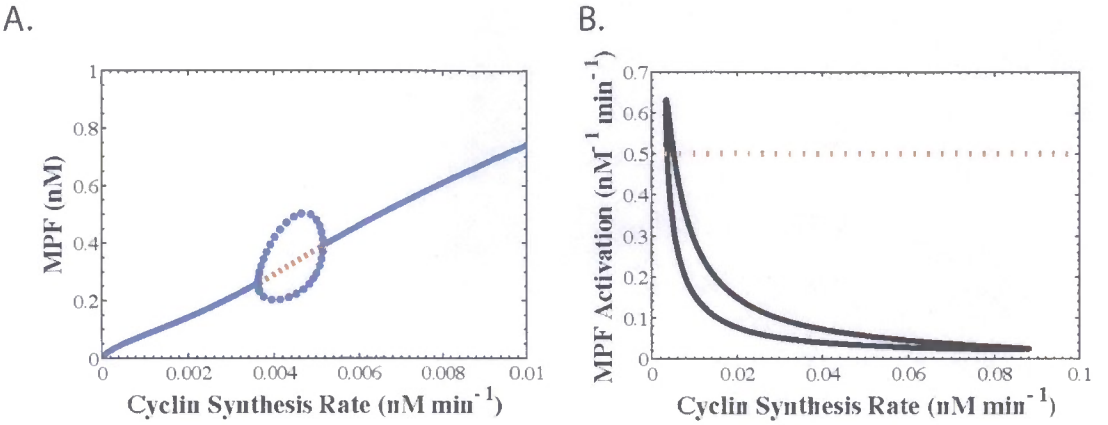

Figure 14 - Simultaneous inactivating phosphorylation. Figure A displays the bifurcation diagram for MPF reaction network D with the base parameter set (**Table 1**). Although the system with sequential inactivating phosphorylations generates realistic cell cycle oscillatory characteristics with multiplicity of steady states and frequency encoded oscillations for this parameter set, the MPF reaction network with simultaneous inactivating phosphorylations does not generate realistic oscillation characteristics. Multiplicity is not observed throughout the MPF activation rate by Cdc25A oscillatory parameter space (Figure B). Solid black line represents Hopf bifurcation points and encloses the oscillatory region (Figure B).

the MPF activation (Figure 14B). The loss of multiplicity is because of the loss in the nonlinear term in the MPF network when the inactivating phosphorylation is assumed to occur in a single step. If the intermediate inactive MPF species is assumed to be at pseudo steady state, $\left(\frac{d[MPF-P]}{dt}=0\right)$, then the resulting ODEs retain the nonlinearity and the system qualitatively exhibits the original system (see Appendix I). The loss of nonlinearity supports my hypothesis that multisite phosphorylation is crucial in the MPF activation network.

5.4. Cdc25A Phosphorylations

After determining that multisite phosphorylation is crucial in the MPF activation network, I investigated multisite phosphorylation on Cdc25A. The system has a region of multiplicity when Cdc25A has linear stabilization (Figure 15D). The nonlinearity is

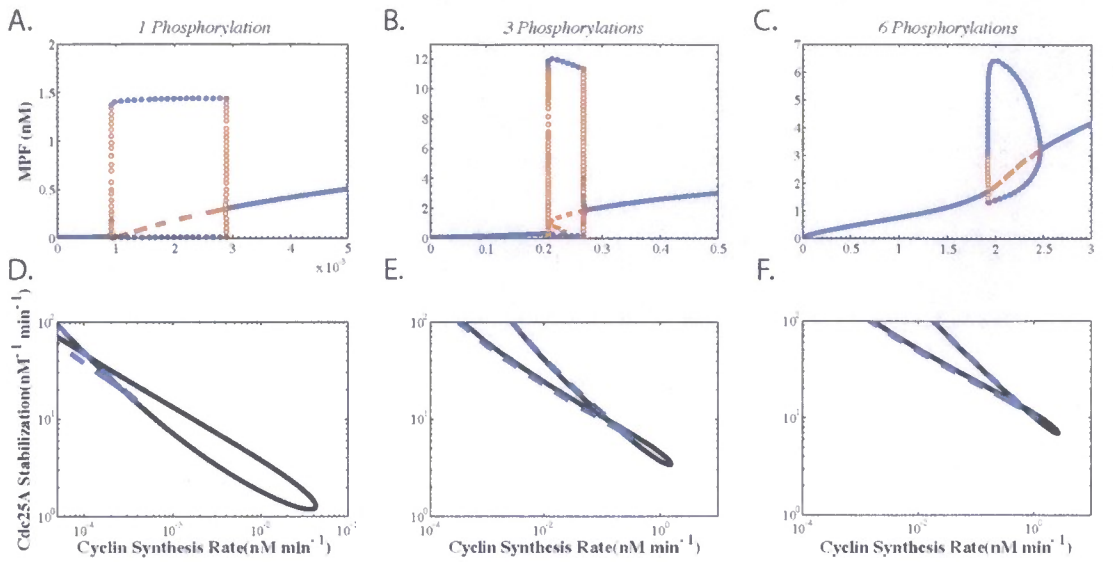

Figure 15 - Effect of sequential Cdc25A phosphorylations. Top figures are bifurcation plots with increasing number of sequential phosphorylations of Cdc25A and constant Cdc25A stabilization rate (k_{11}=7.5 $nM^{-1}min^{-1}$). The Cdc25A species with the maximum number of phosphorylations is considered to be stable for each simulation. All Cdc25A species with less than the maximum number of phosphorylations are considered liable. Bottom figures are two parameter bifurcation plots for Cdc25A stabilization by MPF phosphorylation vs. cyclin B synthesis rate. Increasing the number of Cdc25A phosphorylations has a biphasic effect on the size of the region of multiplicity when the Cdc25A stabilization rate is constant. Initially, the system with 1 phosphorylation does not have a region of multiple steady states. Increasing the system to 2 phosphorylations increases the region of multiple steady states, and an increases to 3 phosphorylations (Figure B) increases the size of the region of multiple steady states further. Further increase in the number of Cdc25A phosphorylations results in a decrease in the size of the region of multiple steady states (Figure C). From the two parameter bifurcation plots (Figure D,E,F), the increase in the number of Cdc25A phosphorylations shifts the region of multiplicity (dashed grey line) further into the region of oscillations (solid black line). The region of oscillations is expanded over a larger region of cyclin Synthesis rate and the minimum Cdc25A stabilization rate where oscillations are observed is increased.

present only in the MPF activation network, which reiterates the importance of sequential inactivating phosphorylations on CDK1.

Increasing the number of Cdc25A phosphorylations increases the size of the oscillatory and multiplicity regions and shifts the oscillatory behavior to higher synthesis rates (Figure 15). Higher Cdc25A stabilization rates are necessary for the system to oscillate while the parameter set is fixed. There is a threshold below which addition of phosphorylations increases the size of the region of multiplicity and amplitude, and the oscillations become more frequency encoded. Above the threshold, additional

phosphorylations decrease the size of the region of multiplicity and amplitude, and the oscillations become less frequency encoded.

Each additional Cdc25A phosphorylation increases the threshold concentration of MPF necessary to stabilize the protein because the parameter set remains constant. Thus, a larger Cdc25A stabilization rate must be utilized in order to maintain the positive feedback strength as the number of phosphorylations increase. If the stabilization rate is held constant and the number of Cdc25A phosphorylations increases, the oscillatory region is eventually destroyed when the concentration of MPF necessary to stabilize Cdc25A exceeds the concentration necessary to activate APC.

5.5. Additional Positive Feedback Loop

To analyze the effect of multiple positive feedback loops this work incorporated Wee1 dynamics into the base mitotic model (Figure 16). Wee1A dynamics introduce two new parameters to the model, k_{15} and k_{16}. The activation rate, k_{15}, is set to unity and the inactivation rate is catalyzed by active MPF. When there is no inactivation of Wee1 (k_{16}=0), the original system dynamics are generated. When the inactivation is increased, which adds the positive feedback, the amplitude of MPF increases (Figure 17). There is also a slight decrease in the region of oscillations and an increase in the region of

Figure 16 - Wee1 Network. Wee1A species with less than N phosphorylations are active. The Wee1A species with N phosphorylations is inactive.

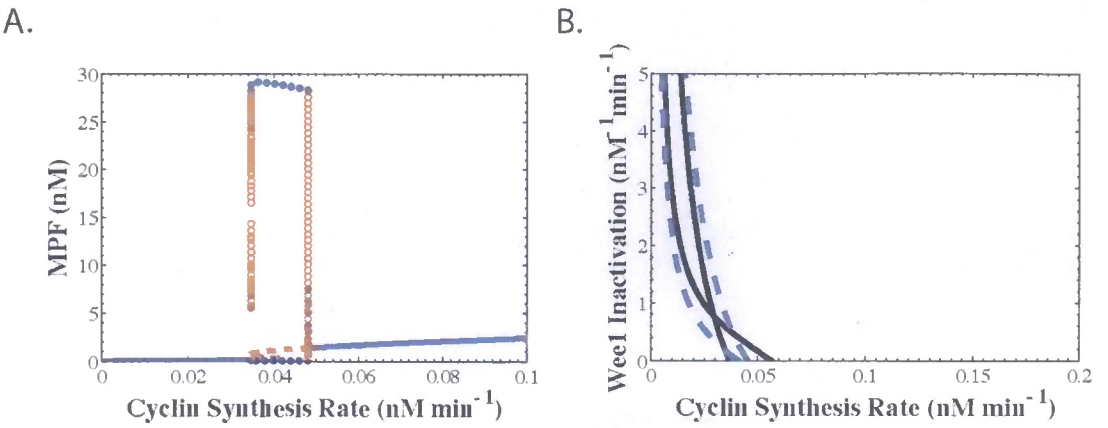

Figure 17 - Incorporation of Wee1 dynamics. The bifurcation diagram for k_{16}=0.2 is shown in figure A. The amplitude of the oscillations is 3 fold larger than the original system. There is a slight decrease and increase in the size of the regions of oscillations and multiplicity, respectively (figure B). Figure B is a two parameter bifurcation of Wee1A inactivation by MPF phosphorylation, k_{16}, vs. cyclin B synthesis rate. Dashed lines are limit points, which enclose the region of multiplicity. Solid lines are Hopf bifurcation points, which enclose the region of oscillations.

multiplicity. By inhibiting Wee1 and stabilizing Cdc25A the system shifts to active MPF. Without a constant inactivation from Wee1, less MPF is necessary to stabilize Cdc25A and more MPF is activated as Wee1 shuts off. Hence, a cell activates MPF more efficiently when both the inhibition of Wee1 and stabilization of Cdc25A are present.

As the number of Wee1A phosphorylations increases, the size of the oscillatory region expands over a larger range of cyclin B synthesis rates at low Wee1A inactivation rates (Figure 18). In the lower Wee1A inactivation rates, the rate of Cdc25A stabilization is faster than Wee1A inactivation. Therefore, Cdc25A is stabilized before Wee1A is inactivated, and the oscillatory characteristics resemble the base system dynamics (Figure 17). As the Wee1A inactivation rate increases, there is an expansion of the oscillatory region to higher cyclin B synthesis rates. The expansion is enhanced as the number of phosphorylations increases (Figure 18B and C). In this region of Wee1A inactivation rates, Wee1A inactivation is faster than Cdc25A stabilization. The oscillatory region generated by Cdc25A stabilization remains the same, and therefore the lower Hopf

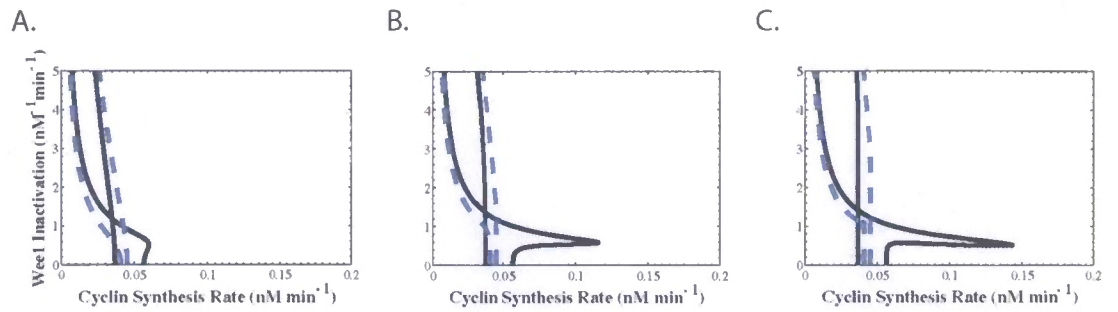

Figure 18 - Multiple Wee1A Phosphorylations. From left to right Wee1A has 2, 4, and 8 phosphorylations, respectively. The two parameter bifurcations plot Wee1A inactivation rate vs. cyclin B synthesis rate. Solid lines are Hopf bifurcation points and enclose the region of oscillations. Dashed lines are the limit points, which enclose the region of multiplicity. As the number of Wee1 phosphorylations increases, the size of the region of oscillations increases at low Wee1A inactivation rates. The size of the region of multiplicity and oscillations increases and decreases, respectively, as the inactivation rate increases further. At high Wee1A phosphorylations, new Hopf bifurcations and limit points are generated which are not observed in the base model (Figure C).

bifurcation point does not move. In the region of expansion to higher cyclin B synthesis rates, Wee1A is inactivated which leads to Cdc25A stabilization. Further increase in Wee1A inactivation rate, increases the positive feedback strength so it is not comparable to the negative feedback strength. Hence for high Wee1A inactivation rates, the system is bistable.

With 8 phosphorylations, the expansion of the region of oscillations has dipped down where it now overlaps with the original region of oscillations (Figure 18C). Thus, for a region of the Wee1A inactivation rate space, there are four Hopf bifurcations. For a slightly larger Wee1A inactivation rates, the limit points begin to overlap and there is a region of the Wee1A inactivation rate space where there are 4 limit points. This phenomenon is enhanced as the number of phosphorylations increases. Although the model can exhibit this behavior, I hypothesize this behavior does not occurs naturally. To observe the generation of additional Hopf and limit points, Wee1 must have 6 to 13 more phosphorylations than Cdc25A. Since Cdc25A has 12 potential sites [39]and Wee1A has 15 CDK phosphorylation sites [29], there is not a significant difference in the

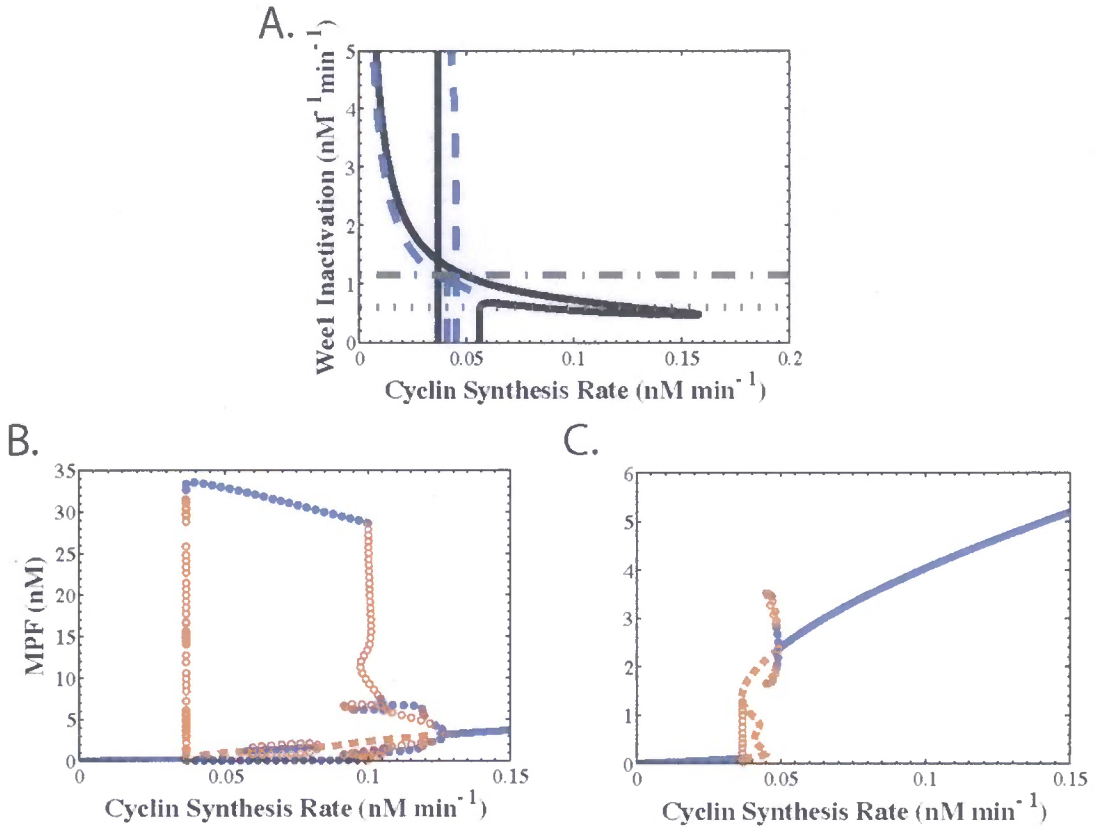

Figure 19 - Wee1A with 15 phosphorylations. The expansion of the region of oscillations to higher cyclin B synthesis rates overlaps for a region of the Wee1A inactivation rates. This results in systems with four Hopf bifurcations (Figure B). In figure B (k_{16}=0.6 nM^{-1}min^{-1}), there is a region of the cyclin B synthesis rate where a steady state exists with a stable limit cycle. There is also birhythmic oscillations, existence of 2 stable limit cycles, at high cyclin B synthesis rates. At higher Wee1A inactivation rates, the limit points overlap generating a parameter range where four limit points coexist (Figure C). In figure C (k_{16}=1.15 nM^{-1}min^{-1}), a double S is observed for a region of the cyclin B synthesis rates where five unstable steady states coexist.

number of phosphorylations necessary to generate the other bifurcation points. Furthermore, the parameter region over which the multiple bifurcation points occur is relatively small. Cell heterogeneity would likely negate these states.

Therefore, the overall role of Wee1 inhibition is to utilize cyclin B more efficiently and generate a larger amplitude of MPF during the initiation of mitosis. In vivo, Wee1 has three more phosphorylations than Cdc25A, thereby leading us to conclude that Cdc25A is activated before Wee1 is inactivated, and the three additional

phosphorylation on Wee1 expand the region of cyclin B synthesis rates over which the system oscillates.

Chapter 6 - Linking a mitotic oscillator to the extracellular environment via ATP

The next step in developing a proliferation model for a bio-artificial tissue regeneration model is to link the proliferation model to the environment. Therefore, I linked the previously developed mitotic oscillator model to the extracellular environment. Specifically, I incorporated ATP, a cellular energy source, into a mitotic oscillator and then correlated the intracellular ATP concentration to the extracellular glucose concentration.

Although a plethora of models has been developed for the cell cycle, relatively few have linked them to the extracellular environment. Obeyesekere and coworkers developed three models for the initiation of DNA synthesis that linked extracellular growth factor concentration directly to cyclin D and cyclin E synthesis [162-164]. Novak and Tyson developed a transition model for the restriction point in which the transcription factors for cyclin D and cyclin E were linked directly to extracellular growth factor [170]. Alarcon incorporated a protein that sensed extracellular oxygen levels into one of Tyson's early mitotic oscillators to include to investigate hypoxia in cancer cells [160]. Most recently, Battogtokh and coworkers linked an external oscillator to the cell cycle by periodically forcing specific species with small amplitude variability [96].

However, this model is the first to link extracellular glucose to a mitotic oscillator. Unlike earlier models, glucose does not be linked directly with protein synthesis, but rather to intracellular ATP, which affects multiple areas of the model. The extracellular environment plays a vital role in wound and tissue regeneration in humans.

During wound healing and regeneration of tissue, cells migrate into the void to proliferate and heal the wound. As cells migrate from the healthy tissue at the periphery into the wound or damaged tissue, their environment changes. Since the extracellular environment modulates cellular division time [10], a model for bio-artificial tissue regeneration must include a cellular proliferation model that is modulated by the extracellular environment.

The following section presents the link between the cell cycle and ATP. The link between the cell cycle and ATP was then incorporated into the mitotic oscillator developed in chapter 5 in the following section. Next, a sensitivity analysis is performed on the model, followed by the model tuning for a relative ATP concentration. Then, a Wee1 inhibition network analysis was performed, and finally, the ATP model is linked to extracellular glucose.

6.1. ATP and the Cell Cycle

Cells uptake nutrients in the environment and convert them into biomass and energy, one form of which is ATP. In 1942, Monod proposed a relationship between cellular growth rate and a main nutrient source [183]:

$$\mu = \frac{\mu_{\max} S}{K_g + S}. \tag{6.1}$$

The cellular growth rate, μ, exhibits saturable kinetics with respect to the main nutrients source, S, with a maximum growth rate of μ_{max}. Recently, Lu and coworkers observed Monod growth kinetics for Chinese hamster ovary cells in limited glucose conditions [10]. The important new aspect of this work was that Lu and coworkers measured intracellular ATP concentrations in limited glucose conditions (Figure 20).

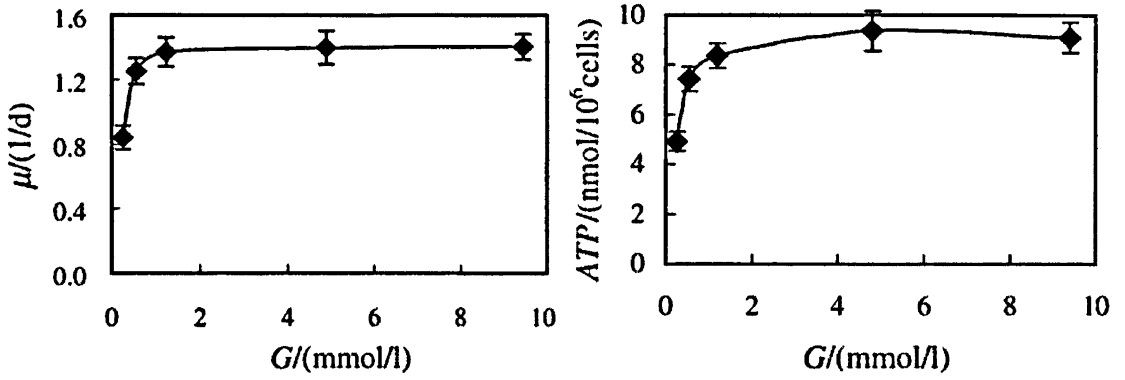

Figure 20 – Growth kinetics and intracellular ATP concentrations for Chinese hamster ovary cells under limited glucose conditions. Growth kinetics, μ, are captured by Monod growth kinetics. Intracellular ATP concentrations follow similar saturable kinetics under limited glucose conditions. Figures reprinted from Lu and coworkers' recent paper [10].

Intracellular ATP concentrations follow similar saturable kinetics as the cellular growth rate. Thus, one mechanism limiting the growth rate is the amount of cellular energy, ATP.

6.2. Model

I began with the final model developed in chapter five and incorporated more of the details of mitosis (Figure 21). The model equations and parameter sets can be found in ATP Model Equations and Parameters . The cyclin B CDK1 dimerization process was expanded to include CAK phosphorylation. CAK phosphorylation on CDK1 is necessary to stabilize the dimer, because the cyclin B-CDK1dimer is not observed without the phosphorylation experimentally [19]. Wee1A is incorporated into the network, because previously in this work Wee1A was observed to be essential to efficiently utilize cyclin B during MPF activation. Synthesis and degradation terms were added to the Wee1A network, because MPF phosphorylation on serine 123 of Wee1A induces a proteolysis cascade, thus up-regulating Wee1A degradation [17, 28]. To reduce the number of

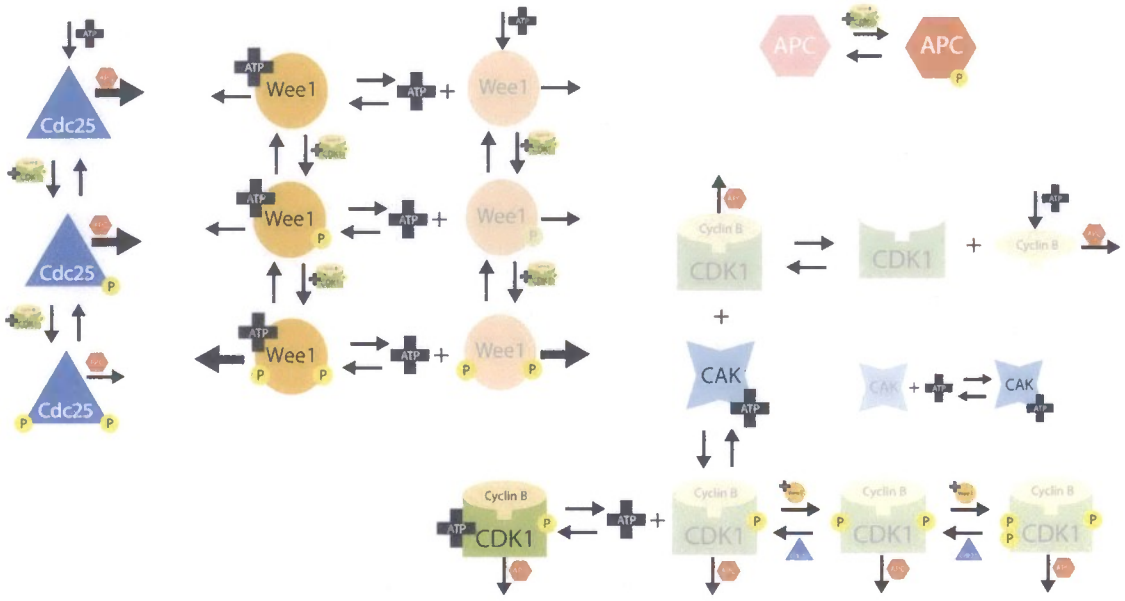

Figure 21 – Mitotic Oscillator with ATP Integrated. Transparent species are not active whereas solid species are in their active form. Arrows pointing away from the protein into space are degradation terms. The larger arrows correlate with increased degradation. The yellow circles with P's in the middle symbolize individual phosphorylations. Enzymes involved in reactions are shown as small icons next to the reaction arrow. In the case of protein synthesis, ATP is a necessary substrate. The central protein in mitosis is MPF that is formed by the trimer of cyclin B, CDK1 and ATP. MPF forms a positive feedback and double negative feedback loop with Cdc25A and Wee1, respectively. MPF stabilizes Cdc25A by phosphorylation that is otherwise highly degraded. Cdc25A removes the inhibitory phosphorylations on inactive species of MPF activating them. Conversely, MPF destabilizes Wee1 by increasing its degradation by phosphorylation. Wee1 inhibits MPF by phosphorylation within MPF's ATP binding pocket. MPF forms a negative feedback loop with APC by activating APC through phosphorylation. Consequently, active APC degrades all cyclin B species and Cdc25A species.

proteins and therefore the model complexity, the model assumes that Wee1A can phosphorylate MPF on both inhibitory phosphorylation sites on CDK1.

The Cdc25A and APC subnetworks remain the same as the base model from the mitotic oscillator. The cyclin B CDK1 dimerization process was expanded to include CAK phosphorylation on CDK1 because the dimer is not observed without the phosphorylation experimentally [19]. CAK activity remains roughly constant throughout the cell cycle [11], and therefore the model assumes that total CAK levels are constant.

I then incorporated ATP into the model. The first process affected by changes in ATP concentration is protein synthesis [184]. I assume that the requirement of ATP for

protein synthesis has saturable kinetics and affects all synthesized proteins in the same manner. Therefore, each protein has a maximum synthesis rate, but all proteins have the same Michaelis-Menten parameter, K_m. Saturable kinetics are a plausible assumption because ATP concentrations are orders of magnitude larger than the proteins involved in the cell cycle [178, 185].

All of the kinases in the model, MPF, Wee1, and CAK require ATP to phosphorylate their substrates [11]. The model assumes that the kinases bind to ATP, which in turn phosphorylate their substrates. Additionally, this model assumes that the kinase-substrate binding and phosphorylation reactions are rapid compared to the kinase substrate interaction, and therefore, that the kinase-substrate complex is not incorporated into the model.

The average intracellular concentration of ATP is modulated by extracellular glucose and remains roughly constant throughout the cell cycle [10, 186]. Therefore, this work employs intracellular ATP concentration as the bifurcation parameter. I performed a sensitivity analysis to elucidate the effect of intracellular ATP on the cell cycle dynamics. Next, I investigated the Wee1 subnetwork to gain insight into the two mechanisms by which MPF can down regulate Wee1 activity at the initiation of mitosis: kinase inhibition and enhanced degradation. Finally, I linked intracellular ATP to the extracellular glucose to connect the cell cycle to the extracellular environment.

6.3. Sensitivity Analysis

Additional details have been incorporated into the mitotic oscillator model. In the expanded model, protein synthesis requires ATP, CAK must phosphorylate the cyclin B

CDK1 dimer for stabilization, and MPF must bind ATP to activate. To begin, this work investigated the requirement of ATP for protein synthesis.

Protein synthesis requires ATP [184]. This model incorporates saturable kinetics, Michaelis-Menten kinetics, for the ATP requirement for protein synthesis. In the base case parameter set, the system exhibits ideal mitotic oscillatory characteristics (Figure 22B). The oscillations are frequency encoded and the MPF-ATP amplitude is the correct order of magnitude. A region of multiplicity of steady states exists along with a lower steady state that models quiescent and G2 arrested cells. The base model equations and parameter set may be found in ATP Model Equations and Parameters . When the ATP requirement for protein synthesis is removed from the model by setting the Michaelis-Menten constant to zero, a second oscillatory region is generated at very low ATP concentrations (Figure 22A). Cells die at very low ATP concentrations [187], and therefore, the model should not induce MPF-ATP oscillations, which simulate proliferation at low ATP concentrations. Since the cell should not be proliferating at low ATP concentrations, I analyzed how the MPF oscillations were generated in the lower oscillatory region.

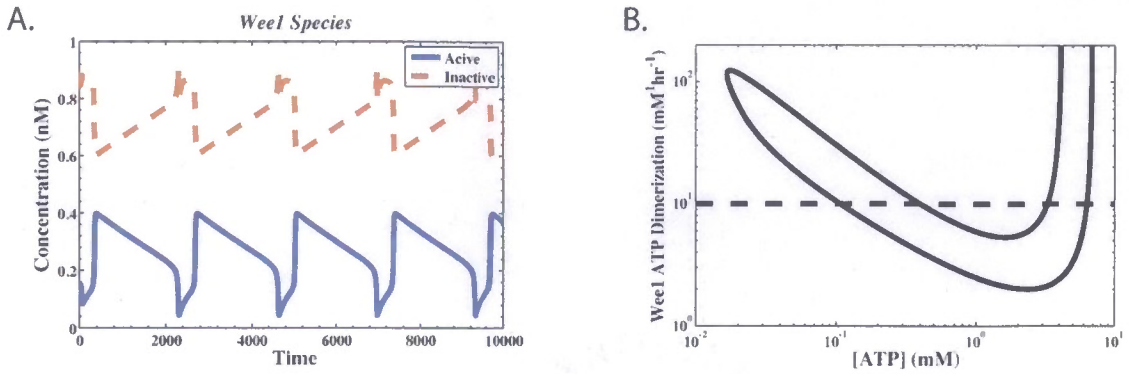

Figure 23 – Wee1 ATP interaction with no requirement of ATP for protein synthesis. In the lower oscillatory region (K_m=0 ATP=0.2 mM), the majority of the Wee1 species do not have ATP bound and therefore are inactive (Figure A). Active Wee1 species have ATP bound and can phosphorylate MPF. Therefore, I investigated the dimerization rate of Wee1 and ATP by two-parameter bifurcation (Figure B). Note the log scale on both axes. The y-axis is the dimerization rate of Wee1 and ATP. The x-axis is the bifurcation parameter, ATP. The solid black line tracks the movement of the Hopf bifurcation points and encloses the region of oscillations. The dashed black line is the dimerization rate of the base case, which has two regions of oscillatory behavior when ATP is not required for protein synthesis (K_m=0). As the Wee1 ATP dimerization rate is increased, the lower oscillatory region is shifted to lower ATP concentrations and is eventually destroyed.

In the lower oscillatory region, the majority of the Wee1 species remain inactive, and therefore, Wee1 is not binding with ATP and inhibiting MPF (Figure 23A). Consequently, cyclin B is synthesized until there is a very high concentration of inactive MPF that pushes the system to activate Cdc25A. ATP does not affect the activity of the Cdc25A species, but Wee1 is not active to inhibit MPF without ATP. Therefore, the decreased inhibition from Wee1 allows Cdc25A to activate MPF at low ATP concentrations. Active MPF then activates APC, which degrades cyclin B and Cdc25A species, resetting the cell cycle.

The lower oscillatory region has a steep change in amplitude because of the amount of active Wee1 (Figure 22A). As the amount of ATP in the system increases, the amount of active Wee1 increases, which inactivates more MPF. Thus, there is more inactive MPF available to be activated, generating a larger amplitude in MPF-ATP

With larger concentrations of active Wee1, all the cyclin B synthesized is dimerized into MPF and inhibited by Wee1. Since Wee1 has a high dimerization rate, it is always in an active form with ATP bound and can counter balance the Cdc25A activation of MPF. Therefore, the Wee1 ATP dimerization, or Wee1 activation, also controls the generation of the lower oscillatory region.

Therefore, there are two mechanisms that ensure that cells do not proliferate at low ATP concentrations: the requirement of ATP for protein synthesis and Wee1-ATP dimerization. When ATP is required for protein synthesis, there is a single region of oscillations with the base case parameter set (Figure 22B). As the Wee1 ATP dimerization is increased, thereby allowing Wee1 to bind ATP more tightly, the lower oscillatory region shifts to smaller ATP concentrations and is eventually destroyed (Figure 23B).

Next, I investigated the effect of cyclin B CDK1 dimerization on the oscillatory features of the system. Cyclin B must bind to CDK1 and be phosphorylated by CAK in order to bind to ATP to phosphorylate the proteins necessary to initiate mitosis. The base case parameter set incorporates rapid cyclin B-CDK1 dimerization and therefore generates the ideal mitotic oscillator characteristics (Figure 22B). When the dimerization process is slow, the oscillatory region is shifted to higher ATP concentrations, and the system loses the region of multiplicity (Figure 24A). More significantly, slow dimerization forces the cell to synthesize more cyclin B to generate the same oscillatory behavior (Figure 24B). Thus, the cell wastes energy and nutrients to synthesize cyclin B that is not dimerized with CDK1 and thus cannot initiate mitosis.

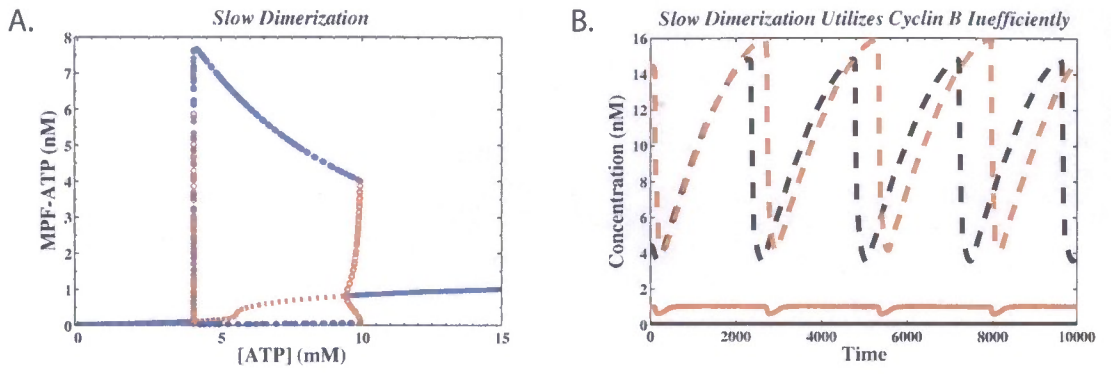

Figure 24- Slow dimerization of cyclin B and CDK1. When the dimerization process is slow (k_5=0.01), the bifurcation diagram maintains most of the key features of the ideal cell cycle (Figure A). However, the region of multiplicity disappeared and the oscillations are less frequency encoded. Furthermore, the oscillatory region has shifted to higher ATP concentrations. The main difference between fast and slow dimerization is the amount of cyclin B not used during the cell cycle (Figure B). The black and red lines are the systems with fast (k_5=1, base case parameter set) and slow dimerization, respectively. The dashed lines are the total concentration of cyclin B in the system and the solid lines are the concentrations of cyclin B monomer. All the cyclin B proteins are dimerized with CDK1 when the system has fast dimerization. There are essentially no cyclin B monomers in the system (solid black line). When there is slow dimerization, some of the synthesized cyclin B never dimerizes with CDK1 (solid red line) and more total cyclin B is necessary to generate the same oscillations (dashed red line). Hence, slow dimerization utilizes cyclin B inefficiently.

The cyclin B-CDK1 dimerization process acts as a throttle for mitosis. For mitosis to run efficiently, the throttle must be fully open. Therefore, dimerization must be a fast process compared to the dynamics of the mitotic oscillator. When the throttle is choked down, the cell is using energy and nutrients to produce the fuel, cyclin B, to initiate mitosis, but not all the fuel is being utilized. Hence, cyclin B-CDK1 dimerization must be fast for the cell to efficiently make use of all the cyclin B it synthesizes.

The cyclin B-CDK1 dimer requires CAK phosphorylation to stabilize [19]. In the base case parameter set, the CAK phosphorylation on CDK1 is stable. When the CAK phosphorylation on CDK1 is unstable, and therefore rapidly removed, the MPF dimer becomes unstable. This system maintains all the key characteristics of the ideal mitotic oscillator, but the amplitude of the oscillations and size of the region of multiplicity have decreased (Figure 25A).

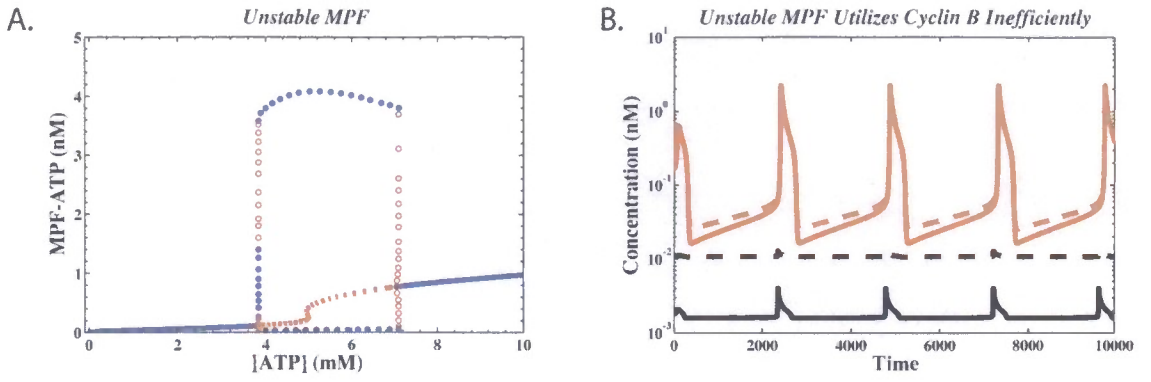

Figure 25 – Unstable MPF Complex. When the CAK phosphorylation is removed at a fast rate (k_7=10), the MPF complex becomes unstable. There is a decrease in the amplitude of MPF-ATP, and the size of the region of multiplicity decreased (Figure A). When the CAK phosphorylation is stable and therefore MPF is stable, there are minimal concentrations of cyclin B monomers and unphosphorylated cyclin B-CDK1 dimers; black dashed and solid lines, respectively (Figure B). Note the log scale on the y-axis. When the CAK phosphorylation is unstable and therefore MPF is unstable, orders of magnitude more cyclin B monomers and unphosphorylated cyclin B-CDK1 dimers are present in the system (red dashed and solid lines, respectively). There is a peak in unphosphorylated cyclin B-CDK1 dimers that corresponds to the activation of MPF. When Cdc25A activates MPF, the unstable CAK phosphorylation is removed and MPF becomes an unphosphorylated cyclin B-CDK1 dimer that cannot bind ATP to phosphorylate substrates. Thus, the cell must synthesize more cyclin to overcome the loss of active MPF because of the unstable active phosphorylation provided by CAK.

When the MPF dimer is unstable, the system maintains higher concentrations of cyclin B monomer and unphosphorylated cyclin B-CDK1 dimer (Figure 25B). The unphosphorylated cyclin B-CDK1 dimer is a highly transient species that is not observed experimentally [19], and therefore should be minimized in the model. Furthermore, the cyclin synthesized by the cell that remains as monomers or unphosphorylated cyclin B-CDK1 dimers is not employed to initiate mitosis. Therefore, the CAK phosphorylation must be stable for the cell to efficiently utilize cyclin B and to minimize the concentration of the unphosphorylated cyclin B-CDK1 dimer, which is not observed experimentally.

Finally, I investigated the addition of MPF-ATP dimerization in the MPF activation network. As the dimerization rate increases, the oscillatory region is shifted to lower ATP concentrations while maintaining all the key features of the ideal mitotic oscillator (Figure 26). I modulated the MPF ATP dimerization rate to tune the model to a relative ATP concentration. Thus, the relative ATP model is a general mitotic oscillator that can be tuned to many different cell lines with different maximum ATP concentrations.

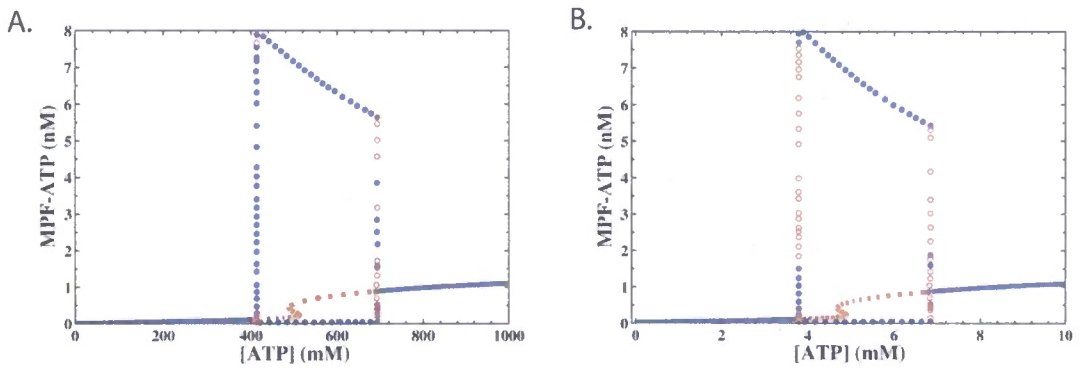

Figure 26 – MPF ATP Dimerization Rate. As the dimerization rate increases, the oscillatory region is shifted to lower ATP concentrations while maintaining all the key characteristics of the ideal mitotic oscillator. In figure A, k_8=0.1 and in figure B, k_8=10, , which is the base case parameter set.

6.4. Model Tuned for Relative ATP Concentration

Since the maximum intracellular ATP concentration is likely to vary between different cell lines, I tuned the model to a relative ATP concentration that is scaled by the maximum concentration. The relative ATP concentration ranges from zero to unity, and the region of oscillations ranges between the relative ATP concentrations of 0.5 to unity as approximated from the experimental data by Lu and coworkers [10].

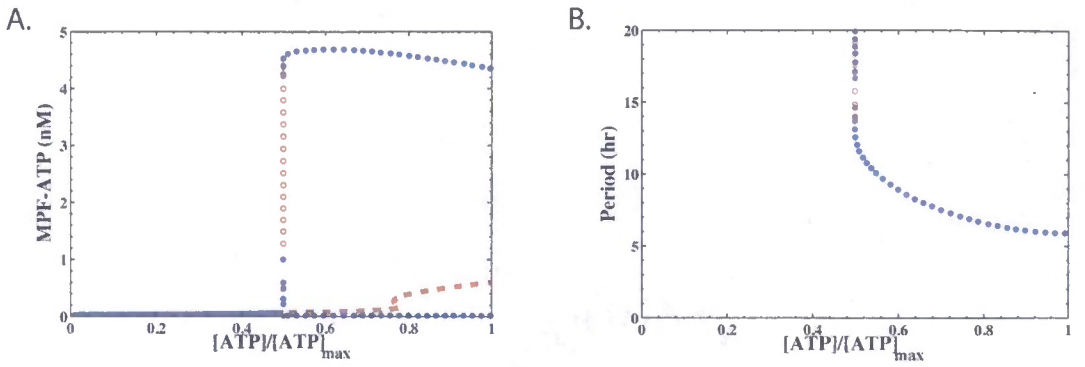

Figure 27 – Model Tuned to Relative ATP Concentration. The ATP concentration has been scaled by a maximum intracellular ATP concentration so that the range of the x-axis is zero to unity (Figure A). The oscillatory region falls between 0.5 and unity as approximated from experimental data [10]. The oscillations are frequency encoded and a region of multiplicity exists. The lower steady state at low relative ATP concentrations models quiescent and G2 arrested cells. The period of the oscillations is characteristic of mammalian cells (Figure B).

The model captures the ideal mitotic oscillator characteristics. The oscillations are frequency encoded. Hysteresis has been observed experimentally [177] with the MPF reaction network. The model captures hysteresis in the region of multiplicity of steady states. Quiescent and G2 arrested cells are modeled by the lower steady state at low relative ATP concentrations. The amplitude of MPF is the correct order of magnitude [178], and the period is characteristic of mammalian cells. The relative ATP tuned model parameter set is presented in ATP Model Equations and Parameters .

Although the model is capable of being linked to glucose at this point, it incorporates only a single inhibitory mechanism for MPF inhibition of Wee1, increased degradation. In nature there are two mechanisms by which MPF can inhibit Wee1, increased degradation and kinase inhibition. Therefore, I analyzed different Wee1 subnetworks to elucidate the effect of different Wee1 inhibition mechanisms on the oscillatory characteristics of the system.

6.5. Wee1 Network Structure

MPF phosphorylation inhibits Wee1A by two different mechanisms. [22]. Two sites, threonine 104 and 150, are conserved across species, including somatic Wee1, and inhibit Wee1 kinase activity during mitosis [22]. Phosphorylation on serine 123 by CDK1 induces a proteolytic cascade, which increases degradation [28]. Up to this point, the mitotic model has only included inhibition by increased degradation. Therefore, I

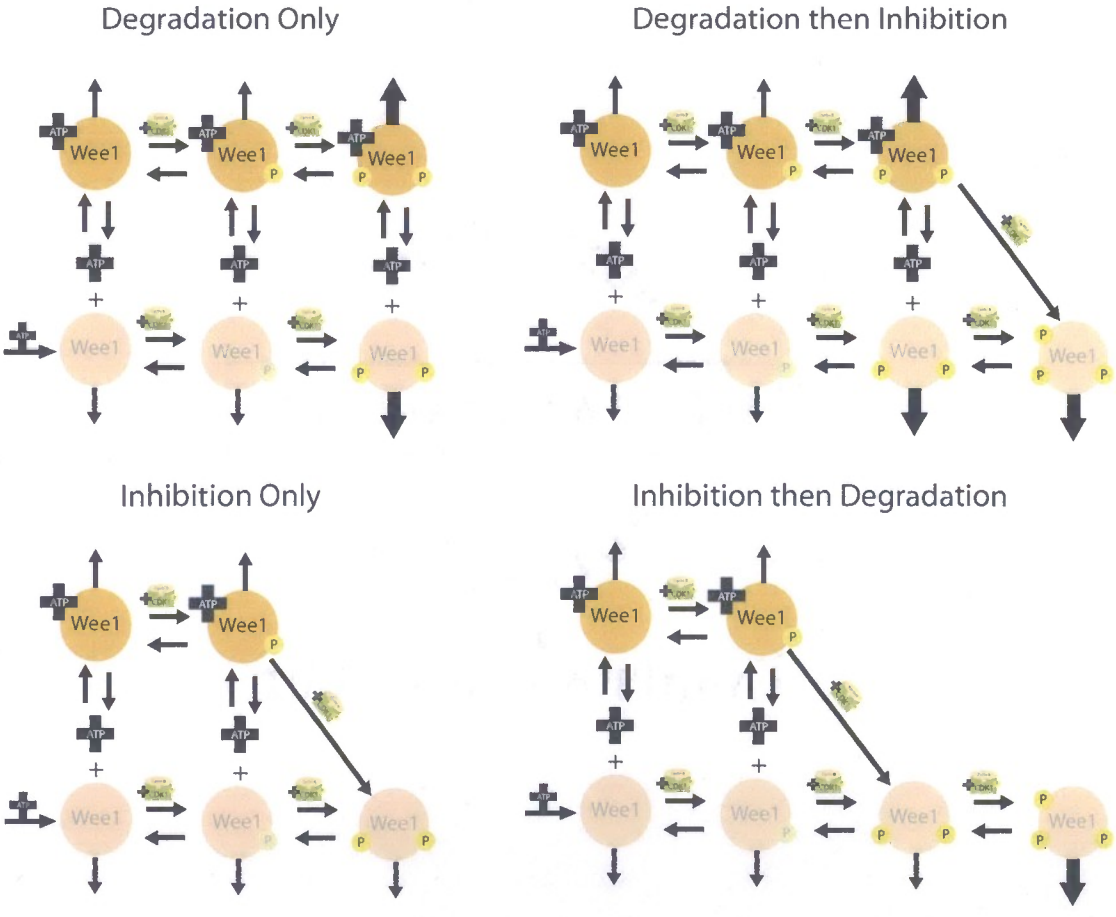

Figure 28 – Wee1 Inhibition Networks. Arrows pointing out into blank space represent degradation. The larger arrows indicate increased degradation. Transparent species are not active and therefore cannot phosphorylate MPF. The small green and yellow species is MPF, which catalyzes the phosphorylation of Wee1. The model analysis to this point incorporated the Wee1 subnetwork where MPF phosphorylation only induces increased degradation. Since MPF phosphorylation induces both kinase inhibition and increased degradation, three other networks were investigated: networks where MPF phosphorylation only induces inhibition, degradation then inhibition, and finally inhibition then degradation.

generated three alternative Wee1 inhibition mechanisms to analyze the effect of Wee1 inhibition on the oscillatory characteristics of the model (Figure 28).

I investigated a Wee1 subnetwork where MPF phosphorylation induced only inhibition. There were also two cases when MPF induced both inhibition and degradation that depend on the order of the inhibitory phosphorylations: one case where the degradation phosphorylation occurs before the inhibitory phosphorylation and vice versa. To keep the same amount of active Wee1 in the systems during interphase, the model assumes that Wee1 must have two phosphorylations before any inhibitory effect occurs. Otherwise, the networks with both inhibitory mechanisms would have less active Wee1 because a single phosphorylation would cause inhibition. Less active Wee1 in the dual inhibition Wee1 mechanisms would not allow equal comparison to the single inhibition Wee1 networks.

Regardless of the MPF inhibition mechanism on Wee1, all the systems displayed the same qualitative oscillatory behavior (Figure 29). All mechanisms generate frequency encoded oscillations and a region of multiplicity. The system with MPF phosphorylation inducing inhibition then degradation has a larger region of multiplicity. The increased positive feedback has slightly shrunk the oscillatory region so that the maximum ATP concentration that induces oscillations is less than unity. Although all Wee1 mechanisms respond qualitatively the same for most parameter changes, one parameter that the systems respond differently to is the increased rate of degradation induced by MPF phosphorylation (Figure 30).

Three of the four inhibition mechanisms are affected by changes in the increased degradation rate of Wee1 by phosphorylation at serine 123. The increased degradation

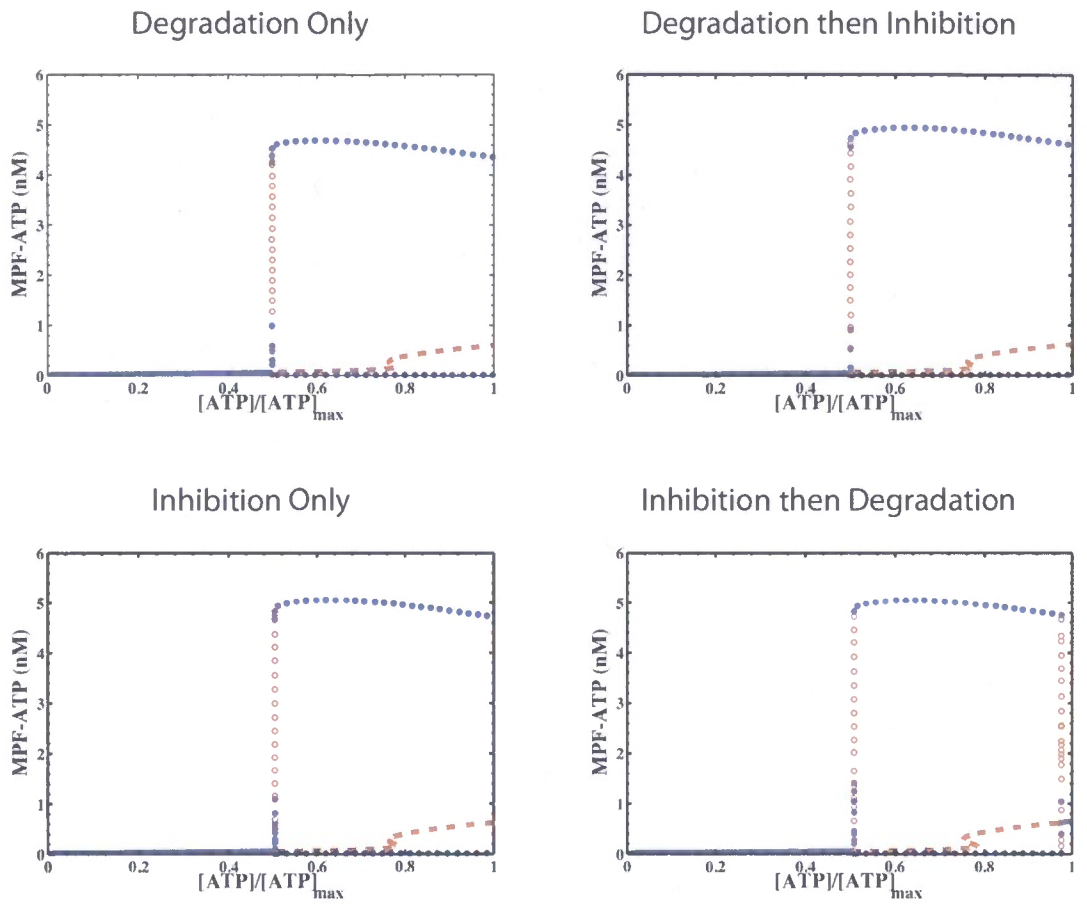

Figure 29 – Wee1 Inhibitory Mechanisms with Relative ATP Parameter Set. All of the Wee1 mechanisms generate the same qualitative oscillatory characteristics that have frequency encoded oscillations and a region of multiplicity of steady states. The system with MPF phosphorylation inducing inhibition then degradation has a larger region of multiplicity of steady states. The size of the oscillatory region has shrunk because of the larger positive feedback.

rate cannot fall below the background degradation rate. Otherwise, MPF phosphorylation induces stabilization, which converts the positive feedback loop into a negative feedback loop.

When MPF induces only increased degradation on Wee1, lowering the degradation rate shrinks the size of the region of multiplicity and increases the size of the region of oscillations. If the degradation rate is lowered below a threshold, the region of multiplicity disappears. Incorporating point mutations in Wee1 that remove the inhibitory phosphorylation sites can generate this system for experimentation, and

therefore, by lowering the degradation rate, the positive feedback loop is lost. Without increased degradation, Wee1 is not inhibited by MPF in this mechanism, and therefore remains at constant activity. Since both inhibitory mechanisms are present in nature, I further investigated these systems.

When MPF phosphorylates the increased degradation site prior to the inhibitory site, similar behavior for the degradation only system is observed. Lowering the degradation rate shrinks the size of the region of multiplicity and increases the size of the oscillatory region. The addition of kinase inhibition does not greatly increase the positive feedback in the model, because the high degradation rate limits the concentrations of the prior active species. Moreover, the inhibited species is also highly degraded, and therefore does not exist in high concentrations. Since there are low concentrations of the highly degraded species and the kinase inhibited species, the addition of kinase inhibition to the down regulation of Wee1 does not reduce the amount of active Wee1 during the initiation of mitosis. However, the additional positive feedback from the kinase inhibition does allow the system to maintain oscillations and multiplicity at lower increased Wee1 degradation rates than the Wee1 inhibition mechanism with degradation only. When the increased degradation is removed, this Wee1 inhibition mechanism becomes a kinase inhibition mechanism with an additional phosphorylation.

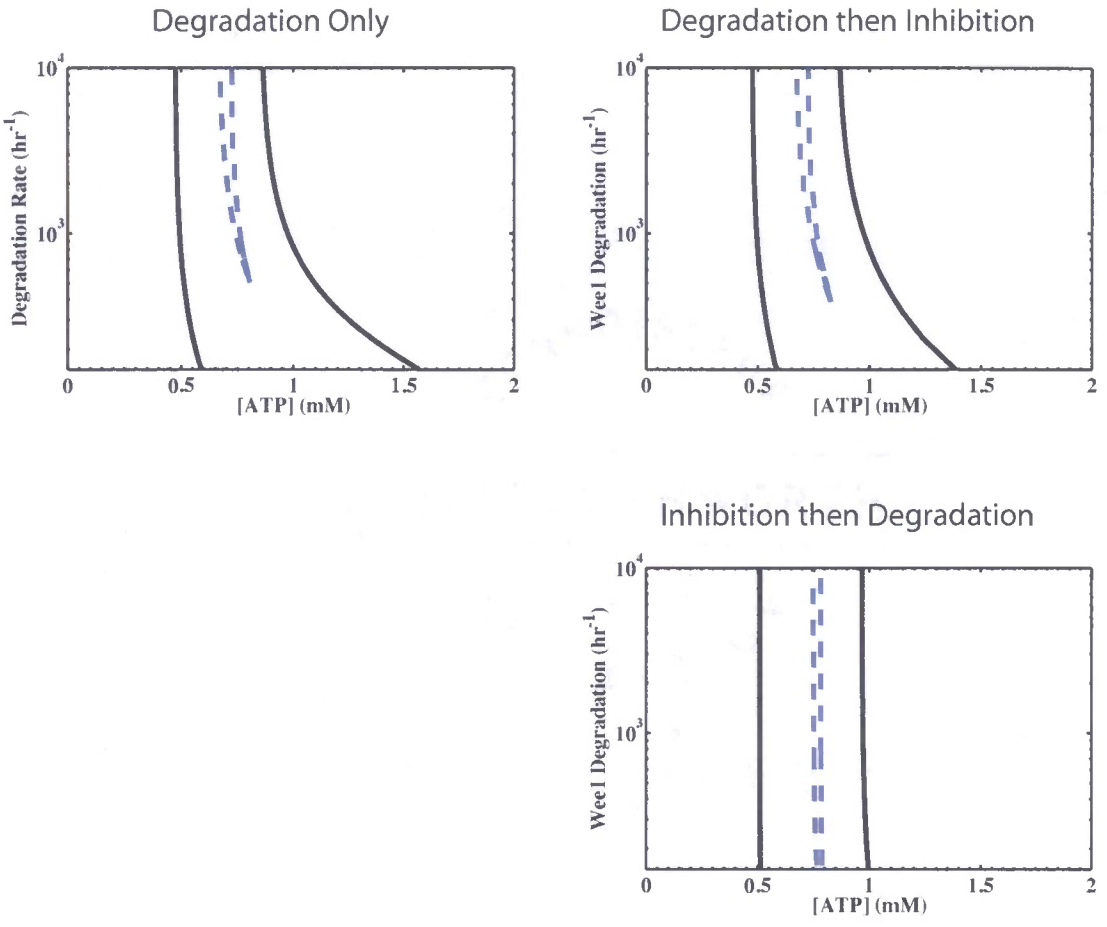

Figure 30 – Two-parameter bifurcation plots for liable Wee1 degradation rate versus ATP concentration. The liable Wee1 species have been phosphorylated by MPF at serine 123 and therefore have increased degradation. The relative ATP concentration parameter set was utilized. However, since the systems are not tuned for relative ATP, the x-axis has units of milimolar. The solid black lines, which enclose the region of oscillations, track the Hopf bifurcation points as the degradation rate of the liable Wee1 protein changes. The dashed blue lines track the limit points of the steady state solutions, which enclose the region of multiplicity. At a limit point, the steady state solution changes the sign of its slope, and therefore overlaps with other steady states. The increased degradation rate cannot be lower than the background degradation rate of Wee1 (k_{17}=150 hr^{-1}). Otherwise, MPF phosphorylation would stabilize Wee1. When MPF inhibits Wee1 only through degradation, as the degradation rate decreases, the size of the oscillatory and multiplicity regions increases and decrease, respectively. When MPF increases degradation and then inhibits Wee1, a decrease in degradation rate shrinks the size of the region of multiplicity and expands the size of the oscillatory region. However, the system does not have a region of multiplicity when the increased degradation becomes equal to background degradation. When MPF inhibits Wee1 then increases Wee1 degradation, changing the degradation rate does not affect the oscillatory region or region of multiplicity. Even when increased degradation becomes background degradation, the system maintains multiplicity and a tuned region of oscillations.

Finally, when MPF phosphorylation induces kinase inhibition and then increased degradation, increasing the degradation rate slightly increases the size of the region of multiplicity and decreases the size of the oscillatory region. Increasing the degradation

rate only reduces the amount of inactive Wee1, and thus there is not a large change in system behavior. From these results, I hypothesize that kinase inhibition followed by increased degradation is the Wee1 inhibition mechanism that is present in cells. By inhibiting Wee1 first, the system can initiate mitosis while maintaining Wee1 concentrations in the inactive form. Therefore, if the cell requires to arrest mitosis, the inhibitory phosphorylation on Wee1 can be removed, thus activating Wee1, which inactivates MPF. If the cell commits to mitosis, the inactive form of Wee1 is then degraded, irreversibly shifting the cell into mitosis.

If increased Wee1 degradation occurs before inhibition, the cell loses the ability to reversibly inhibit Wee1 during the early states of mitosis. Once the protein in degraded, the cell must synthesize new Wee1 if it needs to arrest in mitosis. This is not a logical mechanism for the cell to arrest in mitosis, because it would likely take longer to synthesize new proteins than it would for MPF to complete mitosis.

In summary, regardless of the inhibitory mechanism utilized to down regulate Wee1, the MPF network can generate the ideal cell cycle characteristics (Figure 29). The MPF activation network responds in the same qualitative way as long as Wee1 is inhibited by either or both mechanisms. Although I hypothesize that the inhibitory phosphorylation occurs before the increased degradation phosphorylation, if either mechanism were to be removed, the cell would still be able to accurately initiate mitosis. Hence, the results suggest that the two inhibitory mechanisms are redundant.

6.6. Linking Model to Glucose

Since the results suggest that the two Wee1 inhibitory mechanisms are redundant, any of the Wee1 mechanisms can be tuned for relative ATP concentrations with mitotic

oscillator characteristics. Therefore, I chose to move forward with the model that incorporated Wee1 inhibition followed by increased degradation, because it incorporates both inhibitory mechanisms and maintains the most logical order for the cell to maintain control of the initiation of mitosis.

Following the trend observed between ATP and extracellular glucose in the work by Lu and coworkers, the relative ATP concentration is described by saturable kinetics with glucose [10]. The Michaelis-Menten parameter was utilized an earlier study performed in our lab on fibroblast division times grown in limited glucose concentrations [2].

$$\frac{[ATP]}{[ATP_{\max}]} = \frac{[Glu\cos e]}{K_g + [Glu\cos e]} \tag{6.2}$$

The parameters were scaled to shift the division times to correspond to the experimental data. The glucose parameter set can be found in ATP Model Equations and Parameters . The model maintains the ideal cell cycle behavior and all attributes of the underlying relative ATP model, but now the bifurcation parameter is extracellular glucose concentration (Figure 31). The oscillations are frequency encoded and have an amplitude in the correct order of magnitude for MPF. There is a small steady state region at low glucose concentrations where cell do not proliferate. The model generates a region of multiplicity of steady states and the period is characteristic of fibroblast cells.

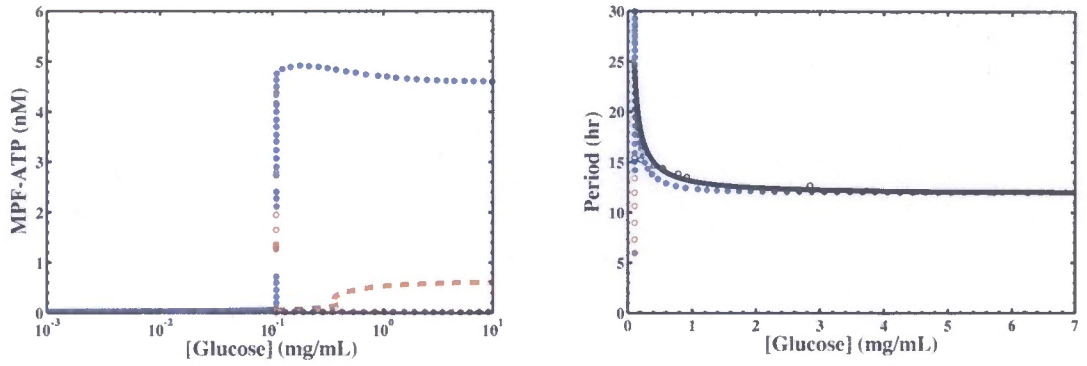

Figure 31 – Mitotic Oscillator Linked to Glucose. Glucose has been linked to the relative intracellular ATP concentration by saturable kinetics. The bifurcation parameter is extracellular glucose. The model maintains all ideal mitotic oscillator characteristics: region of multiplicity, frequency encoded oscillations, a lower steady state at low glucose concentrations where the cells are quiescent, and the correct order of magnitude for MPF amplitude (Figure A). The period of the model has been tuned for the fibroblast data obtained earlier in Dr. Zygourakis's lab at Rice University by Dr. Gang Cheng [2]. The solid blue circles are stable limit cycle periods. The open red circles are unstable limit cycle periods and are not observed experimentally. The open black circles are the data collected by Dr. Cheng in the lab, and the black line is the Monod kinetics fit to the data by Dr. Cheng.

The final model accurately captures the observed phenomena of modulation of the division time by extracellular glucose (Figure 31B). As a cell migrates within an environment with variable extracellular glucose, ATP, which is linked to the glucose, modulates the proteins involved in the cell cycle, and therefore the cell proliferates at a rate proportional to the extracellular glucose. Ultimately, this work developed a mitotic oscillator that is modulated by the extracellular environment through ATP (Figure 32).

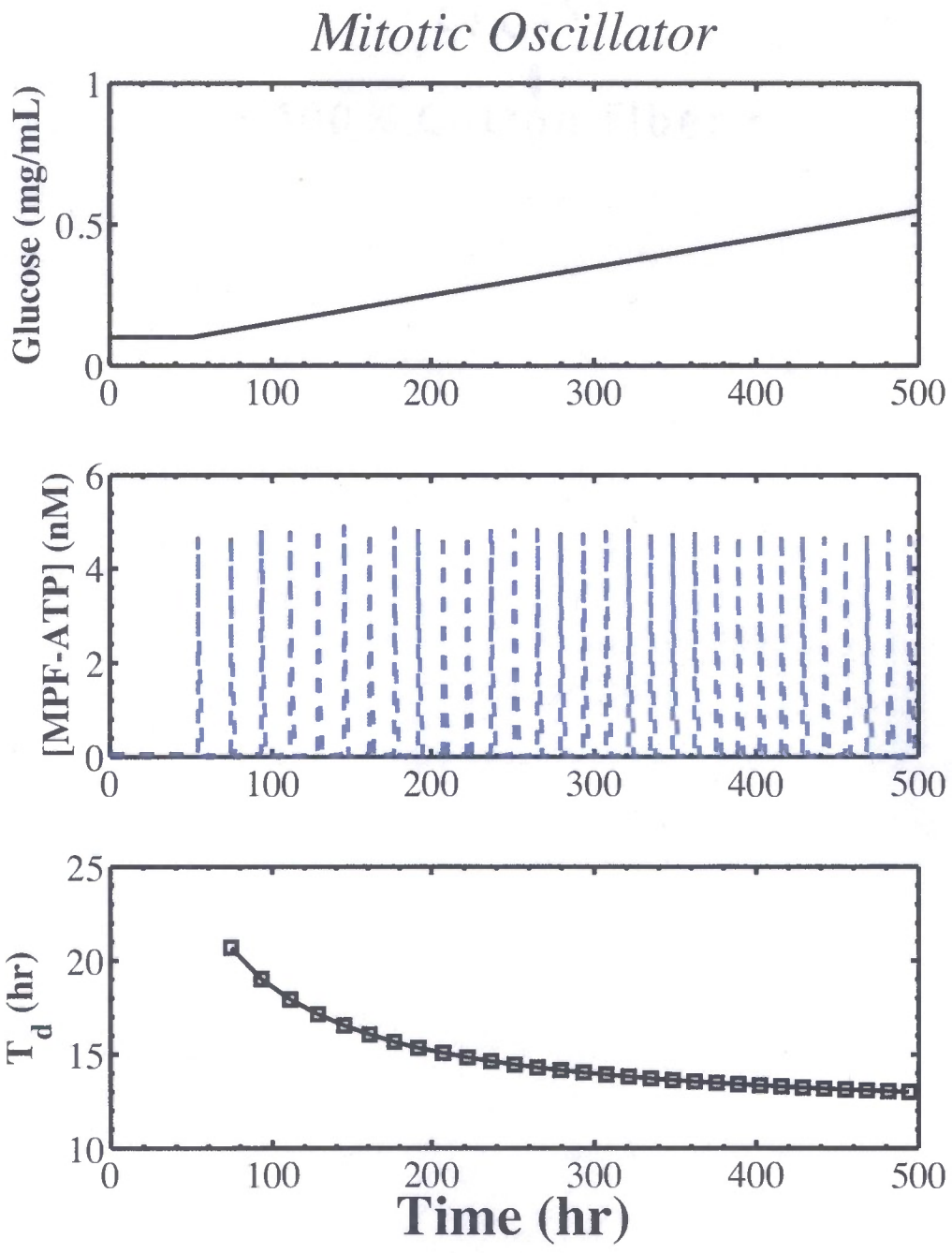

Figure 32 – Effect of Extracellular Glucose on Proliferation. The extracellular glucose concentration increase over time, for instance when a cell migrates towards a nutrient source (top). The mitosis is triggered when MPF-ATP peaks (middle). Thus, the division time (bottom) is modulated by the extracellular glucose. The division time is calculated as the time between MPF-ATP peaks (middle). As the extracellular glucose concentration increases, the doubling time of the cell decreases towards a minimum division at the maximum proliferation rate.

Chapter 7 - Conclusions and Future Work

This thesis work initiated the first vital steps to develop a biologically based proliferation model for a bioartificial tissue regeneration model. Using a bottom-up approach, I first created a base model for mitosis that maintains all of the core aspects of the mitotic oscillator including cyclin B, MPF, Cdc25A, and APC. The effect of the mitotic reaction network structure and multisite phosphorylation on system behavior was elucidated by varying the MPF activation network structure, the number positive feedback loops, and the number of phosphorylations on the positive feedback loop proteins, Wee1 and Cdc25A. Building upon this model, ATP was incorporated into the mitotic network. The inhibitory mechanism for Wee1 is not fully understood, and therefore, to gain insight into Wee1 inhibition during the initiation of mitosis, four mechanisms were analyzed. Using the Wee1 mechanism that allowed the cell to maintain maximum control over the initiation of mitosis, ATP was linked to extracellular glucose, and the model was tuned for fibroblast proliferation.

This mitotic model is the first to utilize the recent biological discoveries that CAK phosphorylation is required for the stabilization of the cyclin B-CDK1 dimer [19], and that the inactive MPF species are phosphorylated and dephosphorylated sequentially [34]. This work is also the first to analyze the effect of multisite phosphorylation and protein network structure on the oscillatory characteristics of a mitotic network.

The results suggest that the MPF reaction network has evolved to efficiently utilize cyclin and maintain maximum control of mitotic initiation. Sequential phosphorylations on CDK1, CAK followed by Wee1 phosphorylations allows the cell to efficiently utilize cyclin B and gives insight about why this sequence of phosphorylations

is observed experimentally [19]. In contrast, parallel phosphorylations on CDK1 by CAK and the Wee1 family of kinases requires the to cell synthesize more cyclin B in order to observe the same dynamics as sequential CAK followed by Wee1 phosphorylation.

When the network incorporates sequential phosphorylation events on CDK1, cyclin B and CDK1 can dimerize into an active or inactive complex. When cyclin B and CDK1 form an active dimer, CDK1 is phosphorylated by CAK to stabilize the dimer, followed by the inactivating phosphorylations by Wee1. This network has a bounded region of oscillations over the MPF activation and unstable Cdc25A degradation rates, allowing the cell to arrest the cell cycle either by raising the Cdc25A degradation or lowering the MPF activation rate. However, when cyclin B and CDK1 form an inactive dimer, the cell loses the ability to arrest the cell cycle by lowering the MPF activation rate or raising the unstable Cdc25A degradation rate. As long as the cell synthesizes enough cyclin B, it maintains the ability to proliferate even at low MPF activation rates or high unstable Cdc25A degradation rates. In addition, to form an inactive cyclin B-CDK1 dimer, all CDK1 phosphorylations must occur simultaneously during dimerization, but these behaviors are contrary to what is observed *in vivo*. Increased Cdc25A degradation has been reported as a mechanism for cell cycle arrest when DNA damage is present [188]. Moreover, CAK phosphorylation is required for cyclin B-CDK1 dimerization [19]. Furthermore, dimerization is required for Wee1 phosphorylation of CDK1 [17], and the inactivating CDK1 phosphorylations occur sequentially [21, 34].

Finally, when the inactive phosphorylations occur sequentially on CDK1, the MPF network maintains the ability to generate nonlinear dynamics that induce sharp

transitions into mitosis. However, when the inactivating phosphorylations occur simultaneously, in a single event, the cell loses the switch like behavior necessary to have a sharp transition between interphase and mitosis. These results from the MPF reaction network analysis indicate that multisite phosphorylation is vital to generate sharp transitions into mitosis and to utilize cyclin B efficiently. Not only is multisite phosphorylation important, but also the order of phosphorylation events plays a major role in the observed behavior of the system, and the ability of the system to be arrested.

Multisite phosphorylation also plays a major role in the positive feedback loop generated by Cdc25A stabilization. The addition of multiple phosphorylations to Cdc25A increases the size of the oscillatory and multiplicity regions allowing the cell to proliferate over a larger range of cyclin synthesis rates while maintaining frequency encoded oscillations. Since the extracellular environment modulates cell growth, and therefore protein synthesis, a larger oscillatory region in the cyclin synthesis rate can be related to a larger region of extracellular conditions over which the cell can proliferate. Incorporating an additional positive feedback loop by including Wee1 dynamics in the model generates a larger amplitude in MPF thereby creating a sharper transition into mitosis and increasing the efficiency of cyclin utilization by activating more MPF. Similar to Cdc25A, additional phosphorylations on Wee1 increase the size of the oscillatory and multiplicity regions.

ATP plays a dual role in the mitotic network and is a vital component in the mitotic process. ATP is required for protein synthesis [184] and for the functionality of all kinases in the cell, including MPF and Wee1 [11]. The average intracellular ATP concentration is modulated by extracellular glucose [10]. Therefore, incorporating

intracellular ATP into the mitotic oscillator model provided a link between mitosis and the extracellular environment.

Initially, the model incorporated a Wee1 network with increased degradation as the only mechanism for down regulation by MPF. However, Wee1 has two inhibition mechanisms, and thus this work analyzed four Wee1 inhibition networks. The results suggest that the two forms of Wee1 inhibition are redundant. All four Wee1 inhibition mechanisms created qualitatively similar behavior. During mitotic initiation, MPF activates regardless of the mechanism that down regulates Wee1. Therefore, from the perspective of MPF activation, the system behavior remains the same regardless of the inhibitory mechanism that down regulates Wee1 as long as a mechanism that down regulates Wee1 exists. Both mechanisms are present in nature, and thus was included in the model.

I hypothesize that the inhibitory phosphorylation occurs before the phosphorylation that increases degradation. Even with increased degradation removed from the network, the model exhibits ideal mitotic oscillator characteristics. Unlike the additional inhibition following increased degradation, the increased degradation after inhibition increases the positive feedback in the system. The size of the region of multiplicity increases and the oscillatory region decreases slightly, both of which are characteristics of increased positive feedback.

Furthermore, inhibition followed by increased degradation for Wee1 down regulation allows a cell to maintain maximum control over the initiation and completion of mitosis. Wee1 can be inhibited during the initiation of mitosis, but if a problem arises, the cell can remove the inhibitory phosphorylation and allow Wee1 to inhibit MPF,

thereby arresting the cell in mitosis. If Wee1 were degraded before being inhibited, then the cell would have to synthesize new Wee1 to inhibit MPF to arrest the cell cycle. Consequently, this would cost the cell energy, and the cell would not likely be able to synthesize Wee1 rapidly enough to arrest when needed.

Therefore, the final model incorporates the Wee1 network with kinase inhibition followed by increased degradation. In the model, ATP is linked to extracellular glucose via saturable kinetics as observed by Lu and coworkers [10], and tuned for fibroblast division times [2]. Ultimately, this project has developed a mitotic oscillator linked to the extracellular environment and tuned for fibroblasts.

This work gives valuable insight into the effect of multisite phosphorylation and protein network structure on the oscillatory characteristics of a mitotic oscillator. Moreover, the model is the first to connect extracellular glucose to a mitotic oscillator utilizing ATP as the link. From this point, there are a number of projects that can advance the model and the knowledge of bioartificial tissue regeneration including heterogeneity, limited glucose time-lapse microscopy experiments, DNA synthesis oscillator models, and further mitotic oscillator network analysis.

This work has made great strides in developing a proliferation model for a bioartificial tissue regeneration model, but cell population heterogeneity must be incorporated into the proliferation model before the model can be integrated into the larger bioartificial tissue regeneration model. This work developed a proliferation model that is modulated by the extracellular environment and simulates the dynamics for the average cell in a population. In nature, cell populations are heterogeneous. Even in a homogeneous environment, cell populations have a distribution of division times [5].

There are a number of different sources that generate cell population heterogeneity. One source is the stochastic nature of the chemical reactions in the cell. The small numbers of proteins that regulate the cell cycle generate discrete, rather than continuous, concentration profiles that may move the reaction network into stochastic reaction kinetics. MPF peak concentration occurs on the order of 1000 molecules, but during interphase there are fewer than 100 molecules [178]. Although the transition into mitosis is highly regulated, variability may exist in the time before initiation. Therefore, the mitotic oscillator developed in this work could be incorporated into Gillespie's algorithm [189] for stochastic chemical kinetics to elucidate the effect of stochastic chemical reactions on the distribution of mitotic times.

Another source of cell population heterogeneity is unequal cell partitioning. Although mother cells partition DNA between daughter cells with high precision, the other cellular material does partition equally, thereby forming two daughter cells with different initial contents. One modeling technique that takes into account unequal portioning is population balances [190-193]. By incorporating the mitotic oscillator into a population balance, the effect of unequal portioning on division times could be analyzed.

Furthermore, individual cells may have slightly different parameters for degradation and synthesis of proteins and their reaction to limited glucose conditions, thereby forming distributions of kinetic parameters. The distributions of kinetic parameters are another source of heterogeneity and could be simulated using ensemble methods, which simulate a population of cells. Ensemble methods have been used to simulate bacteria populations [194, 195]. The Monte Carlo algorithm would isolate the

kinetic parameter distribution to observe the contribution from each source to the distribution of division times.

All prior projects would incorporate a single source of heterogeneity, but to model heterogeneous populations, all the sources of heterogeneity must be included. Recently, a stochastic cell population model has been developed in Dr. Zygourakis's group [196]. It takes into account the major sources of heterogeneity and can isolate the sources to elucidate their contribution. By incorporating this work's mitotic oscillator into the stochastic cell population model, environmental heterogeneity could be simulated as well. The full stochastic cell population model is much too large to incorporate into the bioartificial tissue regeneration model. However, this project would thoroughly analyze the various sources of heterogeneity for the mitotic oscillator, and from the results one could isolate the most prominent sources of heterogeneity to reduce the model size for incorporation into a bioartificial tissue regeneration model.

Division time distributions are necessary to analyze cell proliferation heterogeneity. Prior experiments conducted in Dr. Zygourakis's lab at Rice University measured the distribution of division times with time-lapse video microscopy [5]. In the work, the division time distribution was measured at a single glucose concentration. Since cells are exposed to heterogeneous environments in bioartificial tissue regeneration, distributions of division times are required for varying glucose conditions. Performing time-lapse video microscopy experiments in limited glucose conditions would elucidate the change in the distribution of division times as the extracellular glucose concentration varied. These distributions taken at different homogeneous

glucose concentrations could be compared to the corresponding stochastic modeling efforts to tune and validate the models.

Although incorporating heterogeneity is a necessary step to integrate the proliferation model into the bioartificial tissue regeneration model, further modeling can have an impact on many aspects of the cell cycle. Many components of the cell cycle prior to mitosis can be incorporated into the model. A mammalian cell must pass through a restriction point in interphase and initiate DNA synthesis before initiating mitosis and dividing. Both of the crucial steps occur in every cycle, but there exists uncertainty about the mechanisms involved in passing through the restriction point and to initiate DNA synthesis. Similar to previous mitotic models, the prior restriction point and DNA synthesis models utilized various nonlinear kinetics to describe protein-protein interactions, but without experimental justification [98, 101, 114, 116, 120, 134, 137-147, 160-162, 166, 167, 197-199]. Many of the proteins involved in the earlier aspects of the cell cycle likely have multisite phosphorylation that could generate the assumed nonlinearities. For example, Cdc25A is involved in a positive feedback loop in the initiation of DNA synthesis and has fourteen potential CDK phosphorylation sites [11, 39]. Thus, a model for the restriction point and DNA synthesis incorporating multisite phosphorylation and analyzing the various prior network structures would advance the understanding of the evolution of the biology and the progression of the models in the area. The restriction point and DNA synthesis model could then be combined with this work's mitotic oscillator to create a full scale cell cycle model to reveal the underlying mechanisms involved to ensure that the two processes maintain their order.

Additionally, there are components in mitosis that could be added to the mitotic oscillator to understand their role in the regulation of mitosis and to advance the connectivity to the other components of the bioartificial tissue regeneration model. Since this work took a bottom-up approach, a minimal number of components were incorporated into the model while maintaining the biological integrity. Building complexity into the mitotic model revealed the function of the added components. For instance, two proteins inhibit MPF by phosphorylation, Wee1 and Myt1. The current model incorporates Wee1, but Myt1 can be added to reveal the likely different function of both Wee1 kinases. Wee1 is located in the nucleus and Myt1 is located on the Golgi complex and endoplasmic reticulum in the cytoplasm [18, 27]. The Wee1 kinases bring to light the spatial regulation of the cell cycle proteins. Several models have included spatial regulation of the proteins and have stressed its significance in regulating the cell cycle [134, 169]. Spatial regulation is yet another aspect that can be integrated into the model.

The Cdc25 family of phosphatases has three members, Cdc25A, Cdc25B, and Cdc25C [11]. This work included Cdc25A, which has been shown to be able to compensate for all the roles in the cell cycle [63]. However, the other two proteins do exist in nature and therefore must have had or have a role in the regulation of the cell cycle. Cdc25C is generally regarded as a mitotic protein, and the role of Cdc25B is yet to be understood fully [11]. Including each of these proteins into the model could clarify the role of each of them in the cell cycle.

The negative feedback loop in the mitotic network is highly complex. This work incorporated a simplified feedback loop in which MPF activated APC in a linear fashion.

In reality, APC has two activating proteins, Cdh1 and Cdc20, and all three proteins are regulated by multisite phosphorylation by MPF [11]. There have been a few modeling works to gain insight into this complex activation of APC to exit mitosis, but all previous models have incorporated various nonlinear kinetics for the protein-protein interaction [120, 153, 156]. The APC activation network is another subnetwork of the cell cycle that would benefit from a comprehensive study on prior protein network structures and the effect of multisite phosphorylation on system behavior.

Finally, other environmental factors could be incorporated into the proliferation model, including growth factor concentrations, scaffold configurations with bound signaling proteins, extracellular drugs and waste products, or extracellular oxygen. For example, growth factors have been observed to modulate glucose uptake and therefore cellular metabolism [200]. Therefore, by modulating metabolism, growth factors modulate intracellular ATP, which has already been incorporated into this work's mitotic oscillator.

In conclusion, this work has taken vital steps to develop a proliferation model for a bioartificial tissue regeneration model. As the cell cycle models become more complex through increased biological knowledge, it will be important to analyze models in a mechanistic manner to gain an understanding of the underlying reaction networks. By using this thought process, one can gain insight into why cells evolved the network structures observed today.

Chapter 8 - Bibliography

1. Belgacem, B.Y., K. Zygourakis, and P. Markenscoff. *Modeling the growth of three-dimensional tissues.* in *The First Joint BMES/EMBS Conference Serving Humanity, Advancing Technology.* 1999. Atlanta, GA.

2. Cheng, G., *Hybrid Computational Modeling of Cell Population and Mass Transfer Dynamics in Tissue Growth Processes*, in *Chemical and Biomolecular Engineering.* 2005, Rice University: Houston. p. 300.

3. Cheng, G., et al., *Cell Population Dynamics Modulate the Rates of Tissue Growth Processes.* Biophys. J., 2006. **90**(3): p. 713-724.

4. Feng, J., *Tissue Growth in 3D: A New Computational Model that Integrates Cell Heterogeneity and Diffusional Limitations and Its Parallel Implementation*, in *Electrical and Computer Engineering.* 2005, University of Houston: Houston.

5. Lee, Y., *Computer-Assisted Analysis of Endothelial Cell Migration and Proliferation*, in *Chemical Engineering.* 1994, Rice University: Houston. p. 269.

6. Lee, Y., et al., *A cellular automation model for the proliferaiton of migrating contact-inhibited cells.* Biophys. J., 1995. **69**: p. 1284-1298.

7. Mani, S., *A Parallel Computational Model for Growth of Tissues with Multiple Types of Cells*, in *Electrical and Computer Engineering.* 2002, University of Houston: Houston.

8. Zygourakis, K., R. Bizios, and P. Markenscoff, *Proliferation of anchorage-dependent contact-inhibited cells: I. Development of theoretical models based on cellular automata.* Biotechnology and Bioengineering, 1991. **38**: p. 459-470.

9. Zygourakis, K., P. Markenscoff, and R. Bizios, *Proliferation of anchorage-dependent contact-inhibited cells: II. Experimental results and validation of the theoretical models.* Biotechnology and Bioengineering, 1991. **38**: p. 471-479.

10. Lu, S., X. Sun, and Y. Zhang, *Insight into metabolism of CHO cells at low glucose concentration on the basis of the determination of intracellular metabolites.* Process Biochemistry, 2005. **40**: p. 1917-1921.

11. Krauss, B., *Biochemistry of Signal Transduction and Regulation.* 3 ed. 2003, Weinheim: Wiley-VCH Verlag.

12. Obaya, A.J. and J.M. Sedivy, *Regulation of cyclin-CDK activity in mammalian cells.* Cell. Mol. Life Sci., 2002. **59**: p. 126-142.

13. Evans, T., et al., *Cyclin: A Protein Specified by Maternal mRNA in Sea Urchin Eggs That Is Destroyed at Each Cleavage Division.* Cell, 1983. **33**: p. 389-396.

14. Fung, T.K. and R.Y.C. Poon, *A roller coaster ride with the mitotic cyclins.* Seminars in Cell and Developmental Biology, 2005. **16**: p. 335-342.

15. Gautier, J., et al., *Purified maturation-promoting factor contains the product of a Xenopus homolog of the fission yeast cell cycle control gene cdc2+.* Cell, 1988. **54**(3): p. 433-439.

16. Krauss, G., *Biochemistry of Signal Transduction and Regulation.* 2003, Weinheim: Wiley-WCH Verlag.

17. Squire, C.J., et al., *Structure and inhibition of the human cell cycle checkpoint kinases, Wee1A Kinases: An atypical tyrosine kinase with a key role in CDK1 regulation.* Structure, 2005. **13**: p. 541-550.

18. Liu, F., et al., *The human Myt1 kinase preferentially phosphorylates Cdc2 on Threonine 14 and localizes to the endoplasmic reticulum and golgi complex.* Molecular and Cellular Biology, 1997. **17**(2): p. 571-583.

19. Larochelle, S., et al., *Requirments for CDK7 in the assembly of CDK1/Cyclin B and activation of CDK2 revaled by chemical genetics in human cells.* Molecular Cell, 2007. **25**: p. 839-850.

20. Watanabe, N., M. Broome, and T. Hunter, *Regulation fo the human WEE1Hu CDK tyrosine 15-kinase during the cell cycle.* The EMBO Journal, 1995. **14**(9): p. 1878-1891.

21. Norbury, C., J. Blow, and P. Nurse, *Regulatory phosphorylation of the $p34^{cdc2}$ protein kinase in vertebrates.* The EMBO Journal, 1991. **10**(11): p. 3321-3329.

22. Kim, S.Y., et al., *Multisite m-phase phosphorylation of Xenopus Wee1A.* Molecular and Cellular Biology, 2005. **25**(23): p. 10580-10590.

23. Malumbres, M. and M. Barbacid, *Mammalian cyclin-dependent kinases.* TRENDS in Biochemical Sciences, 2005. **30**(11): p. 630-641.

24. Igarashi, M., et al., *$Wee1^{+}$ - like gene in human cells.* Nature, 1991. **353**: p. 80.

25. Parker, L.L. and H. Piwnica-Worms, *Incactivation of the $p34^{cdc2}$-cyclin B complex by the human wee1 tyrosine kinase.* Science, 1992. **257**: p. 1955-1957.

26. McGowan, C.H. and P. Russell, *Cell cycle regulation of human WEE1.* The EMBO Journal, 1995. **14**(10): p. 2166-2175.

27. Heald, R., M. McLoughlin, and F. McKeon, *Human Wee1 maintains mitotic timing by protecting the nucleus from cytoplasmically activated Cdc2 kinase.* Cell, 1993. **74**: p. 463-474.

28. Watanabe, N., et al., *Cyclin-dependent kinase (CDK) phosphorylation desabilizes somatic Wee1 via multiple pathways.* PNAS, 2005. **102**(33): p. 11663-11668.

29. Kim, S.Y. and J. James E Ferrell, *Substrate competition as a source of ultrasensitivity in the inactivation of wee1.* Cell, 2007. **128**(6): p. 1133-1145.

30. Mueller, P.R., et al., *Myt1: a membrane-associated inhibitory kinase that phosphorylates cdc2 on both threonine-14 and tyrosine-15.* Science, 1995. **270**: p. 86-90.

31. Wells, N.J., et al., *The C-terminal domain of the Cdc2 inhibitory kinase Myt1 interacts with Cdc2 complexes and is required for inhibition of G_2/M progression.* Journal of Cell Science, 1999. **112**: p. 3361-3371.

32. Liu, F., et al., *Overproduction of human Myt1 kinase induces a G_2 cell cycle delay by interfering with the intracellular trafficking of Cdc2-Cyclin B1 complexes.* Molecular and Cellular Biology, 1999. **19**(7): p. 5113-5123.

33. Booher, R.N., P.S. Holman, and A. Fattaey, *Human Myt1 is a cell cycle-regulated kinase that inhibits Cdc2 but not CDK2 activity.* Journal of Biological Chemistry, 1997. **272**(35): p. 22300-22306.

34. Borgne, A. and L. Meijer, *Sequential dephosphorylation of $p34^{cdc2}$ on Thr-14 and Tyr-15 at the prophase/metaphase transition.* Journal of Biological Chemistry, 1996. **271**(44): p. 27847-27854.

35. Russell, P. and P. Nurse, *$cdc25^+$ functions as an inducer in the mitotic control of fission yeast.* Cell, 1986. **45**: p. 145-153.

36. Boutros, R., V. Lobjois, and B. Ducommun, *Cdc25 phosphatases in cancer cells:key players? good targets?* Nature Reviews Cancer, 2007. **7**: p. 495-507.

37. Busino, L., et al., *Cdc25A phosphatase: combinatorial phosphorylation, ubiquitylation and proteolysis.* Oncogene, 2004. **23**: p. 2050-2056.

38. Donzelli, M. and G.F. Draetta, *Regulating mammalian checkpoints through Cdc25 inactivation.* EMBO reports, 2003. **4**(7): p. 671-677.

39. Karlsson-Rosenthal, C. and J.B.A. Millar, *Cdc25: mechanisms of checkpoint inhibition and recovery.* TRENDS in Cell Biology, 2006. **16**(6): p. 285-292.

40. Galaktionov, K., X. Chen, and D. Beach, *Cdc25 cell-cycle phosphatase as a target of c-myc.* Nature, 1996. **382**: p. 511-517.

41. Vigo, E., et al., *Cdc25A phosphatase is a target of E2F and is required for efficient E2F-induced S phase.* Molecular and Cellular Biology, 1999. **19**(9): p. 6379-6395.

42. Wu, L., et al., *E2F-Rb complexes assemble and inhibit cdc25A transcription in cervical carcinoma cells following repression of human papillomavirus oncogene expression.* Molecular and Cellular Biology, 2000. **20**(19): p. 7059-7067.

43. Hoffmann, I., G. Draetta, and E. Karsenti, *Activaiton of the phosphatase activity of human cdc25A by a cdk2-cyclin E dependent phosphorylaiton at the G_1/S transition.* The EMBO Journal, 1994. **13**(18): p. 4302-4310.

44. Blomberg, I. and I. Hoffmann, *Ectopic expression of Cdc25A accelerates teh G_1/S transition and leads to premature activaiton of cyclin E- and cyclin A-dependent kinases.* Molecular and Cellular Biology, 1999. **19**(9): p. 6183-6194.

45. Donzelli, M., et al., *Dual mode of degradation of Cc25 A phosphoatase.* The EMBO Journal, 2002. **21**(18): p. 4875-4884.

46. Mailand, N., et al., *Regulation of G_2/M events by Cdc25A through phosphorylation-dependent modulation of its stability.* The EMBO Journal, 2002. **21**(21): p. 5911-5920.

47. Gabrielli, B.G., et al., *Cytoplasmic accumulation of cdc25B phosphatase in mitosis triggers centrosomal microtuble nucleation in HeLa cells.* Journal of Cell Science, 1996. **109**: p. 1081-1093.

48. Lammer, C., et al., *The cdc25B phosphatase is essential for the G_2/M phase transition in human cells.* Journal of Cell Science, 1998. **111**: p. 2445-2453.

49. Millar, J.B.A., et al., *$p55^{CDC25}$ is a nuclear protien required for the initiation of mitosis in human cells.* PNAS, 1991. **88**: p. 10500-10504.

50. Lindqvist, A., et al., *Cdc25B cooperates with Cdc25A to induce mitosis but has a unique role in activating cyclin B1-CDK1 at the centrosome.* Journal Of Cell Biology, 2005. **171**(1): p. 35-45.

51. Gabrielli, B.G., et al., *Hyperphosphorylation of the N-terminal domain of cdc25 regulates activity toward cyclin B1/Cdc2 but not cyclin A/CDK2.* Journal of Biological Chemistry, 1997. **272**(45): p. 28607-28614.

52. Hoffmann, I., et al., *Phosphorylation and activation of human cdc25-c by cdc2 - cyclin B and its involvement in the self-amplification of MPF at mitosis.* The EMBO Journal, 1993. **12**(1): p. 53-63.

53. Girard, F., et al., *cdc25 is a nuclear protein expressed constitutively throughout the cell cycle in nontransformed mammalian cells.* Journal Of Cell Biology, 1992. **118**(4): p. 785-794.

54. Jinno, S., et al., *Cdc25A is a novel phosphatase function early in the cell cycle.* The EMBO Journal, 1994. **13**(7): p. 1549-1556.

55. Baldin, V., et al., *Phosphorylation of human Cdc25B phosphatase by CDK1-Cyclin A triggers its proteasome-dependent degradation.* Journal of Biological Chemistry, 1997. **272**(52): p. 32731-32734.

56. Kanemori, Y., K. Uto, and N. Sagata, *B-TrCP recognizes a previously undescribed nonphosphorylated destruction motif in Cdc25A and Cdc25B phosphatases.* PNAS, 2005. **102**(18): p. 6279-6284.

57. Sexl, V., et al., *A rate limiting function of cdc25A for S phase entry inversely correlates with tyrosine dephosphorylation of CDK2.* Oncogene, 1999. **18**: p. 573-582.

58. Molinari, M., et al., *Human Cdc25 A incaction in response to S phase inhibition and its role in preventing premature mitosis.* EMBO reports, 2000. **1**(1): p. 71-79.

59. Karlsson, C., et al., *Cdc25B and Cdc25C differ markedly in their properties as initiators of mitosis.* Journal Of Cell Biology, 1999. **146**(3): p. 573-583.

60. Garner-Hamrick, P.A. and C. Fisher, *Antisense phosphorothioate oligonucleotides specifically down-regulate cdc25B causing S-phase delay and persistent antiproliferative effects.* International Journal of Cancer, 1998. **76**: p. 720-728.

61. Turowski, P., et al., *Functional cdc25C dual-specificity phosphatase is required for S-phase entry in human cells.* Molecular Biology of the Cell, 2003. **14**: p. 2984-2998.

62. Chen, M.-S., et al., *Absence of apparent phenotype in mice lacking Cdc25C protein phosphatase.* Molecular and Cellular Biology, 2001. **21**(12): p. 3853-3861.

63. Ferguson, A.M., et al., *Normal cell cycle and checkpoint responses in mice and cells lacking Cdc25B and Cdc25C protein phosphatases.* Molecular and Cellular Biology, 2005. **25**(7): p. 2853-2860.

64. Lincoln, A.J., et al., *Cdc25b phosphatase is required for resumption of meiosis during oocyte maturation.* Nature Genetics, 2002. **30**: p. 446-449.

65. Sachsanmaier, W., U. Remy, and R. Plattner-Schobel, *Initiation of synchronous mitosis in Physarum polycephalum. A model of the control of cell division in eukaryotes.* Exp. Cell Res., 1972. **73**: p. 41-48.

66. Fantes, P., et al., *The regulation of cell size and the control of mitosis.* Journal of Theoretical Biology, 1975. **50**: p. 213-244.

67. Kauffman, S. and J. Wille, *The mitotic oscillator in Physarum polycephalum.* Journal of Theoretical Biology, 1975. **55**: p. 47-93.

68. Hyver, C. and H.L. Guyader, *MPF and cyclin: modelling of the cell cycle minimum oscillator.* Biosystems, 1990. **24**: p. 85-90.

69. Norel, R. and Z. Agur, *A model for the adjustment of the mitotic clock by cyclin and MPF levels.* Science, 1991. **251**(4997): p. 1076-1078.

70. Goldbeter, A., *A minimal cascade model for the mitotic oscillator involving cyclin and cdc2 kinase.* Proc Natl Acad Sci U S A, 1991. **88**(20): p. 9107-11.

71. Hannsgen, K.B. and J.J. Tyson, *Stability of the steady-state size distribution in a model of cell growth and division.* J. Math. Biology, 1985. **22**: p. 293-301.

72. Tyson, J., G. Garcia-Herdugo, and W. Sachsenmaier, *Control of nuclear division in Physarum polycephalum : Comparison of cycloheximide pulse treatment, UV irradiation, and heat shock.* Experimental Cell Research, 1979. **119**(1): p. 87-98.

73. Tyson, J. and W. Sachsenmaier, *Is nuclear division in Physarum controlled by a continuous limit cycle oscillator?* Journal of Theoretical Biology, 1978. **73**(4): p. 723-738.

74. Tyson, J.J., *Size control of cell division.* J Theor Biol, 1987. **126**: p. 381-391.

75. Tyson, J.J., *Effects of asymmetric division on a stochastic model of the cell division cycle.* Mathematical Biosciences, 1989. **96**(2): p. 165-184.

76. Tyson, J.J. and O. Diekmann, *Sloppy size control of the cell division cycle.* J Theor Biol, 1986. **118**: p. 405-426.

77. Tyson, J.J. and K.B. Hannsgen, *The Distribution of cell size and generation time in a model of the cell cycle incorporating size control and random transitions.* J Theor Biol, 1985. **113**: p. 29-62.

78. Tyson, J.J. and K.B. Hannsgen, *Global asymptotic stability of the size distribution in probabilistic models of the cell cycle.* J. Math. Biology, 1985. **22**: p. 61-68.

79. Tyson, J.J. and K.B. Hannsgen, *Cell growth and division: a deterministic/probabilistic model of the cell cycle.* J. Math. Biology, 1986. **23**: p. 231-246.

80. Tyson, J.J., *Modeling the cell division cycle: cdc2 and cyclin interactions.* PNAS, 1991. **88**: p. 7328-7332.

81. Obeyesekere, M.N., S.L. Tucker, and S.O. Zimmerman, *Mathematical models for the cellular concentrations of cyclin and MPF.* Biochemical and Biophysical Research Communications, 1992. **184**(2): p. 782-789.

82. Thron, C.D., *Mathematical analysis of a model of the mitotic clock.* Science, 1991. **254**(5028): p. 122-123.

83. Novak, B. and J.J. Tyson, *Modeling the cell division cycle: M-phase trigger, oscillations, and size control.* J Theor Biol, 1993. **165**: p. 101-134.

84. Novak, B. and J.J. Tyson, *Numerical analysis of a comprehensive model of M-phase control in Xenopus oocyte extracts and intact embryos.* Journal of Cell Science, 1993. **106**: p. 1153-1168.

85. Borisuk, M.T. and J.J. Tyson, *Bifurcation analysis of a model of mitotic control in frog eggs.* J Theor Biol, 1998. **195**: p. 69-85.

86. Marlovits, G., et al., *Modeling M-phase control in Xenopus oocyte extracts: the surveillance mechanism for unreplicated DNA.* Biophysical Chemistry, 1998. **72**: p. 169-184.

87. Romond, P.C., J.M. Guilmot, and A. Goldbeter, *The mitotic oscillator: Temporal self-organization in a phosphorylation-dephosphorylation enzymatic cascade.* Berichte der Bunsen-Gesellschaft für Physikalische Chemie, 1994. **98**: p. 1152-1159.

88. Goldbeter, A. and J. Guilmot, *Arresting the mitotic oscillator and the control of cell proliferation: insights from a cascade model for cdc2 kinase activation.* Experentia, 1996. **52**: p. 212-216.

89. Thron, C.D., *Theoretical dynamics of the cyclin B-MPF system: a possible role for* $p13^{suc1}$. Biosystems, 1994. **32**: p. 97-109.

90. Gardner, T.S., M. Dolnik, and J.J. Collins, *A theory for controlling cell cycle dynamics using a reversibly binding inhibitor.* PNAS, 1998. **95**: p. 14190-14195.

91. Novak, B., et al., *Model Scenarios for Evolution of the Eukaryotic Cell Cycle.* Philosophical Transactions: Biological Sciences, 1998. **353**(1378): p. 2063-2076.

92. Busenberg, S. and B. Tang, *Mathematical models of the early embryonic cell cycle: the role of MPF activation and cyclin degradation.* J. Math. Biol., 1994. **32**: p. 573-596.

93. Romond, P.-C., et al., *Alternating Oscillations and Chaos in a Model of Two Coupled Biochemical Oscillators Driving Successive Phases of the Cell Cycle.* Ann NY Acad Sci, 1999. **879**(1): p. 180-193.

94. Ciliberto, A. and J.J. Tyson, *Mathematical model for early development of the sea urchin embryo.* Bulletin of Mathematical Biology, 2000. **62**: p. 37-59.

95. Gonze, D. and A. Goldbeter, *A Model for a Network of Phosphorylation-dephosphorylation Cycles Displaying the Dynamics of Dominoes and Clocks.* Journal of Theoretical Biology, 2000. **210**(2): p. 167-186.

96. Battogtokh, D. and J.J. Tyson, *Periodic forcing of a mathematical model for the eukaryotic cell cycle.* Physical Review E, 2006. **73**: p. 011910.

97. Battogtokh, D., K. Aihara, and J.J. Tyson, *Synchronization of eukaryotic cells by periodic forcing.* Physical Review Letters, 2006. **96**: p. 148102.

98. Tyson, J.J. and B. Novak, *Regulation of the eukaryotic cell cycle: molecular antagonism, hysteresis, and irreversible transitions.* J Theor Biol, 2001. **210**(2): p. 249-63.

99. Novak, B. and J.J. Tyson, *Modeling the controls of the eukaryotic cell cycle.* Biochem Soc Trans, 2003. **31**(Pt 6): p. 1526-9.

100. Frankel, P., *Tuning the cell cycle: a model based on averaging.* Cell Proliferation, 2002. **35**: p. 363-367.

101. Qu, Z., W.R. MacLellan, and J.N. Weiss, *Dynamics of the cell cycle: checkpoints, sizers, and timers.* Biophys J, 2003. **85**(6): p. 3600-11.

102. Ciliberto, A., et al., *A kinetic model of the cyclin E/CDK2 developmental timer in Xenopus laevis embryos.* Biophysical Chemistry, 2003. **104**(3): p. 573-589.

103. Yang, L., et al., *Multisite phosphorylation and network dynamics of cyclin-dependent kinase signaling in eukaryotic cell cycle.* Biophysical Journal, 2004. **86**: p. 3432-3443.

104. Steuer, R., *Effects of stochasticity in models of the cell cycle: from quantized cycle times to noise-induced oscillations.* Journal of Theoretical Biology, 2004. **228**(3): p. 293-301.

105. Zwolak, J.W., J.J. Tyson, and L.T. Watson, *Parameter estimation for a mathematical model of the cell cycle in frog eggs.* Journal of Computational Biology, 2005. **12**(1): p. 48-63.

106. Allen, N.A., et al., *Computer evaluation of network dynamics models with applicaiton to cell cylce control in budding yeast.* IEE Proc.-Syst. Biol., 2006. **153**(1): p. 13-21.

107. Sible, J.C. and J.J. Tyson, *Mathematical modeling as a tool for investigating clel cycle control networks.* Methods, 2007. **41**: p. 238-247.

108. Pomerening, J.R., S.Y. Kim, and J.E. Ferrell, *Systems-Level Dissection of the Cell-Cycle Oscillator: Bypassing Positive Feedback Produces Damped Oscillations.* Cell, 2005. **122**(4): p. 565-578.

109. Han, Z., et al., *Hysteresis and cell cycle transitions: how crucial is it?* Biophysical Journal, 2005. **88**: p. 1626-1634.

110. Ciliberto, A., F. Capuani, and J.J. Tyson, *Modeling networks of coupled enzymatic reactions using the total quasi-steady state approximation.* PLOS Computational Biology, 2007. **3**(3): p. e45.

111. Novak, B., et al., *Irreversible cell-cycle transitions are due to systems-level feedback.* Nat Cell Biol, 2007. **9**(7): p. 724-728.

112. Novak, B. and J.J. Tyson, *Quantitative analysis of a molecular model of mitotic control in fission yeast.* J Theor Biol, 1995. **173**: p. 283-305.

113. Novak, B. and J.J. Tyson, *Modeling the control of DNA replication in fission yeast.* PNAS, 1997. **94**: p. 9147-9152.

114. Novak, B., et al., *Mathematical model of the fission yeast cell cycle with checkpoint controls at the G1/S, G2/M and metaphase/anaphase transitions.* Biophysical Chemistry, 1998. **72**(1-2): p. 185-200.

115. Sveiczer, A., et al., *Modeling the fission yeast cell cycle: Quantized cycle times in wee1⁻ cdc25Δ mutant cells.* PNAS, 2000. **97**(14): p. 7865-7870.

116. Novak, B., et al., *Mathematical model of the cell division cycle of fission yeast.* Chaos: An Interdisciplinary Journal of Nonlinear Science, 2001. **11**(1): p. 277-286.

117. Sveiczer, A., J.J. Tyson, and B. Novak, *A stochastic, molecular model of the fission yeast cell cycle: role of the nucleocytoplasmic ratio in cycle time regulation.* Biophysical Chemistry, 2001. **92**(1-2): p. 1-15.

118. Sveiczer, A. and B. Novak, *Regularities and irregularities in the cell cycle of the fission yeast, Schizosaccharomyces Pombe.* Acta Microbiologica et Immunologica Hungarica, 2002. **49**(2-3): p. 289-304.

119. Srividhya, J. and M.S. Gopinathan, *A simple time delay model for eukaryotic cell cycle.* J Theor Biol, 2006. **241**: p. 617-627.

120. Novak, B., et al., *Finishing the Cell Cycle.* Journal of Theoretical Biology, 1999. **199**(2): p. 223-233.

121. Chen, K.C., et al., *Kinetic Analysis of a Molecular Model of the Budding Yeast Cell Cycle.* Mol. Biol. Cell, 2000. **11**(1): p. 369-391.

122. Lovrics, A., et al., *Time scale and dimension analysis of a budding yeast cell cycle model.* BMC Bioinformatics, 2006. **7**: p. 494.

123. Ciliberto, A., B. Novak, and J.J. Tyson, *Mathematical model of the morphogenesis checkpoint in budding yeast.* The Journal of Cell Biology, 2003. **163**(6): p. 1243-1254.

124. Battogtokh, D. and J.J. Tyson, *Bifurcation analysis of a model of the budding yeast cell cycle.* Chaos: An Interdisciplinary Journal of Nonlinear Science, 2004. **14**(3): p. 653-661.

125. Chen, K.C., et al., *Integrative Analysis of Cell Cycle Control in Budding Yeast.* Mol. Biol. Cell, 2004. **15**(8): p. 3841-3862.

126. Thornton, B.R., et al., *Cycling without the Cyclosome.* Cell Cycle, 2004. **3**(5): p. 629-633.

127. Li, F., et al., *The yeast cell-cycle network is robustly designed.* PNAS, 2004. **101**(14): p. 4781-4786.

128. Zhang, Y., et al., *Stochastic model of yeast cell-cycle network.* Physica D, 2006. **219**: p. 35-39.

129. Zhang, Y., et al., *Nonequilibrium model for yeast cell cycle*, in *Lecture Notes in Computer Science*. 2006, Springer: Berlin. p. 786-791.

130. Proctor, C.J., et al., *Modelling the checkpoint response to telomere uncapping in budding yeast.* J. R. Soc. Interface, 2007. **4**: p. 73-90.

131. Gi, H., H. Qian, and M. Qian, *Synchronized dynamics and non-equilibrium steady states in a stochastic yeast cell-cycle newtork.* Mathematical Biosciences, 2008. **211**: p. 132-152.

132. Conradi, C., et al., *Subnetwork analysis reveals dynamic features of complex (bio)chemical networks.* PNAS, 2007. **104**(49): p. 19175-19180.

133. Sriram, K., G. Bernot, and F. Képès, *A minimal mathematical model combining several regulatory cycles from the budding yeast cell cycle.* IET Syst. Biol., 2007. **1**(6): p. 326-341.

134. Barberis, M. and E. Klipp, *Insights into the network controlling the G_1/S transition in budding yeast.* Genome Inform., 2007. **18**: p. 85-99.

135. Tyson, J.J., et al., *Checkpoints in the cell cycle from a modeler's perspective.* Progress in Cell Cycle Research, 1995. **1**: p. 1-8.

136. Sabouri-Ghomi, M., et al., *Antagonism and bistability in protien interaction networks.* J Theor Biol, 2008. **250**: p. 209-218.

137. Kohn, K.W., *Functional capabilities of molecular network components controlling the mammalian G1/S cell cycle phase transition.* Oncogene, 1998. **16**: p. 1065-1075.

138. Hatzimanikatis, V., K.H. Lee, and J.E. Bailey, *A mathematical description of regulation of the G1-S transition of the mammalian cell cycle.* Biotech Bioeng, 1999. **65**(6): p. 631-637.

139. Aguda, B.D. and Y. Tang, *The kinetic origins of the restriction point in the mammalian cell cycle.* Cell Proliferation, 1999. **32**: p. 321-335.

140. Deineko, I., et al., *Mathematical model of the mitogen-dependent G1/S transition in mammalian cell cycle.* Interjouranl of Genetics: p. 407.

141. Swat, M., A. Kel, and H. Herzel, *Bifurcation analysis of the regulatory modules of the mammalian G_1/S transition.* Bioinformatics, 2004. **20**(10): p. 1506-1511.

142. Chauhan, A., et al., *A mesoscale mdoel fo G1/S phase transition in liver regeneration.* J Theor Biol, 2008. **252**: p. 465-473.

143. Barberis, M., et al., *Cell size at S phase initiation: An emergent property of the G_1/S network.* PLOS Computational Biology, 2007. **3**(4): p. e64.

144. Pfeuty, B., T. David-Pfeuty, and K. Kaneko, *Underlying principles of cell fate dtermination during G_1 phase of the mammalian cell cycle.* Cell Cycle, 2008. 7(20): p. 3246-3257.

145. Tashima, Y., et al., *Prediction fo key factor contrlling G1/S phase in teh mammalian cell cycle using system analysis.* Journal of Bioscience and Bioengineering, 2008. **106**(4): p. 368-374.

146. Iwamoto, K., et al., *Mathematical modeling and sensitivity analysis of G1/S phase in the cell cycle including the DNA-damage signal transduciton pathway.* Biosystems, 2008. **94**: p. 109-117.

147. Haberichter, T., et al., *A systems biology dynamical model of mammalian G_1 cell cycle progression.* Molecular Systems Biology, 2007. **3**: p. 84.

148. Thron, C.D., *A model for a bistable biochemical trigger of mitosis.* Biophysical Chemistry, 1996. **57**: p. 239-251.

149. Thron, C., *Bistable biochemical switching and the control of the events of the cell cycle.* Oncogene, 1997. **15**: p. 317-325.

150. Aguda, B., *Instabilities in phosphorylation-dephosphorylation cascades and cell cycle checkpoints.* Oncogene, 1999. **18**: p. 2846-2851.

151. Aguda, B.D., *A quantitative analysis of the kinetics of the G2 DNA damage checkpoint system.* PNAS, 1999. **96**: p. 11352-11357.

152. Ibrahim, B., et al., *Mad2 binding is not sufficient for complete Cdc20 sequestering in mitotic transition control (an in silico study).* Biophysical Chemistry, 2008. **134**: p. 93-100.

153. Tóth, A., et al., *Mitotic exit in two dimensions.* J Theor Biol, 2007. **248**: p. 560-573.

154. Alberts, B., et al., *Molecular Biology of the Cell.* Fourth Edition ed. 2002, New York: Garland. 1616.

155. Obeyesekere, M.N., S.L. Tucker, and S.O. Zimmerman, *A model for regulation of the cell cycle incorporating cyclin A, cyclin B and their complexes.* Cell Proliferation, 1994. **27**: p. 105-113.

156. Ciliberto, A., et al., *Rewiring the exit from mitosis.* Cell Cycle, 2005. **4**(8): p. 1107-1112.

157. Aguda, B.D. and C.K. Algar, *A structural analysis of the qualitative networks regulating the cell cycle and apoptosis.* Cell Cycle, 2003. **2**(6): p. 538-544.

158. Ciliberto, A., B. Novak, and J.J. Tyson, *Steady states and oscillations in the p53/Mdm2 network.* Cell Cycle, 2005. **4**(3): p. 488-493.

159. Zhang, T., P. Brazhnik, and J.J. Tyson, *Exploring mechanisms of the DNA-damage response: p53 pulses and their possible relevance to apoptosis.* Cell Cycle, 2007. **6**(1): p. 85-94.

160. Alarcon, T., H.M. Byrne, and P.K. Maini, *A mathematical model of the effects of hypoxia on the cell-cycle of normal and cancer cells.* Journal of Theoretical Biology, 2004. **229**(3): p. 395-411.

161. Obeyesekere, M.N., J.R. Herbert, and S.O. Zimmerman, *A model of the G1 phase of the cell cycle incorporating cyclin E/cdk2 complex and retinoblastoma protein.* Oncogene, 1995. **11**(6): p. 1199-1205.

162. Obeyesekere, M.N., et al., *A mathematical model of the regulation of the G1 phase of Rb +/+ and Rb -/- mouse embryonic fibroblasts and an osteosarcoma cell line.* Cell Proliferation, 1997. **30**(171-194).

163. Obeyesekere, M.N., et al., *A model of cell cycle behavior dominated by kinetics of a pathway stimulated by growth factors.* Bulletin of Mathematical Biology, 1999. **61**(917-934).

164. Bai, S., et al., *Theoretical and experimental evidence for hysteresis in cell proliferation.* Cell Cycle, 2003. **2**(1): p. 46-52.

165. Kaern, M. and A. Hunding, *Dynamics of the Cell Cycle Engine: CDK2-kinase and the Transition into Mitosis.* Journal of Theoretical Biology, 1998. **193**(1): p. 47-57.

166. Chiorino, G. and M. Lupi, *Variability in the timing of G1/S transition.* Mathematical Biosciences, 2002. **177-178**: p. 85-101.

167. Qu, Z., J.N. Weiss, and R. MacLellan, *Regulation of the mammalian cell cycle: a model of the G1 to S transition.* Am J Physiol Cell Physiol, 2003. **284**: p. C349-C364.

168. Qu, Z., J.N. Weiss, and W.R. MacLellan, *Coordination of cell growth and cell division: a mathematical modeling study.* Journal of Cell Science, 2004. **117**(18): p. 4199-4207.

169. Yang, L., et al., *Linking cell division to cell growth in a spatiotemporal model of the cell cycle.* Journal of Theoretical Biology, 2006. **241**: p. 120-133.

170. Novak, B. and J.J. Tyson, *A model for restriction point control of the mammalian cell cycle.* Journal of Theoretical Biology, 2004. **230**(4): p. 563-579.

171. Csikasz-Nagy, A., et al., *Analysis of a generic model of eukaryotic cell-cycle regulation.* Biophyical Journal, 2006. **90**: p. 4361-4379.

172. Glendinning, P., *Stability, instability, and chaos: an introduction to the theory of nonlinear differential equations.* Cambridge Texts in Applied Mathematics. 1994, Cambridge: Cambridge University Press.

173. Strogatz, S.H., *Nonlinear Dynamics and Chaos with Applications to Physics, Biology, Chemistry, and Engineering.* 1994, Cambridge: Westview Press.

174. Ermentrout, B., *XPPAUT.* 2002.

175. Chapra, S.C. and R.P. Canale, *Numerical Methods for Engineers with Software and Programming Applications.* 4 ed. 2002, New York: McGraw Hill.

176. Castedo, M., et al., *Cyclin-dependent kinase-1: linking apoptosis to cell cycle and mitotic catastrophe.* Cell Death and Differentiation, 2002. **9**: p. 1287-1293.

177. Sha, W., et al., *Hysteresis drives cell-cycle transitions in Xenopus laevis egg extracts.* PNAS, 2003. **100**(3): p. 975-980.

178. Arooz, T., et al., *On the concentrations of cyclins and cyclin-dependent kinases in extracts of cultured human cells.* Biochemistry, 2000. **39**: p. 9495-9501.

179. Tassan, J.-P., et al., *Cell cycle analysis of the activity, subcellular localization, and subunit composition of human CAK (CDK-activating kinase).* Journal Of Cell Biology, 1994. **127**(2): p. 467-478.

180. Kraft, C., et al., *Mitotic regulation of the human anaphase-promoting complex by phosphorylation.* The EMBO Journal, 2003. **22**(24): p. 6598-6609.

181. Haese, G.J.D., et al., *The Wee1 protein kinase regulates T14 phosphorylation of fission yeast Cdc2.* Molecular Biology of the Cell, 1995. **6**: p. 371-385.

182. Okamoto, K. and N. Sagata, *Mechanism for inactivation of the mitotic inhibitory kinase Wee1 at M phase.* PNAS, 2007. **104**(10): p. 3753-3758.

183. Bailey, J.E. and D.F. Ollis, *Biochemical Engineering Fundamentals.* Second ed. McGraw-Hill Chemical Engineering Series. 1986, New York: McBraw-Hill Publishing Company.

184. Wieser, W. and G. Krumschnabel, *Hierarchies of ATP-consuming processes: direct compared with indirect measurements, and comparative aspects.* Biochem J., 2001. **355**: p. 389-395.

185. Leist, M., et al., *Intracellular adenosine triphosphate (ATP) concentration: A switch in the decision between apoptosis and necrosis.* J. Exp. Med., 1997. **185**(8): p. 1481-1486.

186. Chapman, J.D., R.G. Webb, and J. Borsa, *ATP pool levels in synchronously growing chinese hamster cells.* Journal of Cell Biology, 1971. **49**: p. 229-233.

187. Eguchi, Y., S. Shimizu, and Y. Tsujimoto, *Intracellular ATP levels determine cell death fate by apoptosis or necrosis.* Cancer Research, 1997. **57**: p. 1835-1840.

188. Mailand, N., et al., *Rapid Destruction of Human Cdc25A in Response to DNA Damage.* Science, 2000. **288**(5470): p. 1425-1429.

189. Gillespie, D.T., *Exact stochastic simulation of coupled chemical reactions.* J. Phys. Chem., 1977. **81**(25): p. 2340 - 2361.

190. Mantzaris, N.V., P. Daoutidis, and F. Srienc, *Numerical solution of multi-variable cell population balance models: I. Finite difference methods.* Computers and Chemical Engineering, 2001. **25**: p. 1411-1440.

191. Ramkrishna, D., *Population balances: theory and applications to particulate systems in engineering.* 2000, San Diego: Academic Press.

192. Fredrickson, A.G., D. Ramkrishna, and H.M. Tsuchiya, *Statistics and Dynamics of Procaryotic Cell Populations.* Mathematical Biosciences, 1967. **1**: p. 327-374.

193. Tsuchiya, H.M., A.G. Fredrickson, and R. Aris, *Dynamics of microbial cell populations.* Advances in Chemical Engineering, 1966. **6**(125-206).

194. Ataai, M.M. and M.L. Shuler, *Simulation of CFSTR through development of a mathematical model for anaerobic growth of Escherichia coli cell population.* Biotechnology and Bioengineering, 1985. **27**: p. 1051-1055.

195. Domach, M.M. and M.L. Shuler, *A finite representation model for an asynchronous culture of E. coli.* Biotechnology and Bioengineering, 1984. **26**: p. 877-884.

196. Stamatakis, M., *Stochasticity and Cell Population Heterogeneity in an Artificial lac Operon Genetic Network*, in *Chemical and Biomolecular Engineering.* 2009, Rice University: Houston.

197. Cross, F.R., et al., *Testing a Mathematical Model of the Yeast Cell Cycle.* Mol. Biol. Cell, 2002. **13**(1): p. 52-70.

198. Stacey, D.W., *Cyclin D1 serves as a cell cycle regulatory switch in actively proliferating cells.* Current Opinion in Cell Biology, 2003. **15**(2): p. 158-163.

199. Sveiczer, A., B. Novak, and J.M. Mitchison, *Mitotic control in the absence of cdc25 mitotic inducer in fission yeast.* Journal of Cell Science, 1999. **112**(7): p. 1085-1092.

200. Heiden, M.G.V., et al., *Growth factors can influence cell growth and survival through effects on glucose metabolism.* Molecular and Cellular Biology, 2001. **21**(17): p. 5899-5912.

Appendix I - Nonlinearity in MPF activation Network

If the intermediate inactive MPF species from the base mitotic model is assumed to be at pseudo steady state, $\left(\frac{d[MPF-P]}{dt}=0\right)$, then the resulting ODEs retain the nonlinearity and the system qualitatively exhibits the original system. Below are the equations for the base MPF activation network.

Original System

$$\begin{aligned}\frac{d[MPF]}{dt} &= k_4[CycB]-k_5[MPF]-k_3[APC-P][MPF]-k_6[Wee1A][MPF]\\ &+k_7\left([Cdc25A]+[Cdc25A-P]+[Cdc25A-PP]\right)[MPF-P]\\ &-k_2[MPF]\end{aligned} \tag{1}$$

$$\begin{aligned}\frac{d[MPF-P]}{dt} &= k_7\left([Cdc25A]+[Cdc25A-P]+[Cdc25A-PP]\right)[MPF-PP]\\ &-k_2[XW]+k_6[Wee1A][MPF]-k_6[Wee1A][MPF-P]\\ &-k_3[APC-P][MPF-P]\\ &-k_7\left([Cdc25A]+[Cdc25A-P]+[Cdc25A-PP]\right)[MPF-P]\end{aligned} \tag{2}$$

$$\begin{aligned}\frac{d[MPF-PP]}{dt} &= -k_7\left([Cdc25A]+[Cdc25A-P]+[Cdc25-PP]\right)[MPF-PP]\\ &-k_2[MPF-PP]-k_3[APC-P][MPF-PP]\\ &+k_6[Wee1A][MPF-P]\end{aligned} \tag{3}$$

Reduced System

To reduce the system, the intermediate inactive species of MPF is assumed to be at pseudo-steady state, $\frac{d[MPF-P]}{dt}=0$, and therefore equation (2) can be solved for MPF-P.

$$[MPF-P]=\frac{k_7\left([Cdc25A]+[Cdc25A-P]+[Cdc25A-PP]\right)[MPF-PP]+k_6[Wee1][MPF]}{k_2+k_3[APC-P]+k_6[Wee1]+k_7\left([Cdc25A]+[Cdc25A-P]+[Cdc25A-PP]\right)} \tag{4}$$

Plugging equation (4) into the differential equations for MPF and MPF-PP retains the nonlinearity generated by the MPF-P species which can be seen in the last two terms of each differential equation. This system produces the same qualitative behavior seen in the base case system (Figure 33).

$$\begin{aligned}\frac{d[MPF]}{dt} &= k_4[CycB]-k_5[MPF]-k_3[APC-P][MPF]-k_6[Wee1A][MPF]-k_2[MPF]\\ &+\frac{k_7^2\left([Cdc25A]+[Cdc25A-P]+[Cdc25A-PP]\right)^2[MPF-PP]}{k_2+k_3[APC-P]+k_6[Wee1]+k_7\left([Cdc25A]+[Cdc25A-P]+[Cdc25A-PP]\right)}\\ &+\frac{+k_6k_7[Wee1]\left([Cdc25A]+[Cdc25A-P]+[Cdc25A-PP]\right)[MPF]}{k_2+k_3[APC-P]+k_6[Wee1]+k_7\left([Cdc25A]+[Cdc25A-P]+[Cdc25A-PP]\right)}\end{aligned} \tag{5}$$

$$\begin{aligned}\frac{d[MPF-PP]}{dt} &= -k_7\left([Cdc25A]+[Cdc25A-P]+[Cdc25-PP]\right)[MPF-PP]\\ &-k_2[MPF-PP]-k_3[APC-P][MPF-PP]\\ &+\frac{k_6k_7[Wee1]\left([Cdc25A]+[Cdc25A-P]+[Cdc25A-PP]\right)[MPF-PP]}{k_2+k_3[APC-P]+k_6[Wee1]+k_7\left([Cdc25A]+[Cdc25A-P]+[Cdc25A-PP]\right)}\\ &+\frac{k_6^2[Wee1]^2[MPF]}{k_2+k_3[APC-P]+k_6[Wee1]+k_7\left([Cdc25A]+[Cdc25A-P]+[Cdc25A-PP]\right)}\end{aligned} \tag{6}$$

In the case of simultaneous inactivating phosphorylations, the last two terms in equations (5) and (6) do not contain the nonlinearity observed in the base mitotic model or in the reduced model. The equations for MPF and MPF-PP for this model are displayed below.

$$\begin{aligned}\frac{d[MPF]}{dt} &= k_4[CycB]-k_5[MPF]-k_3[APC-P][MPF]-k_6[Wee1A][MPF]-k_2[MPF]\\ &+k_7\left([Cdc25A]+[Cdc25A-P]+[Cdc25A-PP]\right)[MPF-PP]\end{aligned} \tag{7}$$

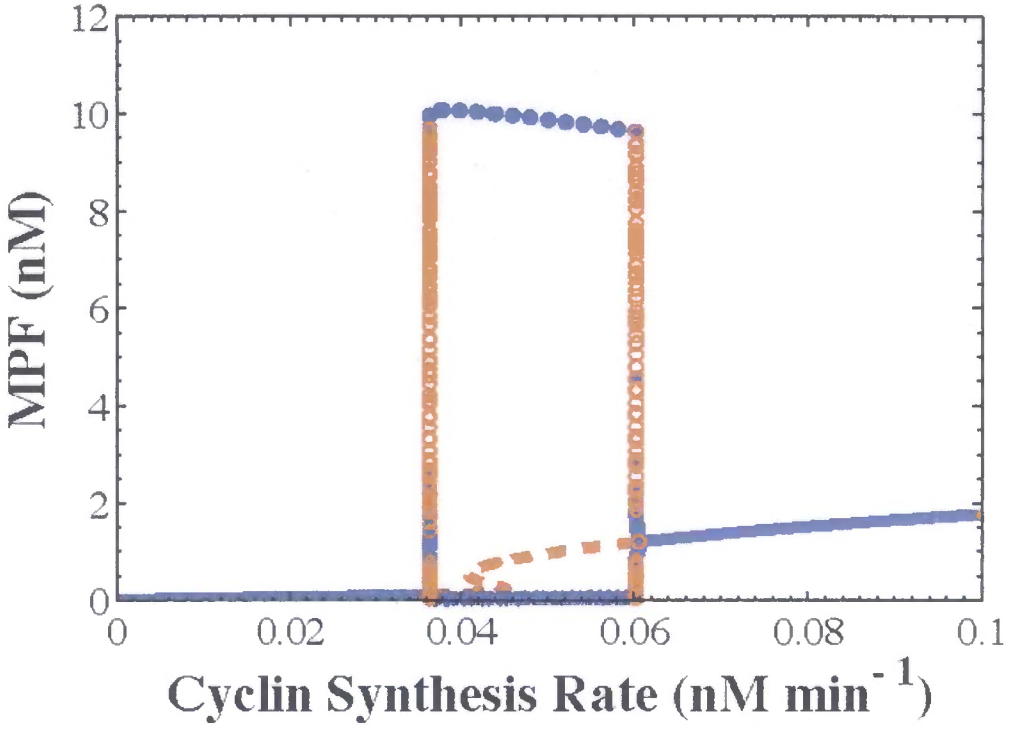

Figure 33 - Quasi-Steady State for Intermediate Inactive MPF species. The system retains the nonlinearity generated by the intermediate species, and therefore displays the same qualitative behavior as the base model.

$$\frac{d[MPF-PP]}{dt} = -k_7\left([Cdc25A]+[Cdc25A-P]+[Cdc25-PP]\right)[MPF-PP] \\ -k_2[MPF-PP]-k_3[APC-P][MPF-PP]+k_6[Wee1][MPF] \tag{8}$$

Neither of the simultaneous terms have the nonlinearity terms observed in the reduced system, and therefore, is the reason why multiplicity and frequency encoding are not observed throughout the MPF activation rate parameter space (Figure 14 p.87).

Appendix II - ATP Model Equations and Parameters

This appendix presents the equations for the ATP model. To begin, the ATP model that incorporates Wee1 inhibition by only degradation is presented in full. The wiring diagram for this system (Figure 21) can be found on page 97. Then, the equations that were changed for the models for Wee1A inhibition by only kinase inhibition, by increased degradation followed by kinases inhibition, and finally kinase inhibition then increased degradation are presented. The wiring diagram for the Wee1A inhibition mechanisms (Figure 28) can be found on page 106. A table of the parameter sets used for the ATP models is presented at the end of this appendix.

ATP Model Incorporating Wee1A Inhibition by only Increased Degradation

The first three equations capture the dynamics of the species involved in cyclin B CDK1 dimerization into active MPF.

$$\frac{d[CAK-ATP]}{dt} = k_1[CAK_{tot}][ATP] - (k_1[ATP] + k_{-1} + k_6[CycB-CDK1])[CAK-ATP] \quad (1)$$

$$\frac{d[CycB]}{dt} = k_2\frac{[ATP]}{K_m+[ATP]} - k_3[CycB] - k_4[APC-P][CycB] - k_5[CycB] + k_{-5}[CycB-CDK1] \quad (2)$$

$$\frac{d[CycB-CDK1]}{dt} = k_5[CycB] + k_7[MPF] - (k_{-5} + k_6[CAK-ATP] + k_3 + k_4[APC-P])[CycB-CDK1] \quad (3)$$

CAK activity has been observed to be roughly constant throughout the cell cycle[11], and thus the model assumes total CAK concentration, CAK_{tot}, is constant. Therefore, only the ATP bound CAK species is incorporated into the model. The dynamics of CAK-ATP are described by equation (1). CAK binds with ATP at a rate of k_1 to form CAK-ATP. CAK concentration is calculated as the total CAK concentration

minus CAK-ATP concentration. CAK-ATP phosphorylates the cyclin B-CDK1 dimer at a rate of k_6, thereby using ATP and becoming CAK.

Cyclin B monomer, CycB, dynamics are generated by equation (2). CycB has saturable rate of protein synthesis with respect to ATP with a maximum rate of k_2. K_m is the Michaelis-Menten parameter for saturable ATP kinetics. All cyclin species including CycB, CycB-CDK1, MPF, MPF-ATP, MPF-P, and MPF-PP have a background degradation rate of k_2 and are also degraded by APC at a rate of k_3 and proportional to the APC-P concentration. CycB dimerizes with CDK1 at a rate of k_5 and dissociates at a rate of k_{-5}. CDK1 is observed to be in excess [178], and therefore, is incorporated into the k_5 constant.

The next equation captures the dynamics of CycB-CDK1, which is the unphosphorylated dimer of cyclin B and CDK1. CycB-CDK1 is formed by and destroyed by dimerization and dissociation of CycB and CDK1. CycB-CDK1 is phosphorylated by CAK-ATP on CDK1 at the activating site, thus forming MPF. The phosphorylation occurs at a rate of k_6 and is proportional to the concentration of CAK-ATP. The activating phosphorylation is removed from CDK1 at a rate of k_7, then converting MPF to CycB-CDK1.

The next four equations capture the dynamics of the active and inactive MPF species. The active form of MPF is bound to ATP (MPF-ATP), and is the species that phosphorylates Wee1, Cdc25A, and APC. The other MPF species are not catalytically active.

$$\frac{d[MPF]}{dt} = k_6[CycB-CDK1][CAK-ATP] + k_{-8}[MPF-ATP]$$
$$-(k_7 + k_8[ATP] + k_3 + k_4[APC-P])[MPF]$$
$$-k_9([Wee1A-ATP]+[Wee1A-P-ATP]+[Wee1A-PP-ATP])[MPF]$$
$$+k_{10}([Cdc25A]+[Cdc25A-P]+[Cdc25A-PP])[MPF-P] \quad (4)$$
$$+k_{14}([Cdc25A]+[Cdc25A-P])[MPF-ATP]$$
$$+k_{19}([Wee1A]+[Wee1A-ATP]+[Wee1A-P]+[Wee1A-P-ATP])[MPF-ATP]$$
$$+k_{22}([APC_{tot}]-[APC-P])[MPF-ATP]$$

$$\frac{d[MPF-ATP]}{dt} = k_8[ATP][MPF] - k_{-8}[MPF-ATP] - k_3[MPF-ATP]$$
$$-k_4[APC-P][MPF-ATP]$$
$$-k_{14}([Cdc25A]+[Cdc25A-P])[MPF-ATP] \quad (5)$$
$$-k_{22}([APC_{tot}]-[APC-P])[MPF-ATP]$$
$$-k_{19}([Wee1A]+[Wee1A-P])[MPF-ATP]$$
$$-k_{19}([Wee1A-ATP]+[Wee1A-P-ATP])[MPF-ATP]$$

$$\frac{d[MPF-P]}{dt} = k_9([Wee1A-ATP]+[Wee1A-P-ATP]+[Wee1A-PP-ATP])[MPF]$$
$$-k_{10}([Cdc25A]+[Cdc25A-P]+[Cdc25A-PP])[MPF-P]$$
$$-k_9([Wee1A-ATP]+[Wee1A-P-ATP]+[Wee1A-PP-ATP])[MPF-P] \quad (6)$$
$$+k_{10}([Cdc25A]+[Cdc25A-P]+[Cdc25A-PP])[MPF-PP]$$
$$-k_3[MPF-P]-k_4[APC-P][MPF-P]$$

$$\frac{d[MPF-PP]}{dt} = k_9([Wee1A-ATP]+[Wee1A-P-ATP]+[Wee1A-PP-ATP])[MPF-P]$$
$$-k_{10}([Cdc25A]+[Cdc25A-P]+[Cdc25A-PP])[MPF-PP] \quad (7)$$
$$-k_3[MPF-PP]-k_4[APC-P][MPF-PP]$$

As stated before, MPF is formed by the phosphorylation of CycB-CDK1 by CAK-ATP at a rate of k_6. All MPF species contain cyclin B, and therefore are degraded at the background rate of k_3 and at a rate of k_4, which is proportional to the concentration of APC. MPF dimerizes with and dissociates from ATP at the rate of k_8 and k_{-8}, respectively. The MPF-ATP species is the active form and phosphorylates the MPF substrates, Wee1, Cdc25A, and APC. When MPF-ATP phosphorylates a substrate, it

uses ATP, and therefore, becomes MPF. Thus, MPF is generated by all MPF-ATP phosphorylation reactions, thus adding the last three terms on equation (4). These terms, k_{14}, k_{19}, and k_{22}, are loss terms in the MPF-ATP equation. The only generation term for MPF-ATP is the dimerization of MPF and ATP at a rate of k_8.

The ATP bound Wee1 species are active, and therefore, phosphorylate MPF at a rate of k_9 that is proportional to the active Wee1 species concentration. Wee1A phosphorylates CDK1 in the ATP binding pocket [23]. Thus phosphorylated MPF species, MPF-P and MPF-PP, cannot bind with ATP and are therefore inactive. The inhibitory phosphorylations are removed from MPF-P and MPF-PP by the Cdc25A family of phosphatases at a rate of k_{10}, which is proportional to the concentration of the Cdc25A species.

The next three equations describe the dynamics of Cdc25A. The unphosphorylated and singly phosphorylated species, Cdc25A and Cdc25A-P, are degraded at a fast rate, k_{12}. The stabilized species, Cdc25A-PP, does not contain this term.

$$\frac{d[Cdc25A]}{dt} = k_{11}\frac{[ATP]}{K_m+[ATP]} - k_{12}[Cdc25A] - k_{13}[APC-P][Cdc25A] - k_{14}[MPF-ATP][Cdc25A] + k_{15}[Cdc25A-P] \tag{8}$$

$$\frac{d[Cdc25A-P]}{dt} = k_{14}[MPF-ATP][Cdc25A] - k_{15}[Cdc25A-P] - k_{14}[MPF-ATP][Cdc25A-P] + k_{15}[Cdc25A-PP] - k_{12}[Cdc25A-P] - k_{13}[APC-P][Cdc25A-P] \tag{9}$$

$$\frac{d[Cdc25A-PP]}{dt} = k_{14}[MPF-ATP][Cdc25A-P] - k_{15}[Cdc25A-PP] - k_{13}[APC-P][Cdc25A-P] \tag{10}$$

Cdc25A is synthesized at a saturable rate with respect to ATP with a maximum rate of k_{11}. MPF-ATP phosphorylates Cdc25A species at a rate of k_{14} that is proportional to the MPF-ATP concentration. The MPF-ATP phosphorylation is removed at a rate of k_{15}. APC degrades all Cdc25A species at a rate of k_{13}. Cdc25A forms a positive feedback loop with MPF. MPF-ATP phosphorylates Cdc25A and stabilizes it [46]. The Cdc25A-PP species that has two MPF-ATP phosphorylations does not have the rapid background degradation term, k_{12}. Cdc25A in turn dephosphorylates the inactive MPF species, MPF-P and MPF-PP, to create MPF. MPF then binds with ATP to form MPF-ATP and can phosphorylate more Cdc25A.

Wee1A dynamics are captured by the following six equations. For this system, MPF down regulation of Wee1A is by degradation only. Wee1A must bind ATP to form an active kinase. The unphosphorylated and singly phosphorylated forms of Wee1A are stable and have low background degradation when compared to the Wee1A species with two MPF phosphorylations that degrades rapidly (k_{21}).

$$\begin{aligned}\frac{d[Wee1A]}{dt} = {} & k_{16}\frac{[ATP]}{K_m+[ATP]} - k_{17}[Wee1A] - k_{18}[ATP][Wee1A] + k_{-18}[Wee1A-ATP] \\ & -k_{19}[MPF-ATP][Wee1A] + k_{20}[Wee1A-P] \\ & +k_9([MPF]+[MPF-P])[Wee1A-ATP]\end{aligned} \tag{11}$$

$$\begin{aligned}\frac{d[Wee1A-ATP]}{dt} = {} & k_{18}[ATP][Wee1A] - k_{-18}[Wee1A-ATP] \\ & -k_{19}[MPF-ATP][Wee1A-ATP] + k_{20}[Wee1A-P-ATP] \\ & -k_{17}[Wee1A-ATP] - k_9([MPF]+[MPF-P])[Wee1A-ATP]\end{aligned} \tag{12}$$

$$\begin{aligned}\frac{d[Wee1A-P]}{dt} = {} & k_{19}[MPF-ATP][Wee1A] - k_{20}[Wee1A-P] \\ & -k_{19}[MPF-ATP][Wee1A-P] + k_{20}[Wee1A-PP] \\ & -k_{18}[ATP][Wee1A-P] + k_{-18}[Wee1A-P-ATP] - k_{17}[Wee1A-P] \\ & +k_9([MPF]+[MPF-P])[Wee1A-P-ATP]\end{aligned} \tag{13}$$

$$\begin{aligned}\frac{d[Wee1A-P-ATP]}{dt} &= k_{19}[MPF-ATP][Wee1A-ATP]-k_{20}[Wee1A-P-ATP]\\ &-k_{19}[MPF-ATP][Wee1A-P-ATP]\\ &+k_{20}[Wee1A-PP-ATP]+k_{18}[ATP][Wee1A-P]\\ &-k_{-18}[Wee1A-P-ATP]-k_{17}[Wee1A-P-ATP]\\ &-k_9([MPF]+[MPF-P])[Wee1A-P-ATP]\end{aligned} \quad (14)$$

$$\begin{aligned}\frac{d[Wee1A-PP]}{dt} &= k_{19}[MPF-ATP][Wee1A-P]-k_{20}[Wee1A-PP]\\ &-k_{18}[ATP][Wee1A-PP]+k_{-18}[Wee1A-PP-ATP]\\ &-k_{21}[Wee1A-PP]+k_9([MPF]+[MPF-P])[Wee1A-PP-ATP]\end{aligned} \quad (15)$$

$$\begin{aligned}\frac{d[Wee1A-PP-ATP]}{dt} &= k_{18}[ATP][Wee1A-PP]-k_{-18}[Wee1A-PP-ATP]\\ &+k_{19}[MPF-ATP][Wee1A-P-ATP]\\ &-k_{20}[Wee1A-PP-ATP]-k_{21}[Wee1A-PP-ATP]\\ &-k_9([MPF]+[MPF-P])[Wee1A-PP-ATP]\end{aligned} \quad (16)$$

The Wee1A species names describe their phosphorylation and ATP bound state. For example, Wee1A-P-ATP has a single MPF phosphorylation and has ATP bound, whereas Wee1A-PP has only two MPF phosphorylations. Wee1A is synthesized at a saturable rate with respect to ATP with a maximum synthesis rate of k_{16}. ATP is assumed to affect all protein synthesis with the same saturable kinetics and therefore, Wee1A synthesis has the same Michaelis-Menten constant as cyclin B and Cdc25A, K_m. All Wee1A species dimerize with ATP at a rate of k_{18}, and dissociate with ATP at a rate of k_{-18}. The ATP bound Wee1A species, Wee1A-ATP, Wee1A-P-ATP, and Wee1A-PP-ATP, are active and thus phosphorylate MPF species to inactivate them. MPF phosphorylation of Wee1 initiates a proteolytic cascade [28]. Therefore, when MPF-ATP phosphorylates Wee1A at a rate of k_{19}, the Wee1A-PP and Wee1A-PP-ATP are degraded at a higher rate, k_{21}. The unphosphorylated and singly phosphorylated Wee1A species have a background degradation rate of k_{17}. The increased degradation parameter, k_{21},

must always be greater than or equal to the background degradation rate, k_{17}. Otherwise, MPF phosphorylation of Wee1 would result in stabilization rather than increased degradation. The MPF phosphorylations on Wee1A species are removed in first order manner at a rate of k_{20}.

When active Wee1A species phosphorylate MPF species, they use their bound ATP. Thus, Wee1A-ATP becomes Wee1A with the other ATP bound species following the same behavior. Thus, the Wee1A species with ATP bound have a sink term for MPF and MPF-P phosphorylation at a rate of k_9, and the Wee1A species without ATP bound have a source term.

The final equation is for the active form of APC. Total APC concentration is assumed to be constant and is set to unity. MPF-ATP activates APC by phosphorylating it at a rate of k_{22}. Inactive APC is calculated as the difference between the total APC, APC_{tot}, minus the active form of APC, APC-P. The MPF phosphorylation on APC is removed at a rate of k_{23}.

$$\frac{d[APC-P]}{dt} = k_{22}[MPF-ATP]([APC_{tot}]-[APC-P]) - k_{23}[APC-P] \tag{17}$$

ATP Model Incorporating Wee1A Inhibition by Kinase Inhibition Only

For this variation of the model, the equations for CAK, CycB, MPF-ATP, the Cdc25A species, APC-P, Wee1A, Wee1A-ATP, and Wee1A-P remain the same. The equations that change are for MPF, MPF-P, MPF-PP, Wee1A-P-ATP, and Wee1A-PP. There is not a Wee1A-PP-ATP species because the model assumes the inhibited form, Wee1A-PP, cannot bind to ATP.

$$\begin{aligned}\frac{d[MPF]}{dt} &= k_6[CycB-CDK1][CAK-ATP]+k_{-8}[MPF-ATP]\\ &-\left(k_7+k_8[ATP]+k_3+k_4[APC-P]\right)[MPF]\\ &-k_9\left([Wee1-ATP]+[Wee1-P-ATP]\right)[MPF]\\ &+k_{10}\left([Cdc25A]+[Cdc25A-P]+[Cdc25A-PP]\right)[MPF-P]\\ &+k_{14}\left([Cdc25A]+[Cdc25A-P]\right)[MPF-ATP]\\ &+k_{19}\left([Wee1]+[Wee1-ATP]+[Wee1-P]+[Wee1-P-ATP]\right)[MPF-ATP]\\ &+k_{22}\left([APC_{tot}]-[APC-P]\right)[MPF-ATP]\end{aligned} \tag{18}$$

$$\begin{aligned}\frac{d[MPF-P]}{dt} &= k_9\left([Wee1-ATP]+[Wee1-P-ATP]\right)[MPF]\\ &-k_{10}\left([Cdc25A]+[Cdc25A-P]+[Cdc25A-PP]\right)[MPF-P]\\ &-k_9\left([Wee1-ATP]+[Wee1-P-ATP]\right)[MPF-P]\\ &+k_{10}\left([Cdc25A]+[Cdc25A-P]+[Cdc25A-PP]\right)[MPF-PP]\\ &-k_3[MPF-P]-k_4[APC-P][MPF-P]\end{aligned} \tag{19}$$

$$\begin{aligned}\frac{d[MPF-PP]}{dt} &= k_9\left([Wee1-ATP]+[Wee1-P-ATP]\right)[MPF-P]\\ &-k_{10}\left([Cdc25A]+[Cdc25A-P]+[Cdc25A-PP]\right)[MPF-PP]\\ &-k_3[MPF-PP]-k_4[APC-P][MPF-PP]\end{aligned} \tag{20}$$

The MPF species equations are changed by only the Wee1A phosphorylation term. Since Wee1A-PP-ATP has been removed from the model, there are only two active forms of Wee1A, Wee1A-ATP and Wee1A-P-ATP. Thus, the inactivation term for MPF phosphorylation, k_9, has two active forms of Wee1A rather than the three from the last model.

$$\begin{aligned}\frac{d[Wee1A-P-ATP]}{dt} &= k_{19}[MPF-ATP][Wee1A-ATP]-k_{20}[Wee1A-P-ATP]\\ &-k_{19}[MPF-ATP][Wee1A-P-ATP]\\ &+k_{18}[ATP][Wee1A-P]-k_{-18}[Wee1A-P-ATP]\\ &-k_{17}[Wee1A-P-ATP]-k_9\left([MPF]+[MPF-P]\right)[Wee1A-P-ATP]\end{aligned} \tag{21}$$

$$\frac{d[Wee1A-PP]}{dt} = k_{19}[MPF-ATP][Wee1A-P]-k_{20}[Wee1A-PP] \\ +k_{19}[MPF-ATP][Wee1A-P-ATP]-k_{17}[Wee1A-PP] \quad (22)$$

Wee1A-P-ATP can now be phosphorylated by MPF-ATP, thereby releasing ATP and forming Wee1A-PP. Wee1A-PP does not dephosphorylate to form Wee1A-P-ATP, and therefore, Wee1A-P-ATP does not have a source term from dephosphorylation, k_{20}, as it did from Wee1A-PP-ATP in the previous model. Wee1A-PP has the additional source term from Wee1A-P-ATP phosphorylation by MPF-ATP at a rate of k_{19}. Wee1A-PP does not bind with ATP and thus these terms have been removed from the equation. Wee1A-PP does not have a source term from phosphorylation of MPF species, because the ATP bound Wee1A-PP-ATP species does not exist in this model. Thus, these terms were removed.

ATP Model Incorporating Wee1A Inhibition by Increased Degradation Followed by Kinase Inhibition

This model was created by augmentation of the ATP model with Wee1A inhibition by only degradation. The equations for MPF-P, MPF-PP, Wee1A, Wee1A-ATP, Wee1A-P, Wee1A-P-ATP, all Cdc25A species, and APC-P remain the same. The equations for MPF, MPF-ATP, Wee1A-PP-ATP, and Wee1A-PP-ATP are altered. To compare the models, the amount of active Wee1A was kept constant. Thus, Wee1A species had to be phosphorylated at two sites before any inhibitory action was implemented. Thus, for the systems with two inhibitory mechanisms, an additional species was added, Wee1A-3P, which was phosphorylated by MPF-ATP at three phosphorylation sites.

With the extra phosphorylations steps occurring in the Wee1A mechanism, the MPF and MPF-ATP equations had to be augmented. MPF-ATP now phosphorylated Wee1A-PP and Wee1A-PP-ATP to form Wee1A-3P. Thus, there were two new sink and source terms for MPF-ATP and MPF, respectively. The new terms can be found in the k_{19} reaction for both species.

$$\begin{aligned}\frac{d[MPF]}{dt} &= k_6[CycB-CDK1][CAK-ATP]+k_{-8}[MPF-ATP]\\ &-(k_7+k_8[ATP]+k_3+k_4[APC-P])[MPF]\\ &-k_9([Wee1A-ATP]+[Wee1A-P-ATP]+[Wee1A-PP-ATP])[MPF]\\ &+k_{10}([Cdc25A]+[Cdc25A-P]+[Cdc25A-PP])[MPF-P]\\ &+k_{14}([Cdc25A]+[Cdc25A-P])[MPF-ATP]\\ &+k_{19}\begin{pmatrix}[Wee1A]+[Wee1A-ATP]+[Wee1A-P]+[Wee1A-P-ATP]\\ +[Wee1A-PP]+[Wee1A-PP-ATP]\end{pmatrix}[MPF-ATP]\\ &+k_{22}([APC_{tot}]-[APC-P])[MPF-ATP]\end{aligned} \tag{23}$$

$$\begin{aligned}\frac{d[MPF-ATP]}{dt} &= k_8[ATP][MPF]-k_{-8}[MPF-ATP]-k_3[MPF-ATP]\\ &-k_4[APC-P][MPF-ATP]\\ &-k_{14}([Cdc25A]+[Cdc25A-P])[MPF-ATP]\\ &-k_{22}([APC_{tot}]-[APC-P])[MPF-ATP]\\ &-k_{19}([Wee1A]+[Wee1A-P]+[Wee1A-PP])[MPF-ATP]\\ &-k_{19}([Wee1A-ATP]+[Wee1A-P-ATP]+[Wee1A-PP-ATP])[MPF-ATP]\end{aligned} \tag{24}$$

The Wee1A-PP and Wee1A-PP-ATP species are now phosphorylated by MPF-ATP to form Wee1A-3P. Thus, there are new sink terms for both at a rate of k_{19} and proportional to MPF-ATP. Wee1A-3P is dephosphorylated at a rate of k_{20} to form Wee1A-PP. The new equation for Wee1A-3P has source terms from MPF-ATP phosphorylation of Wee1A-PP and Wee1A-PP-ATP. Wee1A-3P is dephosphorylated to form Wee1A-PP. All three species have increased degradation rates, k_{21}.

$$\begin{aligned}\frac{d[Wee1A-PP]}{dt} &= k_{19}[MPF-ATP][Wee1A-P]-k_{20}[Wee1A-PP]\\ &-k_{19}[MPF-ATP][Wee1A-PP]+k_{20}[Wee1A-3P]\\ &-k_{18}[ATP][Wee1A-PP]-k_{-18}[Wee1A-PP-ATP]\\ &-k_{21}[Wee1A-PP]+k_9([MPF]+[MPF-P])[Wee1A-PP-ATP]\end{aligned} \tag{25}$$

$$\begin{aligned}\frac{d[Wee1A-PP-ATP]}{dt} &= k_{19}[MPF-ATP][Wee1A-P-ATP]-k_{20}[Wee1A-PP-ATP]\\ &-k_{19}[MPF-ATP][Wee1A-PP-ATP]\\ &+k_{18}[ATP][Wee1A-PP]\\ &-k_{-18}[Wee1A-PP-ATP]-k_{21}[Wee1A-PP-ATP]\\ &-k_9([MPF]+[MPF-P])[Wee1A-PP-ATP]\end{aligned} \tag{26}$$

$$\begin{aligned}\frac{d[Wee1A-3P]}{dt} &= k_{19}[MPF-ATP][Wee1A-PP]-k_{20}[Wee1A-3P]\\ &+k_{19}[MPF-ATP][Wee1A-PP-ATP]-k_{21}[Wee1A-3P]\end{aligned} \tag{27}$$

ATP Model Incorporating Wee1A Inhibition by Kinase Inhibition Followed by Degradation

This variation of the ATP was constructed from the ATP model incorporating Wee1A inhibition by only kinase inhibition. Therefore, the only equations to change are MPF, MPF-ATP, and Wee1A-PP. An additional species, Wee1A-3P was incorporated into the model. To make an equal comparison between the different mechanisms, all models maintained the same number of active Wee1A species. Therefore, two MPF-ATP phosphorylations were required on a Wee1A specie before any inhibition mechanism was initiated. Hence, the additional Wee1A specie with three MPF-ATP phosphorylations, Wee1A-3P, was added to the model to analyze the effect of the extra inhibition mechanism.

Since Wee1A-PP is now phosphorylated by MPF-ATP to form Wee1A-3P, MPF-ATP uses its bound ATP in the reaction. Therefore, a source and sink term must be

added to the MPF and MPF-ATP equations, respectively. This term is found in the k_{19} reaction.

$$\begin{aligned}\frac{d[MPF]}{dt} &= k_6[CycB-CDK1][CAK-ATP]+k_{-8}[MPF-ATP]\\ &-(k_7+k_8[ATP]+k_3+k_4[APC-P])[MPF]\\ &-k_9([Wee1A-ATP]+[Wee1A-P-ATP])[MPF]\\ &+k_{10}([Cdc25A]+[Cdc25A-P]+[Cdc25A-PP])[MPF-P]\\ &+k_{14}([Cdc25A]+[Cdc25A-P])[MPF-ATP]\\ &+k_{19}\begin{pmatrix}[Wee1A]+[Wee1A-ATP]+[Wee1A-P]\\ +[Wee1A-P-ATP]+[Wee1A-PP]\end{pmatrix}[MPF-ATP]\\ &+k_{22}([APC_{tot}]-[APC-P])[MPF-ATP]\end{aligned} \tag{28}$$

$$\begin{aligned}\frac{d[MPF-ATP]}{dt} &= k_8[ATP][MPF]-k_{-8}[MPF-ATP]-k_3[MPF-ATP]\\ &-k_4[APC-P][MPF-ATP]\\ &-k_{14}([Cdc25A]+[Cdc25A-P])[MPF-ATP]\\ &-k_{22}([APC_{tot}]-[APC-P])[MPF-ATP]\\ &-k_{19}([Wee1A]+[Wee1A-P]+[Wee1A-PP])[MPF-ATP]\\ &-k_{19}([Wee1-ATP]+[Wee1-P-ATP])[MPF-ATP]\end{aligned} \tag{29}$$

The Wee1A-PP equation has an additional sink term for MPF-ATP phosphorylation, k_{19}, and a source term for Wee1A-3P dephosphorylation, k_{20}. Conversely, The additional equation for Wee1A-3P has a source term from Wee1A-PP phosphorylation by MPF-ATP, k_{19}, and a sink term for dephosphorylation, k_{20}. Wee1A-3P specie has increased degradation, k_{21}, which is always greater than the background degradation term, k_{17}. Otherwise, MPF-ATP phosphorylation would induce stabilization rather than increased degradation.

$$\frac{d[Wee1A-PP]}{dt} = k_{19}[MPF-ATP][Wee1A-P]-k_{20}[Wee1A-PP] \\ -k_{19}[MPF-ATP][Wee1A-PP]+k_{20}[Wee1A-PP] \\ +k_{19}[MPF-ATP][Wee1A-P-ATP]-k_{17}[Wee1A-PP] \tag{30}$$

$$\frac{d[Wee1A-3P]}{dt} = k_{19}[MPF-ATP][Wee1A-PP]-k_{20}[Wee1A-3P] \\ -k_{21}[Wee1A-3P] \tag{31}$$

Table 2 – ATP Model Parameters with Descriptions. Parameter sets are presented for the base case model, relative ATP models, and the final model that is linked to extracellular glucose.

Parameter	Description	Base Case	Relative ATP - Wee1A Degradation Only	Relative ATP - Wee1A Inhibition then Degradation	Final Model Linked to Glucose	Units
CAK_{tot}	Total Concentraiton of CAK	1	1	1	1	nM
APC_{tot}	Total Concentration of APC	1	1	1	1	nM
k_m	Michaelis-Menten Constant for ATP requirement for Protein Synthesis	0.5	0.05	0.05	0.05	mM
k_1	CAK ATP Dimerization	5	7500	7500	7350	$mM^{-1}hr^{-1}$
k_{-1}	CAK ATP Dissociation	1	150	150	147	hr^{-1}
k_2	Cyclin B Syntheis Rate	0.01	1.5	1.5	1.47	$nM\,hr^{-1}$
k_3	Cyclin B Background Degradation	0.0001	0.015	0.015	0.0147	hr^{-1}
k_4	Cyclin B Degradaiton by APC	1.5	1.15	1.15	1.127	$nM^{-1}hr^{-1}$
k_5	Cyclin B CDK1 Dimerization	1	150	150	147	$nM^{-1}hr^{-1}$
k_{-5}	Cyclin B CDK1 Dissociation	1	150	150	147	hr^{-1}
k_6	CDK1 Activating Phosphorylation by CAK	6	900	900	882	$nM^{-1}hr^{-1}$
k_7	CDK1 Activating Phosphorylation Removal	0.01	1.5	1.5	1.47	hr^{-1}
k_8	MPF ATP Dimerization	10	750	750	735	$mM^{-1}hr^{-1}$
k_{-8}	MPF ATP Dissociation	10	750	750	735	hr^{-1}
k_9	MPF Inhibtion by Wee1	2.1	345	345	338.1	$nM^{-1}hr^{-1}$
k_{10}	MPF Activation by Cdc25A	0.5	250	250	245	$nM^{-1}hr^{-1}$
k_{11}	Cdc25A Synthesis Rate	1.2	180	180	176.4	$nM\,hr^{-1}$
k_{12}	Unstable Cdc25A Degradation Rate	12	1650	1650	1617	hr^{-1}
k_{13}	Cdc25A Degradation by APC	40	75	75	73.5	$nM^{-1}hr^{-1}$
k_{14}	Cdc25A Stabilization by MPF	7.5	1800	1800	1764	$nM^{-1}hr^{-1}$
k_{15}	Cdc25A Destabilization	0.1	15	15	14.7	hr^{-1}
k_{16}	Wee1A Synthesis	1	150	150	147	$nM\,hr^{-1}$
k_{17}	Wee1A Background Degradation	1	150	150	147	hr^{-1}
k_{18}	Wee1A ATP Dimerization	10	15000	15000	14700	$mM^{-1}hr^{-1}$
k_{-18}	Wee1A ATP Dissociation	1	150	150	147	hr^{-1}
k_{19}	Wee1A Inhibition by MPF	0.4	600	550	539	$nM^{-1}hr^{-1}$
k_{20}	Wee1A Activation	1	75	75	73.5	hr^{-1}
k_{21}	Unstable Wee1A Degradation Rate	5	750	750	735	hr^{-1}
k_{22}	APC Activation by MPF	0.001	67.5	67.5	66.15	$nM^{-1}hr^{-1}$
k_{23}	APC Inactivation	0.45	75	75	73.5	hr^{-1}
K_g	Michaelis-Menten Constant for Glucose				0.1085	$mg\,mL^{-1}$